VOLUME 16 NO. 2 |JULY 2022
P-ISSN: 1411-1616 | E-ISSN:2549-8215
Accredited by Kemenristekdikti No. 10/E/KPT/2019 (S3)

JURNAL ILMIAH BERKALA
SAINS DAN TERAPAN KIMIA

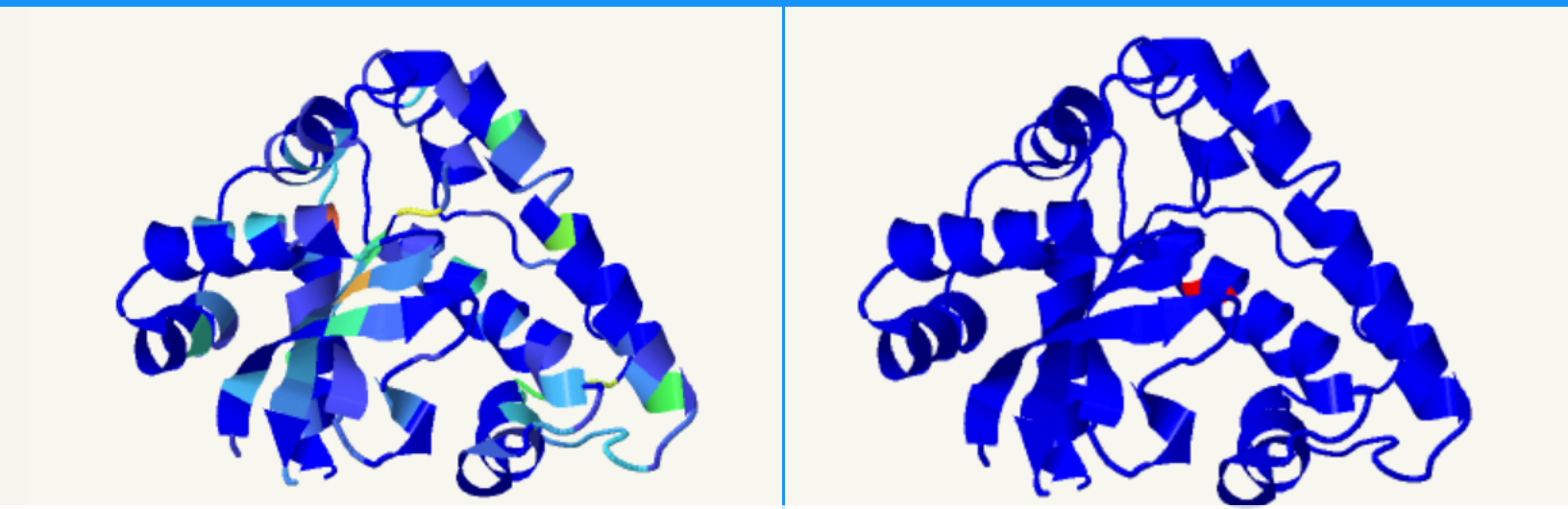

Three Dimension Structure Modeling of The Superoxide Dismutase (SOD) of Rice (Oryza sativa) based on clashes (left) and rotamers (right) (Komari et al, pp. 92)

JURNAL ILMIAH BERKALA
SAINS DAN TERAPAN
KIMIA

PUBLISHED BY:
CHEMISTRY DEPARTMENT, FACULTY OF MATHEMATICS AND NATURAL SCIENCES
LAMBUNG MANGKURAT UNIVERSITY, INDONESIA

SUPERVISORY BOARD

Head of Chemistry Department, Faculty of Mathematics and Natural Sciences, Lambung Mangkurat University

PUBLISHER

Chemistry Department, Faculty of Mathematics and Natural Sciences, Lambung Mangkurat University

MAILING ADDRESS

Jl. A. Yani Km. 36 Banjarbaru, Kalimantan Selatan , Indonesia 70714
Phone: 0511-4773112, 0511-4782899
Email: jstk@ulm.ac.id

FIRST EDITION: 2007

EDITOR IN CHIEF

Utami Irawati, S.Si., MES., Ph.D.

EDITORIAL BOARD

Head of Editorial Board : Prof. Rodiansono, S.Si., M.Si., PhD

Associate Editors : Dahlena Ariyani, S.Si., M.S.
Dewi Umaningrum, S.Si., M.Si.

Section Editors : Noer Komari, S.Si., M.Kes (*regular section*)
Kholifatu Rosyidah, S.Si., M.Si. (SN-STPK *section*)
Maria Dewi Astuti, S.Si., M.Si. (Sainstek 5 *section*)

Editorial Board Members:

Prof. Dr. Rer.nat Drs. Karna Wijaya, M.Eng (UGM, Yogyakarta)
Dr. Hendrik Oktendy Lintang (Universitas Ma Chung, Malang)
Yuana Nurulita,S.Si, M.Si, Ph.D (Universitas Riau, Riau)
Prof. Dr. Abdullah, S.Si, M.Si (Universitas Lambung Mangkurat, Banjarbaru)
Dr. Arnida, S.Si. M.Si. Apt. (Universitas Lambung Mangkurat, Banjarbaru)
Dr. Rahadian Zainul, S.Pd., M.Si. (Universitas Negeri Padang, Padang)
Prof. Sunardi, S.Si., M.Sc., Ph.D. (Universitas Lambung Mangkurat, Banjarbaru)
Edi Mikrianto, S.Si., M.Si. (Universitas Lambung Mangkurat, Banjarbaru)

SITE EDITOR AND ADMINISTRATOR

Ahmad Rusadi Arrahimi, S.Kom., M.Kom.
Shofia Qolby, S.Si.

ABOUT US

(Jurnal Ilmiah Berkala) Sains dan Terapan Kimia publishes scientific articles in the Chemistry field which include, but not limited to, research in chemistry, theoretical chemistry, chemistry education, and applied chemistry. This journal also publishes review articles about the development of chemistry. All the articles in this journal will go through a peer-review process to ensure that the quality of the article meets our standard before being published. Each article submitted to our journal will be reviewed by a reviewer having the expertise in the field. Shall the article submitted is deemed acceptable to be published in our journal, it is the writer's responsibility to make the necessary change and revision as recommended by the reviewer.
This journal is open access journal which means that all content is freely available without charge to users or / institution. Users are allowed to read, download, copy, distribute, print, search, or link to full text articles in this journal without asking prior permission from the publisher or author.

Sains dan Terapan Kimia (Jurnal Ilmiah Berkala) is published twice a year on January and July. There is no fee for authors to submit their manuscripts to be considered for publication in this jurnal. When the article is accepted for the publication. The publication fee is IDR 500.000,00 that covers article processing and DOI processing charge, and one copy of the printed out edition of the journal. The publication fee is for articles being submitted in English. You can still submit the article in Bahasa Indonesia, however, there will be additional IDR 250.000,00 charge for the translation service. The publication fee does not cover shipping fee. If required, authors can ask for additional printed out edition which cost IDR. 60.000,00 per copy. Payment should be made by bank transfer to this account below

Bank : BNI Banjarmasin
Account Number : **0201041846**
Account Name : Dahlena Ariyani

Please send a confirmation of your proof of payment to dariyani@ulm.ac.id

TABLE OF CONTENTS

Characterization of Natural Face Toner from Rice-washed Water 75-85
Tantra Diwa Larasati, Novy Pralisa Putri, Helda Niawanti, Linda Eka Pratiwi, Delthania Ekaristi

Three Dimension Structure Modeling of The Superoxide Dismutase (SOD) of Rice (Oryza sativa) Using Fold Recognition Method Using Phyre^2 Web Server 86-97
Noer Komari, Khairil Anwar, Eko Suhartono

Development of QSAR Model of Caffeic Acid Phenethyl Ester as Anti-Cancer HT-29.... 98-109
Uripto Trisno Santoso, Samsul Hadi, Devi Eka Pratama

Study of Microstructure and Optical Properties of Fe_2O_3/TiO_2 Composites as Functional Materials..... 110-116
Rendy Muhamad Iqbal, Erwin Prasetya Toepak, Dyah Ayu Pramoda Wardani, Elda Alyatikah, Stevin Carolius Angga, Luqman Hakim

Adsorption of Organic Compounds in Leachate using Precipitated Calcium Carbonate (PCC) from Ale-Ale Shells..... 117-124
Yulistya Vidyaning Maulidya, Rudiyansyah, and Nelly Wahyuni

Characteristics and Chemical Composition of Fly Ash From Pulang Pisau's Power Plant as A Potential Material for Synthesis of Aluminosilicate Materials 125-130
Rendy Muhamad Iqbal, Akhmad Damsyik, Retno Agnestisia, Siswo, Ni Wayan Prema Mulya Sari Fildzah 'Adany

Antioxidant and Antibacterial Activity of The Stem Bark Extract of Sterculia Foetida L. 131-139
Theodore Y. K. Lulan, Febri O. Nitbani, Reinner I. Lerrick

JURNAL ILMIAH BERKALA SAINS DAN TERAPAN KIMIA

Jurnal Ilmiah Berkala: Sains dan Terapan Kimia
Vol. 16 No. 2, July 2022

Characterization of Natural Face Toner from Rice-washed Water

Karakteristik *Toner* Wajah Alami Berbahan Baku Air Cucian Beras

Tantra Diwa Larasati[1)], Novy Pralisa Putri[1], Helda Niawanti[1], Linda Eka Pratiwi[1], Delthania Ekaristi[1]

[1]Chemical Engineering, Faculty of Engineering, Mulawarman University, Samarinda, Indonesia

Email: *tantralarasati@ft.unmul.ac.id*

ABSTRACT

Toner is a skin treatment that serves to refresh and clean facial skin. This study used rice-washed water as the main ingredient for producing toner. Rice-washed water is the main ingredient because it contains abundant nutrients such as carbohydrates in the form of starch, fat, protein, gluten, cellulose, hemicellulose, sugar, vitamins, and minerals. This study aims to determine the effect of toner application made from rice-washed water on the skin, storage time on toner quality, and the production process. The method used in this study uses a simple method of soaking with a rice/water with a various ratio (kg/L). The analysis results show that the toner has a pH of 6.4, considered safe for all skin types with good moisture. The effect on skin moisture was analyzed on six respondents. The toner has a viscosity that is not too thick with a cloudy white color caused by rice grains. Rice grains are beneficial for the skin because they can regenerate skin cells. Rice-washed water toner for seven days contains fat, manganese, protein, oil, fat, and is odorless.

Keywords: rice-washed water, toner, skin

ABSTRAK

Toner adalah perawatan kulit yang berfungsi untuk menyegarkan dan membersihkan kulit wajah. Pada penelitian ini air beras digunakan sebagai bahan utama untuk pembuatan toner. Limbah air beras digunakan sebagai bahan utama karena memilik kandungan nutrisi yang berlimpah seperti karbohidrat berupa pati, lemak, protein, gluten, selulosa, hemiselulosa, gula serta mengandung vitamin dan mineral. Penelitian ini bertujuan untuk mengetahui pengaruh penggunaan toner dari air cucian beras terhadap kulit, pengaruh lama penyimpanan toner terhadap kualitas air beras dan reaksi pada kulit serta proses pembuatanya. Metode yang digunakan dalam penelitian ini menggunakan metode sederhana dengan melakukan perendaman dengan rasio beras/air sebesar ½ (kg/L). Berdasarkan metode yang digunakan didapatkan hasil analisa pH 6,4 dimana pH tersebut aman untuk semua jenis kulit dengan kelembaban yang baik. Kelembaban dianalisa oleh 6 responden dengan viskositas toner yang tidak terlalu kental dan memiliki warna yang putih keruh yang diakibatkan butiran beras. Namun, butiran tersebut baik untuk kulit karena dapat meregenerasikan sel-sel kulit. Toner air beras selama 7 hari memiliki kandungan lemak, mangan, protein dan minyak dan lemak. Bahkan toner ini tidak memiliki bau.

Kata Kunci: limbah air beras, toner, kulit

Submitted: June 15, 2021; **Accepted**: June 29, 2022: **Available online**: July 31, 2022

1. INTRODUCTION

Increasing public awareness of physical appearance and skin health has led to a rise in the use of skincare products. According to data from the Ministry of Industry of the Republic of Indonesia, cosmetic consumption increased by 20 % in 2018, four times the national economic growth of 2017. The need for raw materials and additives derived from natural sources increased with the replacement of synthetic components due to the negative impact of synthetic materials on health and the environment. Therefore, natural raw materials are used to manufacture cosmetics, one of which is rice-washed water. Rice-washed water skin care is cheap and effective for various skin problems. Rice-washed water is excellent for all skin types and is a simple facial skin treatment. Rice-washed water contains minerals and vitamins beneficial for skin and hair beauty. Rice grains are rich in ferulic acid, which has anti-inflammatory properties. Ferulic acid is an antioxidant that is rich in allantoin compounds. Besides being one of the gentlest skin cleansing agents, rice-washed water also contains vitamins such as B1, C, E, and minerals, which can shrink pores, tighten, brighten, and soften the skin (Moeskin, 2015).

There are various types of facial skin. Normal skin has good hydration, tone, and resilience produced by a well-functioning epidermis and dermis, well hydrated and supported by adipose tissue (Micalun, 2014). Oily skin is a condition that develops due to an overactive sebaceous. The glands (oil) produce a lot of sebum (oil). Oily skin can be recognized by its shiny, thick, and firm appearance (Micalun, 2014). Dry skin is usually dehydrated and often feels scaly, rough, and itchy. Dry skin can often be very smooth, too delicate, and thin, with barely visible pores (Micalun, 2014). Combination skin occurs when oily, dry, or normal skin types are present together. The most common forms of combination skin tend to be normal in the cheek area with an oily T zone or dry cheeks with a normal T zone (Micalun, 2014).

In this era, there are lots of new brands that sell cosmetics according to the skin problems experienced by consumers. However, sometimes there are still quite a lot of cosmetics on the market that are unsuitable for certain skin types. Therefore, consumers use more natural ingredients, one of which is rice-washed water. Rice has many components, including vitamins, minerals, and phenolic compounds 1. The coarse structure of rice can also be used as a body scrub or facial scrub to remove dead skin cells. Rice is a natural ingredient that has been widely used for various cosmetic purposes, such as masks. The oryzanol substance contained in rice can function as an antioxidant, renew melanin pigment, and neutralize ultraviolet light (Juliano et al., 2005).

Rice-washed water has the potential as an antioxidant and antiaging because of its starch. These carbohydrate group compounds can shed dust and dead skin cells on the face and regenerate skin cells (Samahah et al., 2015). The content of water-soluble micronutrients in rice-washed water is very good for skin health. In addition, rice-washed water can brighten the face because rice-washed water contains oryzanol which can renew the development and formation of melanin pigment, effectively warding off ultraviolet rays (Nisa, 2017). Extract from rice helps increase the production of collagen, which functions to maintain skin elasticity. In addition, the oryzanol substance in rice helps regenerate the melanin pigment in the skin, where the primary function of melanin is as an antidote to UV radiation. Not only that the vitamin E in rice helps nourish the skin so that the skin will look fresher, and the ferulic acid content functions as an antioxidant and an antidote to free radicals (Ijiri et al., 2013).

Table 1. Composition of rice-washed water

Composition	Amount (%)
Carbohydrate	90
Protein	8.77
Fat	1.09
Vitamin B1	70
Vitamin B3	90
Vitamin B6	50
Manganese (Mn)	50
Phosphorus (f)	60
Iron (Fe)	50
Nitrogen (N)	0.015
Magnesium (Mg)	14.525
Potassium (K)	0.02
Calcium (Ca)	2.94

Source: Wardiah, 2014

2. MATERIALS AND METHODS

2.1. Materials

The tools used in this study were various Pyrex beakers (100, 500, 1000 mL), stir bar, spatula, funnel, analytical balance (Ohaus), watch glass, viscometer, bulb, skin analyzer, test tube, measuring flask, dropper, and pH meter (Hanna HI 98107). The materials used were Ramos rice, distilled water, water, 0.2 N NaOH, 0.3 N NaOH, $Fecl_3$, 2% $CuSO_4$, and Whatman filter paper No. 42.

2.2. Methods

A total of 500 grams of rice was washed with water. In the first washing, rice was added with 3 L of water (1:6) and soaked for 1 hour. After 3 hours, the rice-washed water was tested for pH, odor, viscosity, color test for 7 days, moisture test on facial skin for 30 days, protein content, and Vitamin B6. The same method was carried out for other samples with a ratio of raw material: water, namely 1:4 and 1:5.

3. RESULTS AND DISCUSSION

3.1. Odor Test

The odor test was carried out to determine whether the facial toner produced an odor during the storage process. Table 2 shows that rice-washed water stored for seven days is odorless. It is because the toner is made from natural ingredients without adding other chemicals. This odor test was carried out in Baristan Samarinda.

Table 2. Odor Test

Day	Odor
1	Odorless
2	Odorless
3	Odorless
4	Odorless
5	Odorless
6	Odorless
7	Odorless

3.2. Color Test

The color test was carried out in Baristan Samarinda to determine the color change during storage. Tests for seven days of storage are presented in Table 3. Analysis with the platinum-cobalt scale (Pt per Co unit) showed results that fluctuated daily. It is presumably because the toner container is contaminated with other materials.

Table 3. Color Test

Day	Color (Pt.Co)
1	158
2	66.81
3	139
4	78.12
5	138
6	105
7	166

3.3. Viscosity Test

Based on Table 4, it can be seen that on the fourth and fifth days, there is a decrease in toner viscosity, and it start to stabilize again on the sixth and seventh days. It occurs because the storage temperature fluctuates. The higher the temperature, the lower the viscosity. This decrease occurs because the longer the storage time, the longer the toner will be affected by the environment, such as air.

Table 4. Viscosity Test

Day	Viscosity
1	1.8
2	2.03
3	2.06
4	2.06
5	1.8
6	1.8
7	1.7

The longer the storage, the lower the viscosity of the preparation. Decreased viscosity occurs because hygroscopic starch can absorb moisture, thereby increasing the volume of water in the preparation (Sulastri et al., 2016).

Toner with an acidic pH can irritate facial skin, while a pH that is too alkaline can cause a dry effect on the skin (Sulastri et al., 2016). The pH of the toner from the rice-washed water fluctuated, causing pH instability during seven days of storage (Table 5). Changes in room temperature cause instability. However, the pH of the toner produced is still in the pH range of the skin, so it is safe to use.

Table 5. pH Test

Day	pH
1	7
2	6
3	6.1
4	6.5
5	6.3
6	6.8
7	6.4

3.4. Skin Moisture Test

Skin moisture test aims to determine the effect of toner on facial skin moisture before and after application. This test was conducted on six respondents using a skin analyzer. A skin analyzer was used before and after toner's application. Table 6 shows the criteria for facial skin types in general. Each skin type has different water content. The moisture test results before and after toner's application are presented in Table 7 and Table 8.

The skin moisture test on the respondents on the first day before the toner application showed that respondents A, B, D, E, and F had very dry facial skin while respondent C had dry skin. Tests on the seventh day after the toner application showed that respondents A, C, E, and F showed very dry skin, while respondents B and D showed dry facial skin. After toner's application, respondents A, B, C, D, and F showed changes in skin moisture from very dry to dry skin, and for respondent E, the skin moisture became normal. The skin moisture test on the six respondents for 14 days showed a fluctuating percentage of water content. It is thought to be caused by the accuracy factor of the skin analyzer. In addition, different room conditions or air temperatures when checking skin moisture can also affect the results of the skin moisture test.

Table 6. Criteria for Skin Types Based on Water on Facial Skin

Water Content	Skin Types
≤ 33%	Very Dry
34 – 37%	Dry Skin
38 – 42 %	Normal Skin
43 – 46 %	Moist Skin
≥ 47 %	Very Moist

Source: Masluhiya AF and Fidiastuti, 2019.

Table 7. Respondent's Skin Moisture Before Toner Application

Day	Mosture Content (%)					
	A	B	C	D	E	F
1	24.7	24.3	36	31.8	28.5	26
2	31.9	27.9	36.3	35.3	37.3	36
3	30	34.9	26.6	29.1	37.1	31.8
4	34.9	32.6	36	30.9	30.4	35.8
5	34.4	24.5	24.6	28.1	30.4	30
6	33	20	37.4	25.8	35.8	35.1
7	20.7	27.3	29.2	26.1	31.6	34.4
8	27.9	30.4	38	35.7	28.9	36.6
9	26.5	33.1	35.4	35.7	33.4	32.3
10	33.6	33	0	0	34.3	35.8
11	30.1	33.3	29.4	31.1	36.4	35.7
12	30.5	30.7	38.2	0	36.5	32.4
13	29.7	349	37.2	26.8	32.2	32.1
14	27.9	34	31.7	28.8	37.7	37.4

Table 8. Respondent's Skin Moisture After Toner Application

Day	Mosture Content (%)					
	A	B	A	D	A	F
1	36.7	36.9	34.9	36.6	38.2	31.4
2	30.9	31	31.2	32	31.6	32.6
3	21.6	33.6	31.1	32.8	31.2	30
4	23.8	29.7	33.7	35.2	32.8	33.6
5	32.1	27.6	27.9	33.3	32.5	34.7
6	26.2	32.6	31.4	24.1	30.7	34.1
7	24.4	33.4	31.9	33.6	27.6	28.3
8	27.7	25.9	37.8	25.6	31.0	32.5
9	29.0	31.6	34.6	27.7	32.0	30.8
10	29.9	31.6	0.0	0.0	36.0	35.7
11	24.8	33.8	37.0	30.3	36.1	28.3
12	34.1	34.5	34.1	0.0	36.1	37.8
13	31.3	34.1	38.1	24.5	33.9	35.5
14	31.3	34.6	24.5	29.5	32.1	36.8

3.5. Protein Content Test

The protein content test determines the protein content for seven days of storage. Table 9 shows the results of the protein content test for the stirring time for one hour, and Table 10 shows the results of the protein content test for the stirring time for three hours.

Based on the tables above, it can be seen that the toner from rice-washed water contains protein. According to Sumardjo (2008), the protein content test was carried out to show the presence of compounds containing an acidic amide group together with other amide groups. This test gives a positive reaction indicated by the appearance of a red-violet or blue-violet color, as shown in Fig. 1 and Fig. 2.

Table 9. Protein content test for stirring for 1 hour

Day	(1:4)	(1:5)	(1:6)
1	Blue	Blue	Blue
2	Lighter blue	Slightly faded blue	Blue
3	Light blue	Light blue	Light blue
4	Blue	Clear blue	Blue
5	Blue	Blue Blue	Blue
6	Blue	Lighter blue	Blue
7	Blue	Blue	Blue

Table 10. Protein content test for stirring for 3 hour

Day	(1:4)	(1:5)	(1:6)
1	Blue	Blue	Blue
2	Blue	Blue	Blue
3	Light blue	Light blue	Light blue
4	Blue	Blue	Blue
5	Blue	Lighter blue	Blue
6	Blue	Blue	Blue
7	Blue	Blue	Blue

Figure 1. Protein content test results for 1 hour

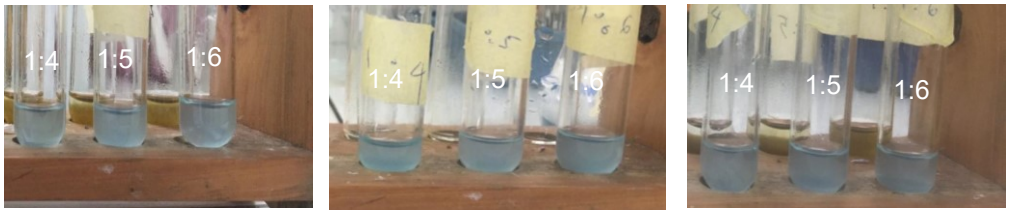

Figure 2. Protein content test results for 3 hour

3.6. Vitamin B6 Content Test

The Vitamin B6 test aims to determine the content of Vitamin B6 for seven days of storage. Table 11 shows the results of the Vitamin B6 content test for the stirring time for one hour, and Table 12 shows the results of the Vitamin B6 content test for the stirring time for three hours.

Based on Fig. 3, Fig. 4, Table 11, and Table 12, toner from rice-washed water contains Vitamin B6. According to Poedjiadi et al. (2009), vitamin B6 consists of three compounds: pyridoxine, pyridoxal, and pyridoxamine. These three vitamins are found in animals and plants, especially rice and wheat. It is characterized by a color change from orange to dark red. This proves that the toner from rice washing water contains vitamin B6.

Table 11. Test the content of Vitamin B6 for 1 hour of stirring

Day	(1:4)	(1:5)	(1:6)
1	Orange	Orange	Orange
2	Orange (with sediment)	Orange (with sediment)	Orange (with sediment)
3	Orange (with sediment)	Orange (with sediment)	Orange (with sediment)
4	Orange (with sediment)	Orange (with sediment)	Orange (with sediment)
5	Orange (with sediment)	Orange (with sediment)	Orange (with sediment)
6	Deep reddish orange (with sediment)	Deep reddish orange (with sediment)	Deep reddish orange (with sediment)
7	Orange (with a lot of sediments)	Orange (with a lot of sediments)	Slightly dark orange (with a lot of sediment)

Tabel 12. Test the content of Vitamin B6 for 3 hour of stirring

Day	(1:4)	(1:5)	(1:6)
1	Orange	Orange	Orange
2	Orange (with sediment)	Orange (with sediment)	Orange (with sediment)
3	Orange (with sediment)	Orange (with sediment)	Orange (with sediment)
4	Orange (with sediment)	Orange (with sediment)	Orange (with sediment)
5	Orange (with sediment)	Orange (with sediment)	Orange (with sediment)
6	Deep reddish orange (with sediment)	Deep reddish orange (with sediment)	Deep reddish orange (with sediment)
7	Orange (with a lot of sediments)	Orange (with a lot of sediments)	Orange (with a lot of sediments)

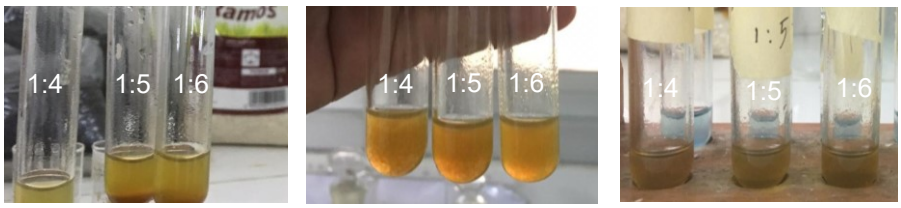

Figure 3. Test results for Vitamin B6 content for 1 hour of stirring

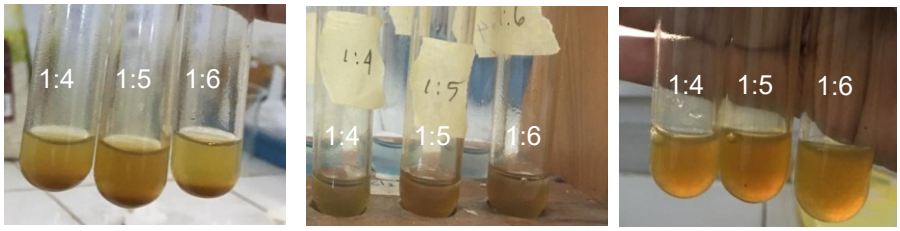

Figure 4. Test results for Vitamin B6 content for 3 hours of stirring

3.7. Fats and Oils Testing

The toner's oil and fat content test was carried out at the Regional Public Service Agency (BLUD) UPTD Health Laboratory of East Kalimantan Province. This test was carried out to determine the oil and fat content contained in toner from rice-washed water which was treated with variations in composition ratio and stirring time. Oil and fat test results are presented in Table 13. On the first day, with a time of 1 hour of stirring, the oil and fat content of 1.028 mg/L was produced, and the time of 3 hours of stirring was 1.049 mg/L. On the seventh day, with a

time of 1 hour of stirring, the oil and fat content of 2.042 mg/L was produced, and the time of 3 hours of stirring was 1.002 mg/L. It can be seen that the oil and fat content after seven days of storage increased. According to Wang (2019), this toner's oil and fat content is helpful as a moisturizer, especially for sensitive skin.

Table 13. Fats and oils testing

Day	t = 1 hour	t = 3 hour
1	1.028 mg/L	1.049 mg/L
7	2.042 mg/L	1.002mg/L

3.8. Manganese Content Test

Manganese testing was carried out at the Regional Public Service Agency (BLUD) UPTD Health Laboratory of East Kalimantan Province. This test aims to determine the manganese content in toner from rice-washed water treated with variations in composition ratio and stirring time. Table 14 shows the manganese content in the toner produced.

On the first day, with a time of 1 hour of stirring, the Manganese content was 0.3493 mg/L, and for 3 hours of stirring, it was 0.2524 mg/L. On the seventh day, with a time of 1 hour of stirring, the manganese content was 0.2524 mg/L, and at 3 hours of stirring, it was 0.2575 mg/L. It indicates that the toner produced contains Manganese. The manganese content in this toner is useful as an antioxidant and overcomes excess oil on facial skin (T. G. Polefka et al., 2012).

Table 14. Manganese content test

Day	t = 1 hour	t = 3 hour
1	0.3493 mg/L	0.2524 mg/L
7	0.2524 mg/L	0.2575 mg/L

4. CONCLUSIONS

Based on the tests that have been carried out, it can be concluded that the toner from rice-washed water is safe for facial skin because it has been proven to contain protein, manganese, vitamin B6, oils, and fats which are known to be good for facial skin. This toner has a color that is not too cloudy, not thick, odorless, and has a pH that is safe for all types of facial skin.

LIST OF REFERENCES

Almatsier, S. (2001). *Prinsip Dasar Ilmu Gizi*. Gramedia Pustaka Utama, Jakarta.

Astuti, P. (2013). *Pemanfaatan Limbah Air Leri Beras IR 64 Sebagai Bahan Baku Pembuatan Sirup Hasil Fermentasi Ragi Tempe dengan Penambahan Kelopak Bunga Rosella Sebagai*

Pewarna Alami. Universitas Muhammadiyah Surakarta, Surakarta.

Bening, C., Rahmatan, & H., Supriatno. (2016). Pengaruh Air Cucian Beras Merah Terhadap Pertumbuhan Vegetatif Tanaman Lada. *Jurnal Ilmiah Mahasiswa Pendidikan Biologi, 1*(1).

Burtis.C.A., E.R. Edward R., Ashwood, D.E., & Bruns. (2008). Tietz Fundamental of Clinical Chemistry and Molecular Diagnosis. *Elsevier, Indian Journal of Clinical Biochemistry*. USA.2012-2238. ISBN: 978-1-4160-6164-9.

Burtis, C., Ashwood, E., & Bruns, D. (2008). *Tietz Fundamentals of Clinical Chemistry.* 6th. Missouri : Saunders, 2008.

Hidayatullah, R. (2012). *Pemanfaatan Limbah Air Cucian Beras Sebagai Substrat Pembuatan Nata De Leri Dengan Penambahan Kadar Gula Pasir Dan Starter Berbeda*. Program Studi Biologi. Fakultas Sains dan Teknologii. Universitas Islam Negri Sunan Kalijaga Yogyakarta.

Ijiri D, Shogo N, Kenji T, Satoru I., & Akira O. (2013). *Effects of Feeding Dried Concentrated Rice-Washing Water On Growth Performance And Skeletal Muscle Lipid Peroxidation In Broiler Chickens*. Japan Poultry Science Association. *50*,370-74.

Juliano, C., Cossu, M., alamanni, MC., & Piu, L. (2005). Antioxidant activity of gamma-oryzanol: Mechanism of action and its effect on oxidative stability of pharmaceutical oils. *International Journal of Pharmaceutic, 299*(1-2), 146-154. https://doi.org/10.1016/j.ijpharm.2005.05.018

Michalun, Mr. Varinia, & Dinardo, Joseph C. (2014). *Milady Skincare and Ingredients Dictionary 4th Edition.* Cengage Learning, USA.

Moeksin, R. (2015). Pembuatan Bioetanol Dari Air Limbah Cucian Beras Menggunakan Metode Hidrolisis Enzimatik Dan Fermentasi. *Jurnal Teknik Kimia*, *21*(1), 14-22.

Muliyawan, D., & Suriana, N. (2013). *A-Z Tentang Kosmetik*. (pp: 14,16-17, 21-25, 141-142, 312). PT Elex Media Komputindo, Jakarta.

Poedjiadi, Anna, & Titin S. (2009). Dasar-Dasar Biokimia. UI press. Jakarta.

Rahmadsyah. (2015). *Pengaruh Air Leri, Air Teh Basi dan Air Kopi Sebagai Larutan Nutrisi Alternatif Terhadap Budidaya Bayam Merah Dengan Metode Nutrien Film Technique.* Skripsi Program Studi Biologi Universias Islam Negeri Sunan Kalijaga, Yogyakarta.

Samahah N., Qomariyah N., Dinda D.R, Eva R., & Rusly H. (2015). Pengolahan Air Leri Menjadi Sabun Pembersih Wajah Alami dan Ekonomis. *Prosiding Seminar Nasional Kimia FMIPA Universitas Negeri,* Surabaya.

Shad, Ray, dkk. (2010). *Analisis Kualitatif Vitamin.* Universitas Islam Negeri, Makassar.

Sugiharto. (1987). *Dasar –Dasar Pengelolaan Air Limbah*. UI press, Jakarta.

T. G. Polefka*, R. J. Bianchini†, & S. Shapiro. (2012). *Interaction of mineral salts with the skin*. *International Journal Of Cosmetic Science USA*, *34*, 416-423.

Thomas, H.W. (1985). *Bailey's Industrial Oil and Fat Product*, *Volume 3*. John Wiley & Sons, New York.

Wang, Y. (2019). *Applications of Rice Bran Oil.* (pp: 159-16).

Wardiah, Linda, & Rahmatan. (2014). Potensi Limbah Air Cucian Beras Sebagai pupuk Organik Cair pada Pertumbuhan Pakchoy (Brassica rapa L.). *Jurnal Biologi Edukasi Edisi 12*, *6*(1), 34-38.

JURNAL ILMIAH BERKALA SAINS DAN TERAPAN KIMIA

Jurnal Ilmiah Berkala: Sains dan Terapan Kimia
Vol. 16 No. 2, July 2022

Three Dimension Structure Modeling of The Superoxide Dismutase (SOD) of Rice (*Oryza sativa*) Using Fold Recognition Method Using Phyre^2 Web Server

Pemodelan Struktur Tiga Dimensi Enzim Superoxide Dismutase (SOD) Padi (*Oryza Sativa*) dengan Metode Fold Recognition Menggunakan Web Server Phyre^2

Noer Komari[1*], Khairil Anwar[1], Eko Suhartono[2]

[1]Chemistry Department, Faculty of Mathematics and Natural Sciences, Lambung Mangkurat University, Banjarmasin, Indonesia
[2]Biochemistry Division, Faculty of Medicine, Lambung Mangkurat University, Banjarmasin, Indonesia

*Email: nkomari@ulm.ac.id

ABSTRACT

Determining the 3D structure of proteins using laboratory instrumentation is time-consuming and expensive. The in silico method can be used as an alternative to predict the 3D structure of proteins, such as the fold recognition method. This study aims to create a 3D structural model of rice's (Oryza sativa) protein superoxide dismutase (SOD). The 3D structure modeling of the protein was carried out with the Phyre2 web server. The protein sequence was obtained from the UniProt KB database with the code A0A6F8FUX1. The results showed that the suitable template used to build the model was the template with the code c1unfX. The c1unfX template has a coverage value of 80%, 100% confidence, and i.d. of 51%. Validation of the model with the PROCHECK program showed that the most favored area on the Ramachandran Plot was 87.8%, and the disallowed area was 1.1%. The disallowed area, which is still below 15%, indicates that the three-dimensional structure model of the SOD protein built from the c1unfX template has good a value.

Keywords: fold recognition, Phyre^2, 3D protein structure, superoxide dismutase

ABSTRAK

Penentuan struktur 3D protein dilakukan menggunakan instrumentasi laboratorium yang memakan waktu dan biaya yang mahal. Metode in silico dapat digunakan sebagai alternatif untuk memprediksi struktur 3D protein, misalnya metode fold recognition. Penelitian ini bertujuan membuat model struktur 3D protein superoxide dismutase (SOD) padi (Oryza sativa). Pemodelan struktur 3D protein dilakukan dengan web server Phyre^2. Sekuen protein didapat dari database UniProt KB dengan kode A0A6F8FUX1. Hasil penelitian menunjukkan bahwa template yang digunakan untuk membangun model adalah template dengan kode c1unfX. Template c1unfX memiliki nilai coverage 80%, confidence 100% dan i.d. 51%. Hasil validasi model menggunakan program PROCHECK menunjukkan daerah most favored pada Ramachandran Plot sebesar 87,8% dan daerah yang disallowed sebesar 1,1%. Daerah disallowed yang masih dibawah 15% menunjukkan model struktur tiga dimensi protein superoxide dismuatse yang dibangun dari template c1unfX bernilai baik.

Kata Kunci: fold recognition, Phyre^2, struktur 3D protein, superoksida dismutase

Received: December 9, 2021; **Accepted**: June 29, 2022 **Available online**: July 31, 2022

1. INTRODUCTION

The 3D structure of the protein was determined using X-ray diffraction instrumentation, Nuclear Magnetic Resonance (NMR), and electron microscopy (Westbrook et al., 2003). This method is time-consuming, expensive, and cannot be applied to some proteins that are difficult to crystallize (Xu et al., 2016). It causes the protein structures available from experiments to be incomparable or significantly smaller than the number of successfully sequenced protein sequences (Schwede, 2013). As of April 2021, the number of protein 3D structures that have been experimentally obtained and stored in the Protein Data Bank (RSCB PDB) is 176,247, while the number of protein sequences that have been mapped and stored in the UniProt KnowledgeBase (UniProt KB) is 546,227. It implies that there are still many other important and essential proteins whose 3D structures are not yet known (Saudale, 2020).

The 3D structure of proteins can be determined by the in-silico method based on the sequence of amino acids. There are three methods: homology/comparative, fold recognition, and ab initio. The homology method is easier and faster than the fold recognition and ab initio methods (Zaki & Brystoff, 2008; Komari et al., 2020). However, the homology method cannot produce an accurate model if the sequence identity between the target and template is low (sequence identity <30%) (Khor et al., 2015). Fold recognition is based on identifying the same fold fragment (fold recognition) from a protein database with evolutionarily related relationships (Saudale, 2020). Modeling with the fold recognition method can be done using the Phyre^2 web server. Phyre^2 is a web server for 3D protein structure prediction where targets are not only based on evolutionarily close but also remote homologous proteins (Kelley et al., 2015).

This study aimed to determine the 3D structure of rice's superoxide dismutase (SOD) protein. SOD is an antioxidant enzyme that plays a role in the metabolism of neutralizing free radicals in the form of Reactivity Oxygen Species (ROS) (Ashraf & Foolad, 2007). SOD is also often the target of research on rice plants (Widowati et al., 2005; Lee et al., 2013). Research to determine the 3D structure of the SOD enzyme has never been carried out, as evidenced by the unavailability of a 3D structure database of the SOD enzyme in the Protein Data Bank (RCSB PDB). Determination of the 3D structure of the SOD enzyme can be carried out in silico using the Phyre2 web server.

2. MATERIALS AND METHODS

2.1. Materials

The materials used were Rice SOD target protein sequences (*Oryza sativa*). The tools used were web server for protein which is UniProt KB database (https://www.uniprot.org/), the ProtParam web server (https://web.expasy.org/protparam/), and the Phyre^2 web server.

2.2. Target Protein Sequence

Rice SOD target protein sequences (*Oryza sativa*) were obtained from the UniProt KB database (https://www.uniprot.org/). The protein sequences of the search results were evaluated for their 3D structure in the Protein Data Bank (RSCB PDB). Selected protein sequences were saved in FASTA format.

2.3. Target Protein Analysis

Target protein analysis was performed on the ProtParam web server (https://web.expasy.org/protparam/). The analysis was carried out to determine the physical and chemical properties of the target protein.

2.4. Template Identification and Protein Modeling

Template identification and modeling were performed on the Phyre^2 web server (http://www.sbg.bio.ic.ac.uk/~phyre2/html/page.cgi?id=index). The target protein sequences in FASTA format were submitted to the Phyre^2 web server for template identification and modeling. The resulting template will be selected based on the 100% confidence value and the i.d. value above 20%. The best template will be selected as the protein model.

2.5. Model Evaluation

The model evaluation was carried out on the Phyre^2 web server after the template

identification and protein modeling processes were completed (http://www.sbg.bio.ic.ac.uk/phyre2/phyre2_output/ca601671cde736c0/summary.html) The model with the highest parameter value was selected and evaluated. The evaluation parameters of the model include the Quality model and the Function model. Quality model parameters were ProQ2 quality assessment, clashes, rotamers, Ramachandran analysis, alignment confidence, and disorder. Function model parameters, namely conservation, pocket detection, and mutational sensitivity.

2.6. Model Validation

Validation of the model used the PROCHECK program on the SAVESv6.0 web server (https://saves.mbi.ucla.edu/). The model file selected on the Phyre2 web server was downloaded in .pdb format and submitted to the SAVESv6.0 web server. Parameters of protein model validation included Ramachandran plot, chi1-chi2 plot, side-chain params, and residue properties.

3. RESULTS AND DISCUSSION

3.1. Selection of Target Protein Sequence

The protein sequence of rice SOD (*Oryza sativa*) on the UniProt KB web server (https://www.uniprot.org/) was searched by entering the keyword "SOD" and by selecting the organism in the other organism column "*Oryza sativa*." A total of eight different types of protein were obtained. Data accessed on April 2021 is depicted in Table 1.

The target protein sequence was selected from a protein that did not yet have a 3D structure, namely protein SOD (Fe-SOD) with UniProt code A0A6F8FUX1. The FASTA format of the SOD protein sequence is presented in Fig. 1.

Sequence data was used to create a 3D protein structure model with the Phyre^2 web server. The protein sequences were copied from the UniProt web server to the Phyre2 web server using the FASTA format, as shown in Fig. 2.

Table 1. SOD Oryza sativa protein on UniProt KB web server

Code	Protein name	Length of amino acid
A0A6F8FQT0	Superoxide dismutase [Cu-Zn]	211
A0A6F8FUX1	Superoxide dismutase	255
A0A6F8F8N3	Superoxide dismutase	231
Q43803	Superoxide dismutase	231
Q01JW6	OSIGBa0147H17.7 protein	316
Q7M238	Superoxide dismutase (Cu-Zn) IV, cy...	57
Q7M240	Superoxide dismutase (Cu-Zn) I, chl...	55
Q7M237	Superoxide dismutase (Cu-Zn) III, c...	48

```
>tr|A0A6F8FUX1|A0A6F8FUX1_ORYSA Superoxide dismutase OS=Oryza sativa OX=4530 GN=Fe-SOD PE=2 SV=1
MAAFASALRVLPSPPAAVPRRLRSREQRQGCRSRRYSKVVAYYALTTPPYKLDALEPYIS
KRTVELHWGKHQQDYVDSLNKQLATSMFYGYTLEELIKEAYNNGNPLPEYNNAAQVWNHH
FFWESMQPEGGGSPGRGVLQQIEKDFGSFTNFREEFIRSALSLLGSGWVWLVLKRKERKF
SVVHTQNAISPLALGDIPLINLDLWEHAYYLDYKDDRRMYVTNFIDHLVSWDTVTLRMMR
AEAFVNLGEPNIPVA
```

Figure 1. SOD Protein Sequences in FASTA format

3.2. Analysis of Protein Target

Protein analysis was carried out to determine the physical and chemical properties of the target protein using the ProtParam web server tool (https://web.expasy.org/protparam/). The physical and chemical properties of the target proteins are presented in Table 2.

Table 2 provides information on the number of amino acids in the target protein, namely 255, molecular weight of 29475.58, and chemical formula of C1338H2041N367O374S7. Its isoelectric point (pI) was 8.84. The pI is the pH value at which the total charge of the positively and negatively charged groups reaches stability (so that the total charge of the amino acid is zero). If the pH is above the isoelectric point, the protein is negatively charged, whereas if it is below the isoelectric point, the protein is positively charged (Thenawidjaja et al., 2017). The estimated half-life of the target protein in mammalian reticulocytes in vitro is 30 hours, yeast in vivo > 20 hours, and Escherichia coli in vivo > 10 hours. The half-life predicts the time required for half of the total protein in the cell to disappear after its synthesis in the cell (Walker, 2002).

The instability index (II) on the target protein was 52.32. The instability index is a protein measure that estimates a protein's stability. A protein whose instability index is less than 40 is predicted to be stable; if it is greater, it is likely to be unstable (Guruprasad et al., 1990). These results indicate that the target protein is unstable. It will affect the process of forming the target protein's 3D structure. The target protein aliphatic index was 82.24. The aliphatic index is the relative volume occupied by amino acids such as alanine, valine, isoleucine, and leucine which have aliphatic side chains in their structure and are considered factors that can increase protein thermostability (Walker, 2002).

GRAVY (grand average of hydropathicity) is a parameter that determines the hydrophobic nature of a protein. The more positive the hydropathic index value of the amino acid, the more hydrophobic the amino acid is. On the other hand, the more negative the hydropathic index value of the amino acid, the more hydrophilic the amino acid is (Nelson & Cox, 2007). The value of the grand average of hydropathicity (GRAVY) of the target protein was -0.413. This value indicates that the target protein is hydrophilic. It dramatically affects an amino acid's folding process in forming its tertiary structure. Generally, proteins rich in hydrophilic amino acid residues are difficult to fold into a good tertiary (3D) structure. The ten highest amino acid compositions of the target proteins are presented in Table 3. The highest amino acid composition is leucine (10.6%), alanine (7.8%), and arginine (7.5%).

Table 2. Physical and chemical properties of the target protein

Physical and chemical properties	Results
Chemical formula	$C_{1338}H_{2041}N_{367}O_{374}S_7$
Number of amino acids	255
Molecular weight	29475.58
Isoelectric point (pI)	8.84
Half-life	30 hours in mammalian reticulocytes (in vitro) >20 hours on yeast (in vivo) >10 hours on Escherichia coli (in vivo)
Instability index (II)	52.32
Aliphatic index	82.24
Grand average of hydropathicity (GRAVY)	-0.413

Table 3. The composition of the ten highest amino acids of rice SOD protein

Amino acid	One letter symbol	Three letter symbols	Amino acid composition	Percentage
Leucine	L	Leu	27	10.6%
Alanine	A	Ala	20	7.8%
Arginine	R	Arg	19	7.5%
Serine	S	Ser	17	6.7%
Valine	V	Val	17	6.7%
Asam glutamate	E	Glu	16	6.3%
Proline	P	Pro	15	5.9%
Glycine	G	Gly	14	5.5%
Tyrosine	Y	Tyr	14	5.5%
Aspargine	N	Asn	13	5.1%

3.3. Template Identification and Protein Modeling

There were 104 templates generated on the Phyre2 web server. The templates showed different confidence values, coverage values, and i.d. values. Templates 1-20 had a protein model, while the rest were not modeled successfully. Information on the 20 templates that have been successfully modeled is presented in Table 3.

The chosen template was the code c1unfX which had a coverage value of 80%, a confidence value of 100%, and an i.d. value of 51%. The model generated by the c1unfX template is visualized in Fig. 2.

The protein model of the SOD enzyme in rice with the c1unfX template comprised of 10 α-helix, 5 β-sheets, and 17 coils. The longest α-helix is shown in number (a1) with 24 amino acids, while the shortest α-helix is shown in (a8) and (a9) with three amino acids each. The longest β-sheet is shown in (b1) and (b2) with eight amino acids each, while the shortest β-sheet has 2 -sheets with one amino acid number each. The longest coil is shown in number (c2) with 23 amino acids, while the shortest has six coils with one amino acid number each.

The c1unfX template information can be found through RCSB PDB (https://www.rcsb.org/) by entering the keyword "1UNF" in the search field. The SOD enzyme in the c1unfX template is a FeSOD enzyme with Fe as a cofactor. This enzyme belongs to the type of oxidoreductase enzyme. The FeSOD enzyme is found in the organism *Vigna unguiculata*, also known as cowpea. The 3D structure of the FeSOD enzyme was discovered using an X-ray diffraction instrument with a resolution of 1.97. The SOD enzyme information on the c1unfX template has been published.

3.4. Model Evaluation

Model evaluation was carried out on the Phyre2 web server (http://www.sbg.bio.ic.ac.uk/phyre2/phyre2_output/ca601671cde736c0/summary.html). The model with the selected parameters was the c1unfX template. The evaluation of the model was carried out with two parameters: quality and function. The quality model showed a value of 7, namely ProQ2 quality assessment, Clashes, Rotamers, Ramachandran analysis, Alignment confidence, and Disorder. The function model had three parameters: Conservation, Pocket detection, and Mutational sensitivity.

3.5. Quality Model

ProQ2 quality assessment showed a value of 0 to 1 (red to blue), where a value of 0 (red) indicates a good value amino acid. The ProQ2 score model shows that the value closest to 1 is 0.396 for amino acids 38 (K), and the value closest to 0 is -0.050 for amino acids 67 (H), 71 (H), 72 (Q), 122 (F), 167-171 (G, W, V, W, L), 199 (L), 202 (L), 204 (L), 205 (W), 230 (S), and 231 (W). Fig. 3 shows that the model is dominated by red, orange, and green colors in the -helix, -sheet, and coil regions, so the model has good value (Ray et al., 2012).

Table 3. Information on 20 successfully modeled templates

No.	Template code	Coverage value (%)	Confidence value (%)	i.d. value (%)
1.	c6bejA	77%	100%	40%
2.	c1xreB	78%	100%	40%
3.	c1gv3B	77%	100%	36%
4.	c1my6A	77%	100%	43%
5.	c3js4C	78%	100%	43%
6.	c6jovC	76%	100%	43%
7.	c4yioB	78%	100%	38%
8.	**c1unfX**	**80%**	**100%**	**51%**
9.	c1mngA	78%	100%	32%
10.	c1gn4B	79%	100%	32%
11.	c3ceiA	78%	100%	33%
12.	c5a9gB	80%	100%	32%
13.	c1y67D	78%	100%	41%
14.	c1ma1E	78%	100%	35%
15.	c1dt0A	79%	100%	43%
16.	c4f2nL	78%	100%	34%
17.	c2rcvA	77%	100%	39%
18.	c5n57B	78%	100%	36%
19.	c4h3eB	78%	100%	32%
20.	c4ffkA	80%	100%	33%

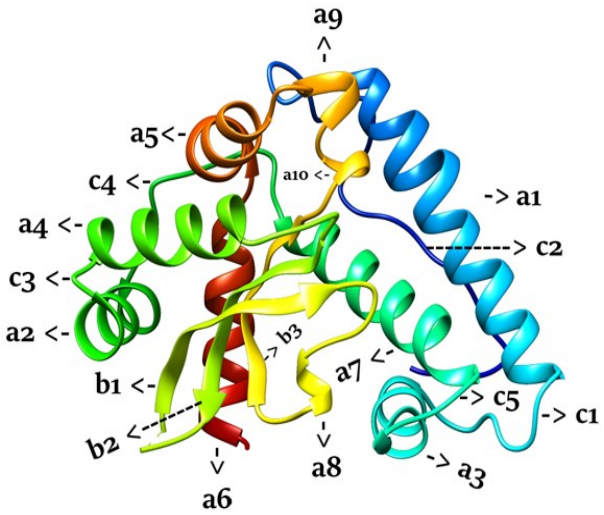

Figure 2. Model visualization with c1unfX template

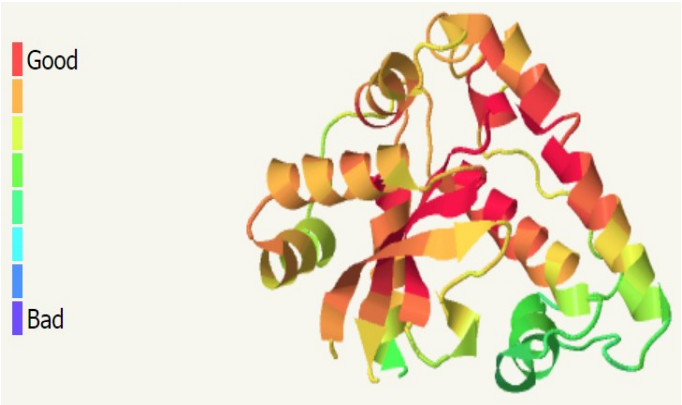

Figure 3. Model based on ProQ2 quality assessment

Clashes show residual clashes with low to high values (blue to red). The clashes model color indicator shows that there are seven amino acids whose color is close to red, namely amino acids 38 (K), 40 (V), 72 (Q), 83 (L), 160 (A), 169 (V) and 204 (L). The color towards purple indicates a residue that has good clashes value (Good). Fig. 4. shows a good value model because it is dominated by purple, light blue, and green in the α-helix, β-sheet, and coil regions.

Rotamers show the number of side chains that are not ideally modeled. From 38-244 residues, only one residue, 120 (H), is problematic. Fig. 5. shows the indicator in red where the residue is not ideally modeled (Bad). The blue indicator shows the ideally modeled residue area (Good). The model is of good value because it is dominated by blue in the α-helix, β-sheet, and coil regions.

The Ramachandran analysis in Fig. 6 shows the residues in the favored (favorable, blue), allowed (allowed, green), and not allowed (disallowed, red) areas. There are 39 allowed residues, namely (V), 49 (P), 70 (K), 85 (T), 103 (N), 136 (R), 187 (N), 194 (L), 195 (G) and 214 (K). In addition, there were 41 disallowed residues, namely (A), 88 (F), 105 (N), and 196 (D). The model is considered a good value because it is dominated by blue in the α-helix region, while green and red are only in some parts of the coil.

Alignment confidence shows the results of the alignment between the template and the target protein sequence, with a value of 0 to 1 (good to poor). Alignment is not good at residues 84 (A) and 85 (T), with a value of 0.54. The color indicator towards red indicates a good alignment confidence value (Good), and the color toward blue is not good (Bad). Fig. 7 shows that the model is dominated by red, yellow, and green colors on the residues in the α-helix and β-sheet regions. Therefore the model is stated to be of good value.

Prediction of disorder is vital to knowing residues that hinder the success of the crystallization of a protein. Values close to one indicate disorder, and values close to 0 indicate order. The disorder areas are found in residues 1-42, 128-135, and 249-255. The color indicator toward red is the residual disorder, while the indicator towards the blue is the order residue. Fig. 8 shows a good value model because the α-helix and β -sheet regions are dominated by blue, light blue, and green, while the areas on the coil are dominated by green and light blue.

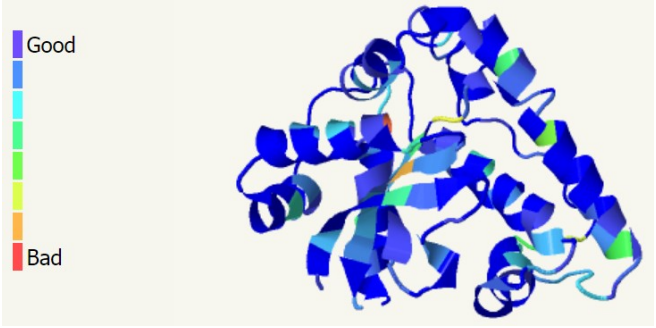

Figure 4. Model based on clashes

Figure 5. Model based on rotamers

Figure 6. Model based on Ramachandran analysis

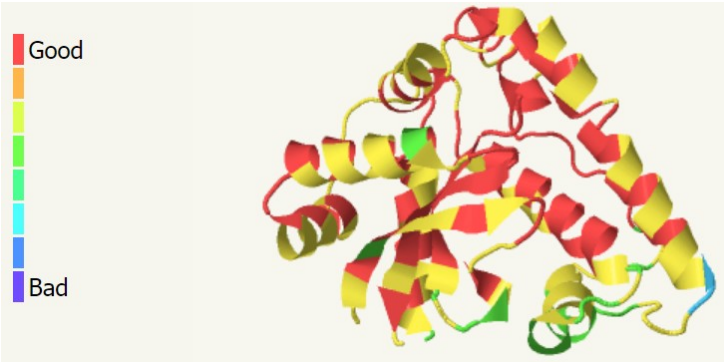

Figure 7. Model based on alignment confidence

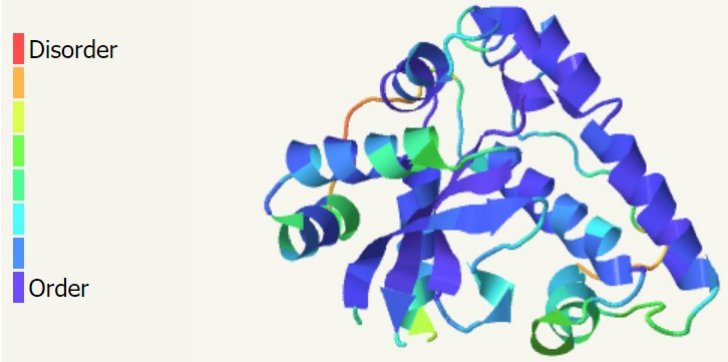

Figure 8. Model based on disorder

3.6. Model Function

Conservation provides information on the presence of functional residues. The color indicator towards red indicates a residue with higher conservation (High). The indicator color towards blue has a lower conservation value (Low). Fig. 9. shows a model dominated by purple, light blue, and green residues in the -helix, -sheet, and coil regions. The red color is found in the residue in one of the -sheets, namely residue 168 (W), and the orange color in one of the α-helix, β-sheet, and coil, namely residues 119 (H), 167 (G), 206 (E), 207 (H) and 209 (Y).

Pocket detection is used to predict amino acids at the active site. The largest pocket is an active site area. The largest pockets are marked in red, as shown in Fig. 10. The residues at the active site are 141 (Q), 144 (K), 145 (D), 173 (L), 175 (R), 176 (K), 178 (R) , 179 (K), 180 (F), 199 (L), 238 (M), 241 (A), and 242 (E).

Mutational sensitivity predicts the occurrence of missense mutations of specific amino acids in the target protein. The

mutation sensitivity score is from 0 to 9, where 0 indicates a low residual mutation value. The color indicator towards red indicates the mutation sensitivity value is getting higher (High). The color indicator towards blue has a lower mutation sensitivity value (Low). Fig. 11 shows the highest mutation value at residue 198 (P), which is indicated by the orange color on the β-sheet. The yellow color indicates the second-highest mutation value in several α-helix, β-sheet, and coils. The model is still dominated by purple, light blue, and green residues with low mutation values.

3.7. Model Validation

Model validation was carried out using the PROCHECK program on the SAVESv6.0 web server (https://saves.mbi.ucla.edu/). The validation results are presented in Table 4 and Fig. 12.

The quality of the protein structure depends on the number of non-glycine residues in the outlier/disallowed regions. The protein structure quality is of good value if the non-glycine residue in the outlier area is <15%, and the smaller it is, the better the protein structure quality (Lovell et al., 2003). Table 4 shows the number of amino acid residues in quadrant I most favored regions (87.8%), quadrant II additional allowed regions (8.9%), quadrant III generously allowed regions (2.2%), and quadrant IV disallowed regions (1.1%). It indicates that the structure of the model has good quality because it has non-glycine residues in the disallowed regions, which are below 15%, namely 1.1%. The quality and stability of the model are indicated by the presence of amino acid residues in the most favored regions, which are larger than the amino acid residues in the disallowed regions (Ho & Brasseur, 2005). Ramachandran plot is an indicator of the intrinsic quality of 3D structure (Petsko & Ringe, 2004).

Table 4 shows that in the All Ramachandran plot, there are ten labeled residues from 201 residues. Labeled is indicated by a red dot with a number above it. The red dot with the number indicates that the residue is in the unfavorable area of the graph. Parentheses containing a number next to the name of the amino acid indicate the number of amino acids present on the graph. The All Ramachandran plot in Fig. 12 shows which residues were labeled out of the ten labeled residues. The ten residues are alanine, aspartic acid, glutamic acid, leucine, lysine, phenylalanine, proline, threonine, and two amino acids valine.

Table 4 shows the results of chi1-chi2 plots that of the 137 residues, there are two labeled residues: histidine and tyrosine. In the side-chain parameters plot, there is one graph with an Inside description, four with BETTER description, and 0 indicating worse. Residual properties plots show how the geometric properties of the protein vary along the sequence of the target protein. This plot provides a visualization of which areas have poor and more normal geometry. Table 6 shows the results that there is a max. deviation of 10.6.

Table 4 shows the Overall G-factor value in the protein model, which is 0.01. The G-factor is a value that measures the stereochemistry of a protein model. A low G-factor value indicates that the protein model has a low conformational probability. The ideal G-factor value is above -0.5. A G-factor value below -1.0 is a non-ideal value (Ahmed et al., 2009). Based on Table 6, the overall G-factor value in the resulting protein model is ideal.

The RMS (Root Mean Square) distance is the distance from the planarity for the various planar groups in the structure. The dotted lines on the graph show different ideal values for aromatic rings (Phe, Tyr, Trp, His) and planar groups (Arg, Asn, Asp, Gln, Glu). The default values are 0.03Å and 0.02Å, respectively. Histogram bars crossing the dotted line are shown as highlighted. Table 4 shows that 0.0% highlighted indicates nothing is highlighted, and 100% within limits shows histogram bars do not cross the dotted line or are still within limits.

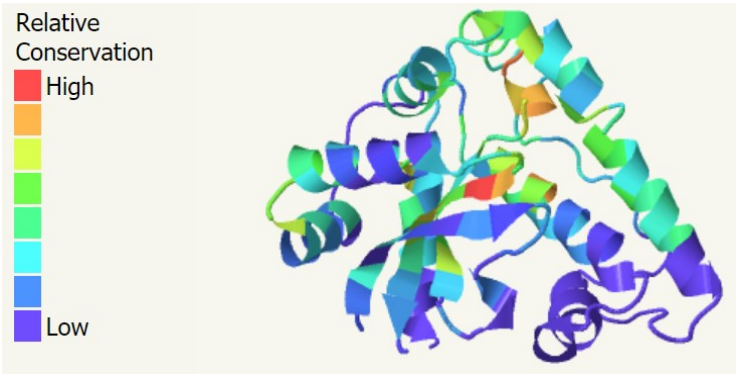

Figure 9. Model based on conservation

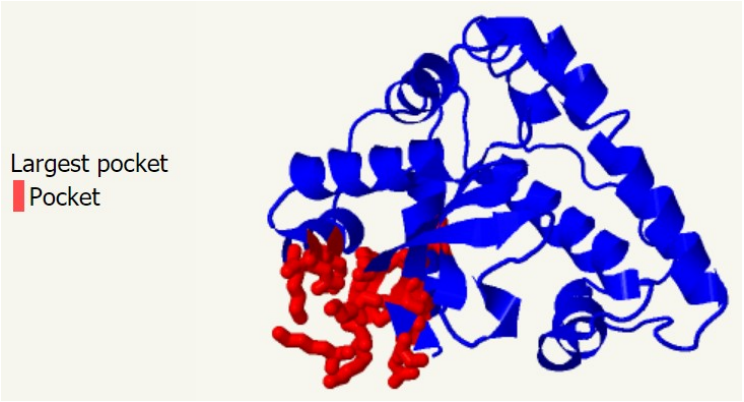

Figure 10. Model based on Pocket detection

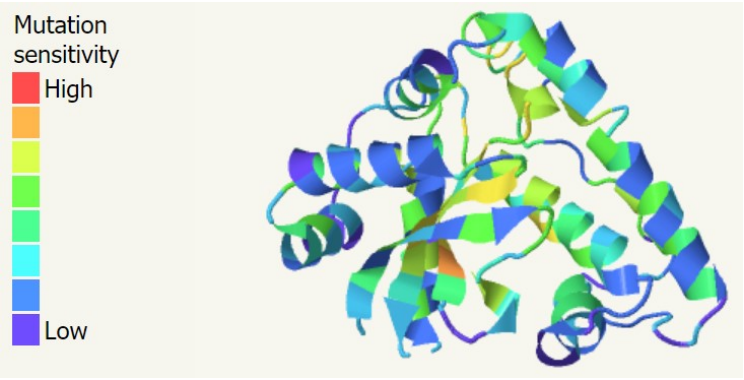

Figure 11. Model based on mutational sensitivity

Table 4. Model validation results using PROCHECK

Parameter	Results
Ramchandran plot	The residue is in the most favored area of 87.8% The residue is in an additional allowed area of 8.9% The residue is in the area that is generously allowed by 2.2% The residue is in the disallowed area of 1.1%
All Ramachandrans	10 labelled residues (out of 201 residues)
Chi1-chi2 plots	2 labelled residues (out of 137 residues)
Side-chain params	4 better, 1 inside, 0 worse
Residue properties	Max. deviation: 10.6
G-factor	Overall: 0.01
Planar groups	100% within limits, 0% highlighted

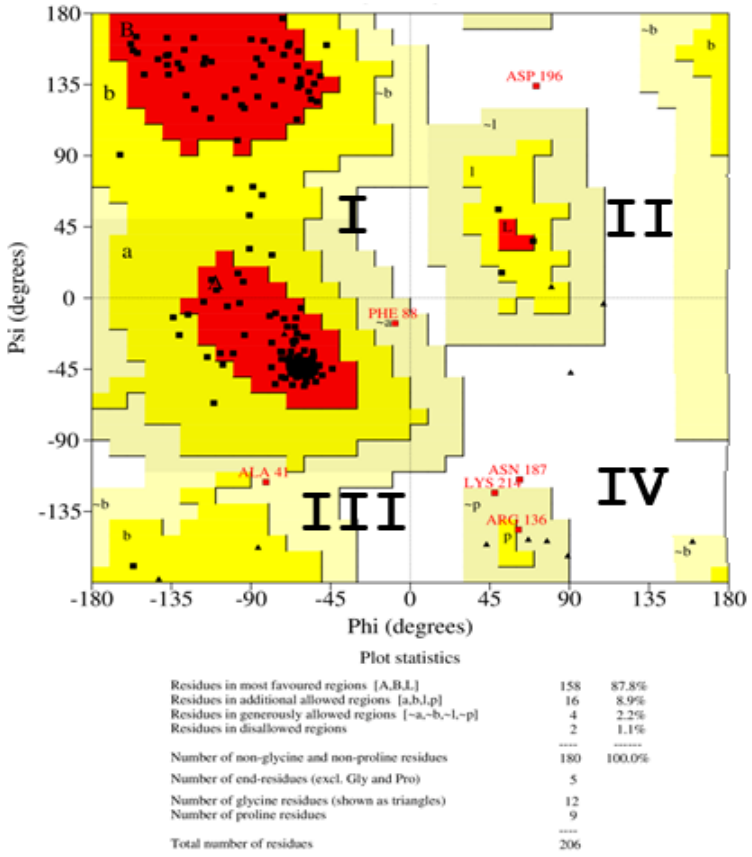

Figure 12. Ramachandran plot of PROCHECK model validation results

4. CONCLUSION

Modeling the 3D structure of the SOD enzyme using the Phyre2 web server produces a model based on the c1unfX template with a coverage value of 80%, a confidence value of 100%, and an i.d. value of 51%. The model's evaluation results include good values based on quality with ProQ2 quality assessment, clashes, rotamers, Ramachandran analysis, alignment confidence, and disorder dominated by good indicators (Good). Evaluation of the model based on function shows that each residue's conservation value and mutational sensitivity value are relatively low. The model validation results on the Ramachandran plot show that the residue in the most favored area was 87.8%, the additional allowed area was 8.9%, the generously allowed area was 2.2%, and the disallowed area was 1.1%. The resulting model is of good value because the residue in the disallowed area is still below 15% and smaller than the most favored area of 87.8%.

ACKNOWLEDGEMENT

Acknowledgments are conveyed to Mr. Sunardi, the head of the chemistry study program, FMIPA ULM, who has facilitated the use of the bioinformatics laboratory for this research.

LIST OF REFERENCES

Ahmed, A., Koller, A., & Gohlke, H. (2009). Multi-scale modelling of macromolecular conformational changes. In *Chemistry Central Journal,* 3(1). https://doi.org/10.1186/1752-153X-3-S1-P53

Ashraf, M., & Foolad, M. R. (2007). Roles of glycine betaine and proline in improving plant abiotic stress resistance. *Environmental and Experimental Botany*, *59*(2), 206–216. https://doi.org/10.1016/j.envexpbot.2005.12.006

Guruprasad, K., Reddy, B. V. B., & Pandit, M. W. (1990). Correlation between stability of a protein and its dipeptide composition: A novel approach for predicting in vivo stability of a protein from its primary sequence. *Protein Engineering, Design and Selection*. https://doi.org/10.1093/protein/4.2.155

Haryanto, T., & Budiman, B. (2015). Penggunaan Fitur Kimia Fisik dan Posisi Atom untuk Prediksi Struktur Sekunder Protein. *Jurnal Edukasi Dan Penelitian Informatika (JEPIN)*, *1*(2). https://doi.org/10.26418/jp.v1i2.11919

Ho, B. K., & Brasseur, R. (2005). The Ramachandran plots of glycine and pre-proline. *BMC Structural Biology*, *5*, 1–11. https://doi.org/10.1186/1472-6807-5-14

Kelley, L. A., Mezulis, S., Yates, C. M., Wass, M. N., & Sternberg, M. J. E. (2015). The Phyre2 web portal for protein modeling, prediction and analysis. *Nature Protocols*, *10*(6), 845–858. https://doi.org/10.1038/nprot.2015.053

Khor, B. Y., Tye, G. J., Lim, T. S., & Choong, Y. S. (2015). General overview on structure prediction of twilight-zone proteins. *Theoretical Biology and Medical Modelling*, *12*(1). https://doi.org/10.1186/s12976-015-0014-1

Komari, N., Hadi, S., & Suhartono, E. (2020). *Pemodelan Protein dengan Homology Modeling menggunakan SWISS-MODEL Protein Modeling with Homology Modeling using SWISS-MODEL*, *2*(2), 65–70.

Lee, M. H., Cho, E. J., Wi, S. G., Bae, H., Kim, J. E., Cho, J. Y., Lee, S., Kim, J. H., & Chung, B. Y. (2013). Divergences in morphological changes and antioxidant responses in salt-tolerant and salt-sensitive rice seedlings after salt stress. *Plant Physiology and Biochemistry*, *70*. https://doi.org/10.1016/j.plaphy.2013.05.047

Lovell, S. C., Davis, I. W., Iii, W. B. A., de Bakker, P. I. W., Word, J. M., Prisant, M. G., Richardson, J. S., & Richardson, D. C. (2003). Structure validation by Calpha geometry: Phi,psi and Cbeta deviation. *Proteins*, *50*(3).

Petsko, G. a, & Ringe, D. (2004). From Sequence to Function : Case Studies in Structural and Functional Genomics. In *Protein Structure and Function*.

Ray, A., Lindahl, E., & Wallner, B. (2012). Improved model quality assessment using ProQ2. *BMC Bioinformatics*. https://doi.org/10.1186/1471-2105-13-224

Rosmawati, T. (2013). Lama perebusan terhadap kandungan protein pada kerang darah (Anadara granosa). *Jurnal Biology Science & Education*, *2*(2), 103–109.

Saudale, F. Z. (2020). Biokimia di Era Big Data Genomik: Tantangan, Aplikasi dan Peluang Inovasi. *Chem. Notes*, *1*(2), 21–43.

Schwede, T. (2013). Protein modeling: What happened to the “protein structure gap”?. In *Structure*. https://doi.org/10.1016/j.str.2013.08.007

Walker, J. M. (2002). Protein Protocols Handbook, The. In *Protein Protocols Handbook, The*. https://doi.org/10.1385/1592591698

Westbrook, J., Feng, Z., Chen, L., Yang, H., & Berman, H. M. (2003). The Protein Data Bank and structural genomics. *Nucleic Acids Research*, *31*(1), 489–491. https://doi.org/10.1093/nar/gkg068

Widowati, W., Safitri, R., Rumumpuk, R., & Siahaan, M. (2005). Penapisan Aktivitas Superoksida Dismutase pada Berbagai Tanaman. *JKM*, *5*(1).

JURNAL ILMIAH BERKALA SAINS DAN TERAPAN KIMIA

Jurnal Ilmiah Berkala: Sains dan Terapan Kimia
Vol. 16 No. 2, July 2022

Development of QSAR Model of Caffeic Acid Phenethyl Ester as Anti-Cancer HT-29

Pengembangan Model HKSA Senyawa *Caffeic Acid Phenethyl Ester* (CAPE) sebagai Antikanker HT-29

Uripto Trisno Santoso[1,2,*], Samsul Hadi[3], Devi Eka Pratama[3]

[1]Computational Chemistry Laboratory, Laboratory of Mathematics and Natural Sciences, Lambung Mangkurat University, Jl. A. Yani KM. 36 Banjarbaru 70714, Kalimantan Selatan
[2]Chemistry Department, Faculty of Mathematics and Natural Sciences, Lambung Mangkurat University, Jl. A. Yani KM. 36 Banjarbaru 70714, Kalimantan Selatan
[3]Pharmacy Department, Faculty of Mathematics and Natural Sciences, Lambung Mangkurat University, Jl. A. Yani KM. 36 Banjarbaru 70714, Kalimantan Selatan

*Email: utsantoso@ulm.ac.id

ABSTRACT

Caffeic Acid Phenethyl Ester (CAPE) compounds are potentially colorectal anticancer drugs. HKSA (Quantitative Structure-Activity Relationship) research on the CAPE compound class has been carried out, but the model in the previous study did not meet the goodness of fit criteria. The development of the CAPE compound HKSA model as a colorectal anticancer was carried out to obtain a model that meets the goodness of fit criteria and is valid. Eighteen CAPE compounds were used to build the HKSA model using the Multiple Linear Regression (MLR) technique. The descriptor selection was carried out using the backward elimination method and the validation test using the internal leave one out (LOO) cross-validation. The results showed that the HKSA model with four descriptors, namely MDEC22, MDEC23, JGI1, and molecular weight (BM), met the goodness of fit and Q^2(LOO) criteria. The development of the HKSA model by adding the LogP descriptor resulted in the HKSA 5 descriptor model with higher goodness of fit level than the HKSA model without the LogP descriptor. Both of these HKSA models have the potential to be used as predictors in the development of a new class of CAPE compounds as anticancer agents against HT-29 cells.

Keywords: Caffeic Acid Phenethyl Ester (CAPE), Quantitative Structure-Activity Relationship (QSAR), Multiple Linear Regression, Internal Validation.

ABSTRAK

Senyawa Caffeic Acid Phenethyl Ester (CAPE) memiliki potensi sebagai obat antikanker kolorektal. Penelitan HKSA (Hubungan Kuantitatif Struktur-Aktivitas) tentang golongan senyawa CAPE telah dilakukan tetapi model pada penelitian sebelumnya tidak memenuhi kriteria goodness of fit. Pengembangan model HKSA senyawa CAPE sebagai antikanker kolorektal dilakukan untuk mendapatkan model yang memenuhi kriteria goodness of fit dan bersifat valid. Sebanyak 18 senyawa CAPE digunakan untuk membangun model HKSA dengan menggunakan teknik Regresi Linier Berganda (RLB). Pemilihan deskriptor dilakukan dengan metode eliminasi backward dan uji validasinya menggunakan validasi silang internal leave one out (LOO). Hasil penelitian menunjukkan bahwa model HKSA dengan 4 deskriptor, yaitu MDEC22, MDEC23, JGI1, dan berat molekul (BM) memenuhi kriteria goodness of fit dan Q^2(LOO). Pengembangan model HKSA dengan menambahkan deskriptor LogP menghasilkan model HKSA 5 deskriptor dengan tingkat goodness of fit yang lebih baik daripada model HKSA tanpa deskriptor LogP. Kedua model HKSA ini berpotensi untuk dijadikan prediktor dalam pengembangan golongan senyawa CAPE yang baru sebagai antikanker terhadap sel HT-29.

Kata Kunci: Caffeic Acid Phenethyl Ester (CAPE), Hubungan Kuantitatif Struktur-Aktivitas (HKSA), Regresi Linier Ganda, Validasi Internal.

Received: January 27, 2022; **Accepted**: June 29, 2022: **Available online**: July 31, 2022

1. INTRODUCTION

Cancer is the second leading cause of death in the world. The number of new cases in 2020 shows the three most extensive cancers, namely lung cancer, breast cancer, and colon cancer. Asia has notable cases, 49.3% of the total 19,292,789 people. Asia's cancer mortality rate in 2020 was 58.3% of the total 9,958,133 people (IARC, 2020). Colon cancer is the third largest cancer in the world and the fourth most recent case in Indonesia. Data from IARC (2020) states that there are 10% of the latest cases worldwide and 8.6% of the newest cases in Indonesia. The risk of developing colorectal cancer, according to the American Cancer Society (2020), is 1 in 23 (4.3%) in men and 1 in 25 (4.0%) in women.

Radiotherapy and chemotherapy are frequently employed cancer treatments. Radiation therapy is generally remarkably effective, but there is a risk of damaging normal cells and tumor cells developing radio resistance. The development of radio resistance causes patients' cancer to recur with a more aggressive phenotype. There are several chemotherapy drugs for colorectal cancer, namely 5-fluorouracil, capecitabine, irinotecan, and oxaliplatin (Katzung et al., 2013). Hand-foot syndrome is a side effect of chemotherapy drugs such as capecitabine or 5-Fluorouracil (American Cancer Society, 2020). 5-Fluorouracil has toxic effects such as nausea, mucositis, diarrhea, bone marrow depression, and neurotoxicity (Katzung et al., 2013). Therefore, new compounds for treating colorectal cancer with antitumor action that has high effectiveness and selectivity of cancer cells, as well as low toxicity of normal cells, are urgently needed. Recently, interest in natural compounds has increased significantly as some compounds exhibit significant cytotoxic, antiproliferative, and proapoptotic effects to inhibit cancer cell growth (Kabała-Dzik et al., 2017).

Recent studies have shown that caffeic acid phenethyl ester (CAPE), a component of honeybee propolis, is a natural compound with a strong chemo preventive effect, including cell cycle inhibition and proapoptotic action. These CAPE compounds have potential as colorectal anticancer drugs (Wadhwa et al., 2016). Analysis of the HKSA (Quantitative Structure-Activity Relationship) of CAPE compounds as colorectal anticancer can be used to learn more about the structural parameters that influence the activity of these compounds as colorectal anticancer.

Ketabforoosh et al. (2013) synthesized several CAPE compounds and their derivatives and evaluated their inhibitory activity on HeLa, SK-OV-3, and HT-29 cells. Evaluation of cytotoxic activity showed that the compound had the potential to inhibit HT-29 cancer cells, which are colorectal cancer cells. Using electronegativity molecular descriptors, topological indices, and steric factors, Ketabforoosh et al. (2013) analyzed CAPE compounds HKSA. The results of the reported HKSA model show that this model has a correlation coefficient value (R) = 0.66, a determination coefficient (R^2) = 0.44, and a Leave-One-Out or Q^2 (LOO) cross-validation value = 0.44. According to Golbraikh et al. (2003), a model may have good predictive power if the model meets several criteria, including $R^2 > 0.6$ and $Q^2(LOO) > 0.5$. Thus, this model cannot be said to have good predictive power.

This study describes the development of the CAPE compound HKSA model as a colorectal anticancer using topological and physicochemical descriptors to obtain a model that meets the goodness-of-fit criteria and the validity of Q2 (LOO). The modeling was performed by using the multiple linear regression techniques, and descriptor selection was made by the backward elimination method. Given that one of the factors that may affect the absorption of a drug compound in the target tissue is the level of polarity or hydrophobicity factor, the descriptor selection is conducted while maintaining the presence of a hydrophobic descriptor in each selected model.

2. MATERIALS AND METHODS

2.1. Materials

The materials used were chemical structure data and pIC_{50} values of 18 Caffeic Acid Phenethyl Ester (CAPE) compounds, the lead compound was shown in Fig. 1. The pIC_{50} value is the negative value of log IC_{50}, or pIC_{50} = -log(IC_{50}). The IC_{50} value is the concentration at which a drug or active compound can inhibit certain biological processes with an inhibition level of 50%. Because the nature of this potential inhibitory value is logarithmic, the decrease in potential from the micromolar to nanomolar level is a logarithmic change, not a linear change, so for linear regression studies, the use of the pIC_{50} value as the dependent variable will be more appropriate than the IC_{50} value. Data on the inhibitory activity of HT-29 cancer cells with CAPE compounds were obtained from a molar sample (Ketabforoosh et al., 2013) and converted to pIC_{50} (Table 1).

The tools used in this study consisted of hardware and software. The hardware was the Asus ZenBook UX305 laptop with specifications: Processor type Intel(R) Core(TM) M3-6Y30 CPU @ 0.90GHz 1.51 GHz, 8 GB Random Access Memory (RAM). The software used was the Windows 10 Home operating system, Marvin Beans 20.19.0, Microsoft Exel 2010, Mordred Descriptor web UI, and HyperChem 8.0.10. The Modred UI web server can be accessed for free at the link https://modred.phs.osaka-u.ac.jp.

2.2. Methdos

Eighteen structures of CAPE compounds obtained from the research of Ketabforoosh et al. (2013) were drawn using HyperChem software. Each structure was then optimized using the Polak-Ribiere algorithm with a convergence limit of 0.1 kcal/(Åmol) and the semi-empirical calculation method Recief Model 1 (RM 1). The structural image files optimized by HyperChem were saved in the file type (*.HIN) format. Furthermore, with the help of the Marvin Beans program, this file type was converted into *.SMI or *.SMILES format. The calculations of descriptor value were performed using three software, HyperChem, Marvin Beans, and Modred Descriptor web UI. The modeling was conducted using the multiple linear regression techniques and the descriptor selection was done by the backward elimination method. The selected model was validated using the Leave-One-Out (LOO) cross-validation technique using equation (1).

$$Q^2(LOO) = 1 - \frac{\sum(Y-\hat{Y})^2}{\sum(Y-\bar{Y})^2} = 1 - \frac{PRESS}{\sum(Y-\bar{Y})^2} \quad (1)$$

Y is the value of the experimental activity, $\hat{Y}$ is the predictive activity value, and $\bar{Y}$ is the average value of the experimental activity. A model is declared valid if it has a value of $Q^2 > 0{,}5$.

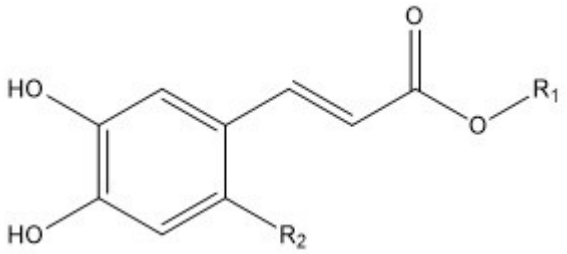

Figure 1. Structure of caffeic acid phenethyl ester (CAPE) with R_1 and R_2 substituent

Table 1. The structure and pIC_{50} value of CAPE compounds

Compound	R_1	R_2	pIC_{50} HT-29
1	-	-	4.600
2	-	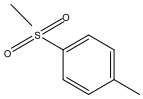	4.288
3	-	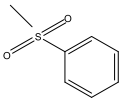	4.314
4	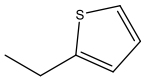	-	4.427
5	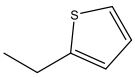	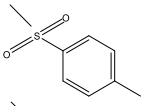	4.075
6	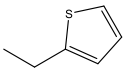	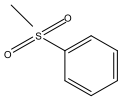	4.270
7		-	3.728
8		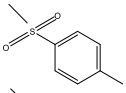	3.619
9		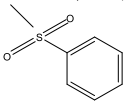	3.489
10		-	3.896
11		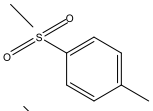	3.678
12	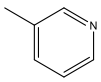	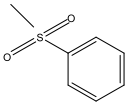	3.740
13	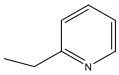	-	4.365
14	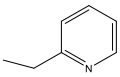	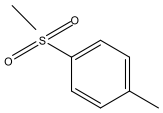	4.130
15	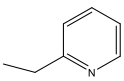	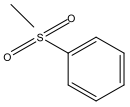	3.740
16		-	4.242
17	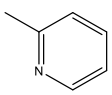	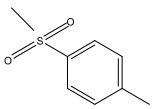	4.017
18	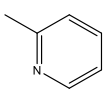	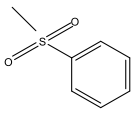	4.135

Source: Data structure and pIC_{50} values from Ketabforoosh et al. (2013) processed.

3. RESULTS AND DISCUSSION

3.1. Calculation and Selection of Descriptors

The method of calculating the electronic structural properties used in this study was RM1 (Recife Model 1). In general, the RM 1 method is superior to other semi-empirical methods seen from the average error in calculating the heat of formation parameter, dipole moment, ionization potential, and interatomic distance. The compounds used in the RM1 parameterization include various compounds containing C, H, N, O, P, S, F, Cl, Br, and I atoms (Rocha et al., 2006) so that the RM 1 method will be suitable if used as a method of calculating the structural descriptor of CAPE and its derivative compounds consisting of C, H, O, N and S atoms. Three applications (software) were used to calculate the descriptor value: HyperChem, Modred UI, and Marvin Beans.

The selection of descriptors in this study begins with a multicollinearity test. The multicollinearity test aims to avoid correlation or multicollinearity between descriptors so that all selected descriptors are not correlated with each other. The descriptor from Marvin Beans had a high correlation, so this descriptor was not used for further testing. The results of the multicollinearity test on 47 descriptors from Modred UI and 11 descriptors from HyperChem obtained ten descriptors that did not show high multicollinearity (Table 2). Therefore, these descriptors were chosen for the trial development of the HKSA model.

The steric parameter is an effect that correlates with the spatial arrangement of molecules in three-dimensional space. It is important to monitor the binding of chemicals to biological receptors (Roy et al., 2015). The steric properties affect the molecular energy, the reaction and conformational pathways, the reaction rate and equilibrium, the binding affinity between the ligand and the receptor, and other thermodynamic properties (Todeschini & Consonni, 2000). The steric constant of the substituents can be measured based on the appearance of groups and the effect of the groups on drug contact with adjacent receptor sites (Siswandono, 2016). The descriptors MDEC22, MDEC23, and molecular weight (BM) in Table 2 are the steric parameters evaluated in this study.

Topological descriptors were calculated based on the graphical representation of the molecule. They do not require estimating physicochemical properties or the rigorous computations involved in deriving quantum chemical descriptors (Roy et al., 2015). The topological charge index can evaluate charge transfer between pairs of atoms (Todeschini & Consonni, 2000). The ability to describe the charge distribution of a molecule is determined by relating it to the dipole moment of a heterogeneous set of hydrocarbons, the boiling temperatures of alkanes and alcohols, and the enthalpies of evaporation of alkanes (Galvez et al., 1994). Based on Table 2, the descriptors associated with the topological load index in this study are JGI1, JGI8, and JGI10.

The descriptor related to the hydrophobicity factor (lipophilicity) often used in HKSA is the logarithm of the partition coefficient (logP). The compound's hydrophobicity represents how likely it is for the compound to enter through the cell membrane causing damage and the ability of the compound to interact with its receptors. The logP value can describe the distribution of the drug in the body. If the logP value is positive, the compound tends to be in a non-polar phase (hydrophobic), and if the logP value is negative, the compound tends to be in a polar phase (hydrophilic). SlogP is an octanol-water partition coefficient developed by Wildman and Crippen (1999) to overcome several problems in calculating the logP value. SlogP and LogP in Table 2 are descriptors representing hydrophobic properties.

Electronic descriptors can affect how easily a drug can pass through a cell membrane or how strongly a drug can bind to a receptor. Electronic descriptors also affect the drug distribution process and the penetration of biological membranes, which is strongly influenced by the solubility of the drug in fat/water as well as in the structure-activity relationship and how strong these effects can interact between drugs and receptors (Siswandono, 2016). The groups with a dipolar function (with a dipole moment) are the ester group and CAPE, which is included in the ester group. The hydration energy and dipole moment in Table 2 are descriptors that represent electronic properties.

Table 2. List of selected descriptors that are not correlated

No	Name	Group	Description
1	MDEC22*	Steric	The length of the molecular distance edge connecting the secondary C atoms
2	MDEC23*	Steric	The length of the molecular edge connecting the secondary and tertiary C atoms
3	SlogP*	Hydrophobic	LogP Wildman-Crippen
4	JGI1*	Topology	1-Ordered Mean Topological Charge Index (1-Ordered Mean Topological Charge)
5	1JGI8*	Topology	8 order average topological charge index
6	JGI10*	Topology	10 order topological charge index
7	Hydration Energy**	Electronics	The energy released when one mole of ions is hydrated
8	BLogP**	Hydrophobic	Logarithm of partition coefficient between octanol and water
9	BM**	Steric	Relative molecular weight
10	dipole moment**	Electronics	A vector quantity used to express the polarity of a molecule

* = Descriptors in Modred UI
** = Descriptors in HyperChem

3.2. HKSA Model Development

Ten selected descriptors (Table 2) were tested for developing the HKSA model using multiple linear regression techniques. The best model was explored by selecting the appropriate descriptor through the backward elimination method. Based on the trial, we obtained the best eight models (Model 1-8) with a coefficient of determination (R^2) ≥ 0,6 and a $F_{ratio} > 1$, as listed in Table 3. Models 9 and 10 did not meet the goodness of fit criteria because of the $R^2 < 0,6$ and $F_{ratio} < 1$.

Table 3. Linear regression statistical data for ten HKSA equation as the model candidate

Model	F_{rasio}	R^2	R	SE	Adj R^2
1[a]	1.991	0.912	0.955	0.148	0.786
2[b]	2.696	0.911	0.955	0.138	0.812
3[c]	3.527	0.910	0.954	0.131	0.830
4[d]	4.137	0.901	0.949	0.131	0.831
5[e]	4.080	0.934	0.873	0.141	0.804
6[f]	4.499	0.853	0.924	0.145	0.792
7[g]	3.682	0.783	0.885	0.170	0.716
8[h]	2.424	0.635	0.797	0.212	0.556
9[i]	0.611	0.231	0.480	0.298	0.128
10[j]	0.480	0.119	0.345	0.309	0.064

[a]Descriptors: MDEC22, MDEC23, SlogP, JGI1, JGI8, JGI10, Energy of Hydration, LogP, BM, Dipole Moment
[b]Descriptors: MDEC22, MDEC23, JGI1, JGI8, JGI10, Energy of Hydration, LogP, BM, Dipole Moment
[c]Descriptors: MDEC22, MDEC23, JGI1, JGI8, JGI10, LogP, BM, Dipole Moment
[d]Descriptors: MDEC22, MDEC23, JGI1, JGI8, LogP, BM, Dipole Moment
[e]Descriptors: MDEC22, MDEC23, JGI1, JGI8, LogP, BM
[f]Descriptors: MDEC22, MDEC23, JGI1, LogP, BM
[g]Descriptors: MDEC22, MDEC23, JGI1, BM
[h]Descriptors: MDEC22, MDEC23, JGI1
[i]Descriptors: MDEC22, MDEC23
[j]Descriptors: MDEC23

F_{ratio} value > 1 can be achieved if the value of $F_{count} > F_{table}$. The F-test, in this case, is the overall significance test used to evaluate whether the regression model provides higher goodness of fit when compared to models that do not contain independent variables. Regression models that do not contain predictors are also known

as intercept-only models. The hypothesis for this significance test is as follows:

- Null hypothesis: there is no significant difference in the level of goodness of fit between the model containing only the intercept (without the descriptor) and the proposed model (containing the selected descriptor),
- Alternative hypothesis: there is a significant difference in the goodness of fit between the model without descriptors and the proposed model.

The data in Table 3 shows that models 1 to 8 have a $F_{ratio} > 1$ while models 9 and 10 have a $F_{ratio} < 1$. Based on this F_{ratio} value, only models 1 to 8 have the null hypothesis rejected. Thus, only models 1 to 8 have descriptors that significantly affect the goodness of fit as a whole.

The goodness of fit in this model can be seen from the coefficient of determination (R^2) value. This value shows the proportion of the value of the variation of biological activity that can be explained by the predicted results of the model (OECD, 2007). The higher value of R^2 (closer to 1 or -1) can be obtained if the data distribution gets closer to the trend line. In linear regression, it indicates the stronger the linear relationship between the dependent variable and the independent variable. Thus, the value of R^2 can be a requirement that the model meets the goodness of fit in multiple linear regression. The criteria for the model selected based on the value of R^2 is a model with a value of $R^2 \geq 0.6$. The value of $R^2 \geq 0.6$ can be interpreted that the model can explain 60% of the variation in biological activity. Judging from the R^2 value, only models 1 to 8 meet these criteria (model 9 and model 10 do not meet the criteria).

However, the value of R^2, in general, tends to increase when the number of independent variables (descriptors) increases, even though it does not contribute a significant effect. Therefore, another parameter is needed for correction, namely adjusted R^2 (R^2_{adj}). R^2_{adj} is the value of R^2 that has been adjusted or corrected concerning the number of descriptors. This value will decrease if additional descriptors have no significant effect (OECD, 2007). The difference between the accepted values of R^2 and R^2_{adj} is less than 0.3 (Veerasamy et al., 2011). All models (1-8) have a difference R^2 value and R^2_{adj} smaller than 0.3. Therefore, the number of descriptors used in the model is still acceptable.

A p-value analysis was carried out to see the descriptors that had a significant effect on the compound's activity, and the results are presented in Table 4. Based on Table 4, each descriptor model 6, model 7, model 9, and model 10 has a p-value descriptor < 0.05. Because model 9 and model 10 have a value of $R^2 \geq 0.6$, if the p-value requirements are combined with the R^2 value requirements, only model 6 and model 7 meet the R2 value and p-value criteria.

Models 6 and 7 of this study, compared with the previous model (Ketabforoosh et al., 2013), show that these two models have a better level of goodness of fit (Table 5). Models 6 and 7 have $R^2 \geq 0.6$, while the previous model has $R^2 \leq 0.6$. Model 6 uses MDEC22, MDEC23, JGI1, LogP, and BM descriptors. Model 7 uses MDEC22, MDEC23, JGI1, and BM descriptors, while the previous research model uses GATS1e and GATS3v. It indicates that the selection of the descriptor type can affect the quality of the obtained HKSA model. The goodness of fit level is very closely related to the significance of the descriptor effect as the independent variable and activity as the dependent variable. The higher fit in models 6 and 7 compared to the previous model indicates that the descriptor used in models 6 and 7 has a more significant effect than the descriptor in the previous model.

Table 4. Regression coefficient and p-value data from ten HKSA equation models

Model	1		2		3		4		5	
	Coefficient	**p-value**	**Coefficient**	**p-value**	**Coefficient**	**p-value**	**Coefficient**	**p-value**	**Coefficient**	**p-value**
Intercept	-9.940	0.211	-9.275	0.164	-10.984	0.005	-8.952	0.002	-8.441	0.003
MDEC22	0.525	0.024	0.501	0.005	0,.523	0.001	0.452	0.000	0.433	0.000
MDEC23	-0.789	0.039	-0,.759	0.018	-0.816	0.001	-0.669	0.000	-0.633	0.000
SlogP	-0.063	0.842	-	-	-	-	-	-	-	-
JGI1	83.418	0.065	78.601	0.024	86.361	0.000	83.469	0.000	80.362	0.000
JGI8	262.317	0.250	260.266	0.221	229.392	0.194	78.026	0.123	64.409	0.217
JGI10	207.046	0.395	204.134	0.368	167.397	0.360	-	-	-	
Hydrating Energy	0.058	0.750	0.054	0.750	-	-	-	-	-	-
LogP	-0.575	0.211	-0.532	0.155	-0.442	0.046	-0.376	0.061	-0.417	0.051
BM	0.009	0.138	0.008	0.051	0.008	0.032	0.006	0.025	0.007	0.023
Dipole Moment	0.022	0.546	0.025	0.377	0.026	0.328	0.038	0.126	-	-

Model	6		7		8		9		10	
	Coefficient	***p-value***	**Coefficient**	***p-value***	**Coefficient**	***p-value***	**Coefficient**	***p-value***	**Coefficient**	***p-value***
Intercept	-9.639	0.001	-6.548	0.005	-4.982	0.054	4.289	6.27E-09	4.530	4.6E-10
MDEC22	0.478	0.000	0.352	0.000	0.319	0.001	0.053	1.60E-01	-	-
MDEC23	-0.691	0.000	-0.603	0.000	-0.419	0.001	-0.054	5.21E-02	-0.025	1.6E-01
SlogP	-	-	-	-	-	-	-	-	-	-
JGI1	89.760	0.000	66.870	0.000	59.376	0.001	-	-	-	-
JGI8	-	-	-	-	-	-	-	-	-	-
JGI10	-	-	-	-	-	-	-	-	-	-
Hydrating Energy	-	-	-	-	-	-	-	-	-	-
LogP	-0.463	0.033	-	-	-	-	-	-	-	-
BM	0.008	0.006	0.008	0.011	-	-	-	-	-	-
Dipole Moment	-	-	-	-	-	-	-	-	-	-

Table 5. Results of statistical analysis of model 6, model 7, and previous research

Statistical Parameters	Model 6	Model 7	Previous Model*	Criteria
F_{rasio}	4,499	3,682	1,447	>1
R^2	0,853	0,783	0,415	≥ 0,6
R^2_{adj}	0,792	0,716	0,337	-
(R^2 - R^2_{adj})	0,061	0,067	0,078	< 0,3

Note: *Model according to Ketabforoosh *et al.* (2013)

Based on Table 5 and Table 4, two models of HKSA equations that meet these criteria can be drawn up: Equation (2) and Equation (3).

$$\boldsymbol{pIC_{50}} = -9{,}639 + 0{,}478\boldsymbol{MDEC22} - 0{,}691\boldsymbol{MDEC23} + 89{,}760\boldsymbol{JGI1} - 0{,}463\boldsymbol{logP} - 0{,}008\boldsymbol{BM} \quad (2)$$

$$\boldsymbol{pIC_{50}} = -6{,}548 + 0{,}352\boldsymbol{MDEC22} - 0{,}603\boldsymbol{MDEC23} + 66{,}870\boldsymbol{JGI1} - 0{,}008\boldsymbol{BM} \quad (3)$$

The HKSA model in Equation 2 contains a logP descriptor, while the HKSA model in Equation 3 does not contain a logP descriptor. The logP coefficient in Equation 2 is negative. If the logP is positive, the greater the logP value will result in a lower pIC_{50} activity value. On the other hand, if the logP is negative, the larger the logP value, the higher the pIC_{50} activity value. A positive logP value indicates the compound tends to be in a non-polar phase (hydrophobic). Conversely, a negative logP value indicates that the compound tends to be more soluble in a polar phase (hydrophilic). Thus, for non-polar compounds, there is a tendency that increasing the logP value will decrease the activity (pIC_{50}) of CAPE derivatives. On the other hand, for polar compounds, there is a tendency that increasing the logP value (which is negative) will increase the activity (pIC50) of CAPE derivatives. Thus, this logP parameter becomes particularly important in the design or development of CAPE derivative compounds, considering that CAPE compounds can be developed into polar or non-polar compounds (Hashimoto et al., 2021).

The HKSA model of equation (2) and equation (3) show that the JGI1 descriptor is the descriptor that has the most positive influence on the pIC_{50} value than the other descriptors. It indicates that the 1-Ordered Mean Topological Charge index is also important to consider in the design of CAPE-derived compounds with high potential as colorectal anticancer HT-29 cells.

3.3. Model Validation

The estimation of the two HKSA models' predictive power (equation (2) and equation (3)) was carried out using the LOO cross-validation technique test. The validity criterion used is that a model is said to be valid if the value of Q^2(LOO) > 0.5 (Veerasamy et al., 2011). The validation test results on Model 6 and Model 7 show that Model 6 has a Q^2(LOO) value of 0.702 while Model 7 has a Q^2(LOO) value of 0.569. Thus, these two models can be declared valid based on the Q^2(LOO) criteria.

In addition to estimating how robust the model predictions are for new compounds that are not in the data, the Q^2 value can also be used as a reference to assess the possibility of overfitting. This value can also be an indication of overfitting in the model, which is characterized by the difference between R^2 and Q^2 > 0.3 (Veerasamy et al., 2011). Based on Q^2 and R^2 values, it can be seen that model 6 has a Q^2 and R^2 difference of 0.151, while model 7 has a Q^2 and R^2 difference of 0.214. Therefore, it can be declared that there is no overfitting in model 6 and model 7.

Based on the Q^2(LOO) internal cross-validation test, it appears that model 6 and model 7 meet the criteria as valid models. However, if viewed from the value of the F_{ratio} and R^2, it appears that model 6 is better than model 7. In addition, model 6 has a PRESS value of 0.516 while model 7 was 0.745. It indicates that the addition of the hydrophobicity descriptor (logP) can improve the quality of the CAPE compound HKSA model as an anticancer HT-29. The comparison of the quality of model 6 (Equation (2)) and model 7 (Equation (3)) can be seen in the scatter diagram of the predicted activity value versus the

experimental activity value in Fig. 2. Fig. 2 shows that the goodness of fit level of model 6 is better than model 7.

Fig. 3 shows a comparison diagram of the predicted activity values of model 6 and model 7, which are very close to the experimental values. Fig. 3 also shows that model 6 has a predictive activity value closer to the experimental activity value than model 7. Overall, it can be stated that model 6 and model 7 are models that meet the Q^2(LOO) validity criteria, but model 6 has highest goodness of fit level than model 7. Based on Table 3, model 6 has a correlation coefficient value (r) of 0.924 while model 7 has a correlation coefficient value of 0.885. Thus, Equation (2) (derived from model 6) tends to have better predictive ability than Equation (3) (from model 7).

Based on Equation (2), to obtain CAPE-derived compounds with higher colorectal anticancer activity in HT-29 cells, new compounds can be developed by: increasing the value of the MDEC22 descriptor and increasing the value of JGI1 or decreasing the value of the MDEC23 descriptor. It should be noted that the derivatization in the production of new compound will generally result in a larger molecular weight even though the effect is relatively small, so the addition of a new group or side chain should not be too large. The design of new CAPE-derived compounds must also pay attention to molecular polarity. For non-polar compounds, a decrease in the logP value will tend to increase activity. On the other hand, for polar compounds, an increase in the logP value will increase the activity (pIC_{50}) of CAPE derivatives.

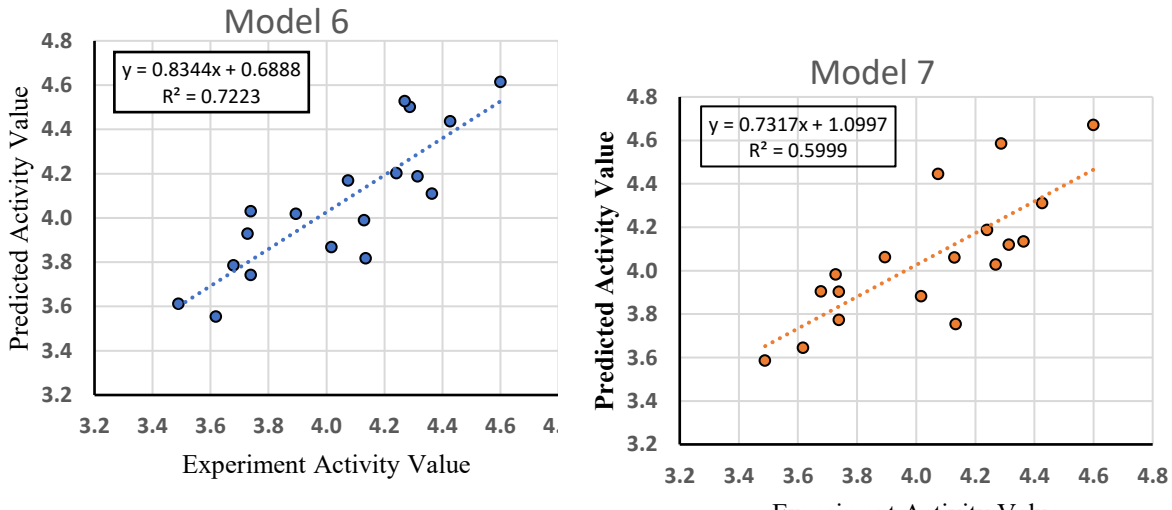

Figure 2. Scatter diagram of the relationship between the experimental activity value vs. the predicted activity value from the HKSA model Equation (2) and Equation (3).

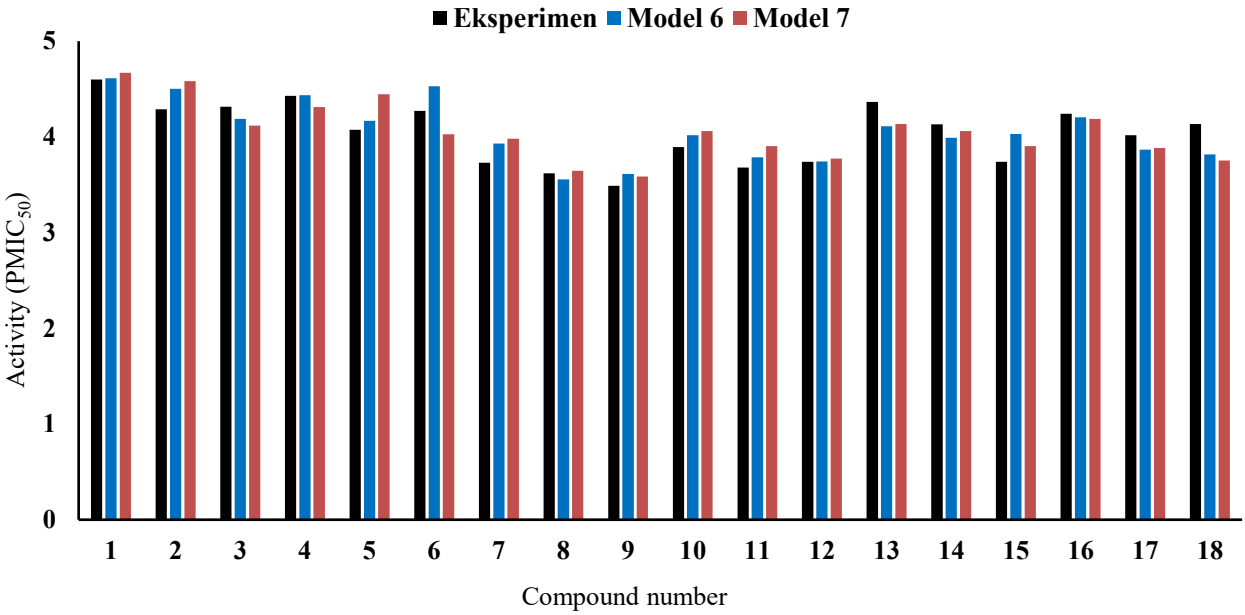

Figure 3. The predictive activity value diagram of the HKSA model Equation 2 and the HKSA model Equation 3 are compared with the experimental activity values.

4. CONCLUSIONS

Based on the data from the research and discussion described, it can be concluded that by using four descriptors, namely MDEC22, MDEC23, JGI1, and BM, the HKSA model meets the validity criteria of Q^2(LOO). The addition of the LogP hydrophobic factor descriptor also resulted in an HKSA model that met the Q^2(LOO) validity criteria. The development of the HKSA model by adding the LogP descriptor resulted in the 5 descriptor HKSA model with higher goodness of fit level than the HKSA model without the LogP descriptor. Based on the goodness of fit and the validity of Q^2(LOO), these two HKSA models have the potential to be used as predictors or aids in the development of a new class of CAPE compounds as anticancer against HT-29 cells with higher activity.

LIST OF REFERENCES

American Cancer Society. (2020). *General Counsel American Cancer Society. Inc*. Atlanta, Georgia.

Galves, J., R. Garcia, M. T. Salabert, R. Soler. (1994). Charge Indexes New Topological Descriptors. *Journal of Chemical Information and Modeling*, *34*(3): 520-525.

Golbraikh A., Shen M., Xiao Z., Xiao Y.D., Lee K.H. & Tropsham A. (2003). Rational selection of training and test sets for the development of validated QSAR models. *Journal of Computer-Aided Molecular Design, 17*, 241–253. https://doi.org/10.1023/A:1025386326946

Hashimoto R, Lai H, Fujita R, Hanaya K, Higashibayashi S, Inoue H, & Sugai T. (2021). *Global Cancer Observatory: Cancer Today*.Chemoenzymatic semisynthesis of caffeic acid β-phenethyl ester, an antioxidative component in propolis, from raw coffee bean extract. *Bioscience, Biotechnology, and Biochemistry*, *85* (3), 476-480. https://doi.org/10.1093/bbb/zbaa077

Kabała-Dzik, A., Rzepecka-Stojko, A., Kubina, R, Jastrzebska-Stojko Z., Stojko, R., Wojtyczka, R.D., and Stojko, J. (2017). Comparison of Two Components of Propolis: Caffeic Acid (CA) and Caffeic Acid Phenethyl Ester (CAPE) Induce Apoptosis and Cell Cycle Arrest of Breast Cancer

Cells MDA-MB-231. *Molecules*, *22*(1554), 1-15.

Katzung, B. G., S. B. Masters & A. J. Trevor. (2013). Farmakologi Dasar & Klinik. EGC, Jakarta.

Ketabforoosh S.H.E., Amini M, Vosooghi M, Shafiee A, Azizi E. & Kobarfard F. (2013). Synthesis, evaluation of anticancer activity and QSAR study of heterocyclic esters of caffeic acid. *Iranian Journal of Pharmaceutical Research*, *12*(4), 705–719.

OECD. (2007). *Guidance Document On the Validation of (Quantitative) Structure-Activity Relationships [(Q)SAR] Models*. Organisation de Coopération et de Développement Economiques, France.

Roy, K., S. Kar & R. N. Das. (2015). *A Primer on QSAR/QSPR Modeling Fundamental Concepts*. Springer, New York.

Rocha, G. B., R. O. Freire, A. M. Simas & J. J. P. Stewart. (2006). RM1: A Reparameterization of AM1 for H, C, N, O, P, S, F, Cl, Br and I. *Wiley InterScience, 27*(10),1101-1111.

Siswandono. (2016). *Kimia Medisinal Jilid 1*. Airlangga Universitas Press, Jakarta.

Todeschini, R. & V. Consonni. (2000). *Handbook of Molecular Descriptor*. Wiley-VCH, Germany.

Veerasamy, R., H. Rajak, A. Jain, S. Sivadasan, C. P. Varghesel & R. K. Agrawal. (2011). Validation of QSAR Models Strategies and Importance. *International Journal of Drug Desain and Discovery, 2*, 511-519.

Wadhwa, R., Nigam, N., Bhargava, P, Dhanjal, J.K., Goyal, S, Grover, A., Sundar, D., Ishida, Y., Terao, K., Kau, S. (2016). Molecular characterization and enhancement of anticancer activity of caffeic acid phenethyl ester by γ cyclodextrin. *Journal of Cancer*, *7*(13), 1755–1771. https://doi. org/10.7150/jca.15170

Wildman, S. A. & G. M. Crippen. (1999). Prediction of Physicochemical Parameters by Atomic Contributions. *J.Chem.Inf.Comput.Sci, 39*(5), 868-873. https://doi.org/10.1021/ci9903071

JURNAL ILMIAH BERKALA SAINS DAN TERAPAN KIMIA

Jurnal Ilmiah Berkala: Sains dan Terapan Kimia
Vol. 16 No. 2, July 2022

Development of QSAR Model of Caffeic Acid Phenethyl Ester as Anti-Cancer HT-29

Pengembangan Model HKSA Senyawa *Caffeic Acid Phenethyl Ester* (CAPE) sebagai Antikanker HT-29

Uripto Trisno Santoso[1,2,*], Samsul Hadi[3], Devi Eka Pratama[3]

[1]Computational Chemistry Laboratory, Laboratory of Mathematics and Natural Sciences, Lambung Mangkurat University, Jl. A. Yani KM. 36 Banjarbaru 70714, Kalimantan Selatan

[2]Chemistry Department, Faculty of Mathematics and Natural Sciences, Lambung Mangkurat University, Jl. A. Yani KM. 36 Banjarbaru 70714, Kalimantan Selatan

[3]Pharmacy Department, Faculty of Mathematics and Natural Sciences, Lambung Mangkurat University, Jl. A. Yani KM. 36 Banjarbaru 70714, Kalimantan Selatan

*Email: utsantoso@ulm.ac.id

ABSTRACT

Caffeic Acid Phenethyl Ester (CAPE) compounds are potentially colorectal anticancer drugs. QSAR (Quantitative Structure-Activity Relationship) research on the CAPE compound class has been carried out, but the model in the previous study did not meet the goodness of fit criteria. The development of the CAPE compound QSAR model as a colorectal anticancer was carried out to obtain a model that meets the goodness of fit criteria and is valid. Eighteen CAPE compounds were used to build the QSAR model using the Multiple Linear Regression (MLR) technique. The descriptor selection was carried out using the backward elimination method and the validation test using the internal leave one out (LOO) cross-validation. The results showed that the QSAR model with four descriptors, namely MDEC22, MDEC23, JGI1, and molecular weight (BM), met the goodness of fit and Q^2(LOO) criteria. The development of the QSAR model by adding the LogP descriptor resulted in the QSAR 5 descriptor model with higher goodness of fit level than the QSAR model without the LogP descriptor. Both of these QSAR models have the potential to be used as predictors in the development of a new class of CAPE compounds as anticancer agents against HT-29 cells.

Keywords: Caffeic Acid Phenethyl Ester (CAPE), Quantitative Structure-Activity Relationship (QSAR), Multiple Linear Regression, Internal Validation.

ABSTRAK

Senyawa Caffeic Acid Phenethyl Ester (CAPE) memiliki potensi sebagai obat antikanker kolorektal. Penelitan HKSA (Hubungan Kuantitatif Struktur-Aktivitas) tentang golongan senyawa CAPE telah dilakukan tetapi model pada penelitian sebelumnya tidak memenuhi kriteria goodness of fit. Pengembangan model HKSA senyawa CAPE sebagai antikanker kolorektal dilakukan untuk mendapatkan model yang memenuhi kriteria goodness of fit dan bersifat valid. Sebanyak 18 senyawa CAPE digunakan untuk membangun model HKSA dengan menggunakan teknik Regresi Linier Berganda (RLB). Pemilihan deskriptor dilakukan dengan metode eliminasi backward dan uji validasinya menggunakan validasi silang internal leave one out (LOO). Hasil penelitian menunjukkan bahwa model HKSA dengan 4 deskriptor, yaitu MDEC22, MDEC23, JGI1, dan berat molekul (BM) memenuhi kriteria goodness of fit dan Q^2(LOO). Pengembangan model HKSA dengan menambahkan deskriptor LogP menghasilkan model HKSA 5 deskriptor dengan tingkat goodness of fit yang lebih baik daripada model HKSA tanpa deskriptor LogP. Kedua model HKSA ini berpotensi untuk dijadikan prediktor dalam pengembangan golongan senyawa CAPE yang baru sebagai antikanker terhadap sel HT-29.

Kata Kunci: Caffeic Acid Phenethyl Ester (CAPE), Hubungan Kuantitatif Struktur-Aktivitas (HKSA), Regresi Linier Ganda, Validasi Internal.

Received: January 27, 2022; **Accepted**: June 29, 2022: **Available online**: July 31, 2022

1. INTRODUCTION

Cancer is the second leading cause of death in the world. The number of new cases in 2020 shows the three most extensive cancers, namely lung cancer, breast cancer, and colon cancer. Asia has notable cases, 49.3% of the total 19,292,789 people. Asia's cancer mortality rate in 2020 was 58.3% of the total 9,958,133 people (IARC, 2020). Colon cancer is the third largest cancer in the world and the fourth most recent case in Indonesia. Data from IARC (2020) states that there are 10% of the latest cases worldwide and 8.6% of the newest cases in Indonesia. The risk of developing colorectal cancer, according to the American Cancer Society (2020), is 1 in 23 (4.3%) in men and 1 in 25 (4.0%) in women.

Radiotherapy and chemotherapy are frequently employed cancer treatments. Radiation therapy is generally remarkably effective, but there is a risk of damaging normal cells and tumor cells developing radio resistance. The development of radio resistance causes patients' cancer to recur with a more aggressive phenotype. There are several chemotherapy drugs for colorectal cancer, namely 5-fluorouracil, capecitabine, irinotecan, and oxaliplatin (Katzung et al., 2013). Hand-foot syndrome is a side effect of chemotherapy drugs such as capecitabine or 5-Fluorouracil (American Cancer Society, 2020). 5-Fluorouracil has toxic effects such as nausea, mucositis, diarrhea, bone marrow depression, and neurotoxicity (Katzung et al., 2013). Therefore, new compounds for treating colorectal cancer with antitumor action that has high effectiveness and selectivity of cancer cells, as well as low toxicity of normal cells, are urgently needed. Recently, interest in natural compounds has increased significantly as some compounds exhibit significant cytotoxic, antiproliferative, and proapoptotic effects to inhibit cancer cell growth (Kabała-Dzik et al., 2017).

Recent studies have shown that caffeic acid phenethyl ester (CAPE), a component of honeybee propolis, is a natural compound with a strong chemo preventive effect, including cell cycle inhibition and proapoptotic action. These CAPE compounds have potential as colorectal anticancer drugs (Wadhwa et al., 2016). Analysis of the QSAR (Quantitative Structure-Activity Relationship) of CAPE compounds as colorectal anticancer can be used to learn more about the structural parameters that influence the activity of these compounds as colorectal anticancer.

Ketabforoosh et al. (2013) synthesized several CAPE compounds and their derivatives and evaluated their inhibitory activity on HeLa, SK-OV-3, and HT-29 cells. Evaluation of cytotoxic activity showed that the compound had the potential to inhibit HT-29 cancer cells, which are colorectal cancer cells. Using electronegativity molecular descriptors, topological indices, and steric factors, Ketabforoosh et al. (2013) analyzed CAPE compounds QSAR. The results of the reported QSAR model show that this model has a correlation coefficient value (R) = 0.66, a determination coefficient (R^2) = 0.44, and a Leave-One-Out or Q^2 (LOO) cross-validation value = 0.44. According to Golbraikh et al. (2003), a model may have good predictive power if the model meets several criteria, including $R^2 > 0.6$ and $Q^2(LOO) > 0.5$. Thus, this model cannot be said to have good predictive power.

This study describes the development of the CAPE compound QSAR model as a colorectal anticancer using topological and physicochemical descriptors to obtain a model that meets the goodness-of-fit criteria and the validity of Q^2 (LOO). The modeling was performed by using the multiple linear regression techniques, and descriptor selection was made by the backward elimination method. Given that one of the factors that may affect the absorption of a drug compound in the target tissue is the level of polarity or hydrophobicity factor, the descriptor selection is conducted while maintaining the presence of a hydrophobic descriptor in each selected model.

2. MATERIALS AND METHODS

2.1. Materials

The materials used were chemical structure data and pIC_{50} values of 18 Caffeic Acid Phenethyl Ester (CAPE) compounds, the lead compound was shown in Fig. 1. The pIC_{50} value is the negative value of log IC_{50}, or pIC_{50} = -log(IC_{50}). The IC_{50} value is the concentration at which a drug or active compound can inhibit certain biological processes with an inhibition level of 50%. Because the nature of this potential inhibitory value is logarithmic, the decrease in potential from the micromolar to nanomolar level is a logarithmic change, not a linear change, so for linear regression studies, the use of the pIC_{50} value as the dependent variable will be more appropriate than the IC_{50} value. Data on the inhibitory activity of HT-29 cancer cells with CAPE compounds were obtained from a molar sample (Ketabforoosh et al., 2013) and converted to pIC_{50} (Table 1).

The tools used in this study consisted of hardware and software. The hardware was the Asus ZenBook UX305 laptop with specifications: Processor type Intel(R) Core(TM) M3-6Y30 CPU @ 0.90GHz 1.51 GHz, 8 GB Random Access Memory (RAM). The software used was the Windows 10 Home operating system, Marvin Beans 20.19.0, Microsoft Exel 2010, Mordred Descriptor web UI, and HyperChem 8.0.10. The Modred UI web server can be accessed for free at the link *https://modred.phs.osaka-u.ac.jp.*

2.2. Methods

Eighteen structures of CAPE compounds obtained from the research of Ketabforoosh et al. (2013) were drawn using HyperChem software. Each structure was then optimized using the Polak-Ribiere algorithm with a convergence limit of 0.1 kcal/(Åmol) and the semi-empirical calculation method Recief Model 1 (RM 1). The structural image files optimized by HyperChem were saved in the file type (*.HIN) format. Furthermore, with the help of the Marvin Beans program, this file type was converted into *.SMI or *.SMILES format. The calculations of descriptor value were performed using three software, HyperChem, Marvin Beans, and Modred Descriptor web UI. The modeling was conducted using the multiple linear regression techniques and the descriptor selection was done by the backward elimination method. The selected model was validated using the Leave-One-Out (LOO) cross-validation technique using equation (1).

$$Q^2(LOO) = 1 - \frac{\sum(Y-\hat{Y})^2}{\sum(Y-\bar{Y})^2} = 1 - \frac{PRESS}{\sum(Y-\bar{Y})^2} \quad (1)$$

$\hat{Y}$ Y is the value of the experimental activity, is the predictive activity value, and $\bar{Y}$ is the average value of the experimental activity. A model is declared valid if it has a value of Q^2 > 0,5.

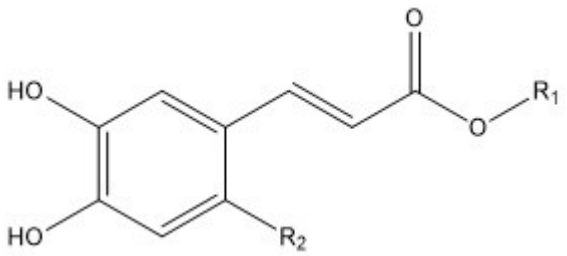

Figure 1. Structure of caffeic acid phenethyl ester (CAPE) with R_1 and R_2 substituent

Table 1. The structure and pIC_{50} value of CAPE compounds

Compound	R_1	R_2	pIC_{50} HT-29
1	-	-	4.600
2	-	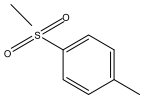	4.288
3	-	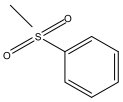	4.314
4	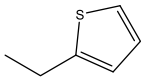	-	4.427
5	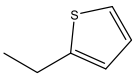	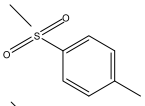	4.075
6	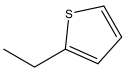	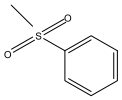	4.270
7		-	3.728
8		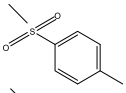	3.619
9		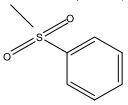	3.489
10		-	3.896
11		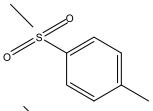	3.678
12	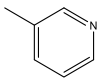	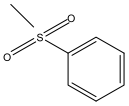	3.740
13	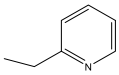	-	4.365
14	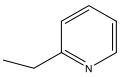	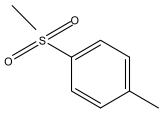	4.130
15	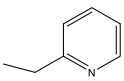	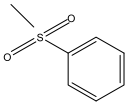	3.740
16	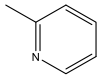	-	4.242
17	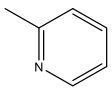	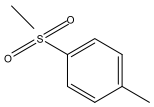	4.017
18	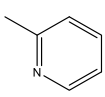	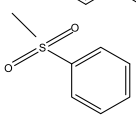	4.135

Source: Data structure and pIC_{50} values from Ketabforoosh et al. (2013) processed.

3. RESULTS AND DISCUSSION

3.1. Calculation and Selection of Descriptors

The method of calculating the electronic structural properties used in this study was RM1 (Recife Model 1). In general, the RM 1 method is superior to other semi-empirical methods seen from the average error in calculating the heat of formation parameter, dipole moment, ionization potential, and interatomic distance. The compounds used in the RM1 parameterization include various compounds containing C, H, N, O, P, S, F, Cl, Br, and I atoms (Rocha et al., 2006) so that the RM 1 method will be suitable if used as a method of calculating the structural descriptor of CAPE and its derivative compounds consisting of C, H, O, N and S atoms. Three applications (software) were used to calculate the descriptor value: HyperChem, Modred UI, and Marvin Beans.

The selection of descriptors in this study begins with a multicollinearity test. The multicollinearity test aims to avoid correlation or multicollinearity between descriptors so that all selected descriptors are not correlated with each other. The descriptor from Marvin Beans had a high correlation, so this descriptor was not used for further testing. The results of the multicollinearity test on 47 descriptors from Modred UI and 11 descriptors from HyperChem obtained ten descriptors that did not show high multicollinearity (Table 2). Therefore, these descriptors were chosen for the trial development of the QSAR model.

The steric parameter is an effect that correlates with the spatial arrangement of molecules in three-dimensional space. It is important to monitor the binding of chemicals to biological receptors (Roy et al., 2015). The steric properties affect the molecular energy, the reaction and conformational pathways, the reaction rate and equilibrium, the binding affinity between the ligand and the receptor, and other thermodynamic properties (Todeschini & Consonni, 2000). The steric constant of the substituents can be measured based on the appearance of groups and the effect of the groups on drug contact with adjacent receptor sites (Siswandono, 2016). The descriptors MDEC22, MDEC23, and molecular weight (BM) in Table 2 are the steric parameters evaluated in this study.

Topological descriptors were calculated based on the graphical representation of the molecule. They do not require estimating physicochemical properties or the rigorous computations involved in deriving quantum chemical descriptors (Roy et al., 2015). The topological charge index can evaluate charge transfer between pairs of atoms (Todeschini & Consonni, 2000). The ability to describe the charge distribution of a molecule is determined by relating it to the dipole moment of a heterogeneous set of hydrocarbons, the boiling temperatures of alkanes and alcohols, and the enthalpies of evaporation of alkanes (Galvez et al., 1994). Based on Table 2, the descriptors associated with the topological load index in this study are JGI1, JGI8, and JGI10.

The descriptor related to the hydrophobicity factor (lipophilicity) often used in QSAR is the logarithm of the partition coefficient (logP). The compound's hydrophobicity represents how likely it is for the compound to enter through the cell membrane causing damage and the ability of the compound to interact with its receptors. The logP value can describe the distribution of the drug in the body. If the logP value is positive, the compound tends to be in a non-polar phase (hydrophobic), and if the logP value is negative, the compound tends to be in a polar phase (hydrophilic). SlogP is an octanol-water partition coefficient developed by Wildman and Crippen (1999) to overcome several problems in calculating the logP value. SlogP and LogP in Table 2 are descriptors representing hydrophobic properties.

Electronic descriptors can affect how easily a drug can pass through a cell membrane or how strongly a drug can bind to a receptor. Electronic descriptors also affect the drug distribution process and the penetration of biological membranes, which is strongly influenced by the solubility of the drug in fat/water as well as in the structure-activity relationship and how strong these effects can interact between drugs and receptors (Siswandono, 2016). The groups with a dipolar function (with a dipole moment) are the ester group and CAPE, which is included in the ester group. The hydration energy and dipole moment in Table 2 are descriptors that represent electronic properties.

Table 2. List of selected descriptors that are not correlated

No	Name	Group	Description
1	MDEC22*	Steric	The length of the molecular distance edge connecting the secondary C atoms
2	MDEC23*	Steric	The length of the molecular edge connecting the secondary and tertiary C atoms
3	SlogP*	Hydrophobic	LogP Wildman-Crippen
4	JGI1*	Topology	1-Ordered Mean Topological Charge Index (1-Ordered Mean Topological Charge)
5	1JGI8*	Topology	8 order average topological charge index
6	JGI10*	Topology	10 order topological charge index
7	Hydration Energy**	Electronics	The energy released when one mole of ions is hydrated
8	BLogP**	Hydrophobic	Logarithm of partition coefficient between octanol and water
9	BM**	Steric	Relative molecular weight
10	dipole moment**	Electronics	A vector quantity used to express the polarity of a molecule

* = Descriptors are available in Modred UI
** = Descriptors are available in HyperChem

3.2. QSAR Model Development

Ten selected descriptors (Table 2) were tested for developing the QSAR model using multiple linear regression techniques. the best model was explored by selecting the appropriate descriptor through the backward elimination method. Based on the trial, we obtained the best eight models (Model 1-8) with a coefficient of determination (R^2) ≥ 0,6 and a F_{ratio} > 1, as listed in Table 3. Models 9 and 10 did not meet the goodness of fit criteria because of the R^2 < 0,6 and F_{ratio} < 1.

Table 3. Linear regression statistical data for ten QSAR equation as the model candidate

Model	F_{rasio}	R^2	R	SE	Adj R^2
1[a]	1.991	0.912	0.955	0.148	0.786
2[b]	2.696	0.911	0.955	0.138	0.812
3[c]	3.527	0.910	0.954	0.131	0.830
4[d]	4.137	0.901	0.949	0.131	0.831
5[e]	4.080	0.934	0.873	0.141	0.804
6[f]	4.499	0.853	0.924	0.145	0.792
7[g]	3.682	0.783	0.885	0.170	0.716
8[h]	2.424	0.635	0.797	0.212	0.556
9[i]	0.611	0.231	0.480	0.298	0.128
10[j]	0.480	0.119	0.345	0.309	0.064

[a]Descriptors: MDEC22, MDEC23, SlogP, JGI1, JGI8, JGI10, Energy of Hydration, LogP, BM, Dipole Moment
[b]Descriptors: MDEC22, MDEC23, JGI1, JGI8, JGI10, Energy of Hydration, LogP, BM, Dipole Moment
[c]Descriptors: MDEC22, MDEC23, JGI1, JGI8, JGI10, LogP, BM, Dipole Moment
[d]Descriptors: MDEC22, MDEC23, JGI1, JGI8, LogP, BM, Dipole Moment
[e]Descriptors: MDEC22, MDEC23, JGI1, JGI8, LogP, BM
[f]Descriptors: MDEC22, MDEC23, JGI1, LogP, BM
[g]Descriptors: MDEC22, MDEC23, JGI1, BM
[h]Descriptors: MDEC22, MDEC23, JGI1
[i]Descriptors: MDEC22, MDEC23
[j]Descriptors: MDEC23

F_{ratio} value > 1 can be achieved if the value of $F_{count} > F_{table}$. The F-test, in this case, is the overall significance test used to evaluate whether the regression model provides higher goodness of fit when compared to models that do not contain independent variables. Regression models that do not contain predictors are

also known as intercept-only models. The hypothesis for this significance test is as follows:

- Null hypothesis: there is no significant difference in the level of goodness of fit between the model containing only the intercept (without the descriptor) and the proposed model (containing the selected descriptor),
- Alternative hypothesis: there is a significant difference in the goodness of fit between the model without descriptors and the proposed model.

The data in Table 3 shows that models 1 to 8 have a $F_{ratio} > 1$ while models 9 and 10 have a $F_{ratio} < 1$. Based on this F_{ratio} value, only models 1 to 8 have the null hypothesis rejected. Thus, only models 1 to 8 have descriptors that significantly affect the goodness of fit as a whole.

The goodness of fit in this model can be seen from the coefficient of determination (R^2) value. This value shows the proportion of the value of the variation of biological activity that can be explained by the predicted results of the model (OECD, 2007). The higher value of R^2 (closer to 1 or -1) can be obtained if the data distribution gets closer to the trend line. In linear regression, it indicates the stronger the linear relationship between the dependent variable and the independent variable. Thus, the value of R^2 can be a requirement that the model meets the goodness of fit in multiple linear regression. The criteria for the model selected based on the value of R^2 is a model with a value of $R^2 \geq 0.6$. The value of $R^2 \geq 0.6$ can be interpreted that the model can explain 60% of the variation in biological activity. Judging from the R^2 value, only models 1 to 8 meet these criteria (model 9 and model 10 do not meet the criteria).

However, the value of R^2, in general, tends to increase when the number of independent variables (descriptors) increases, even though it does not contribute a significant effect. Therefore, another parameter is needed for correction, namely adjusted R^2 (R^2_{adj}). R^2_{adj} is the value of R^2 that has been adjusted or corrected concerning the number of descriptors. This value will decrease if additional descriptors have no significant effect (OECD, 2007). The difference between the accepted values of R2 and R2adj is less than 0.3 (Veerasamy et al., 2011). All models (1-8) have a difference R^2 value and R^2_{adj} smaller than 0.3. Therefore, the number of descriptors used in the model is still acceptable.

A p-value analysis was carried out to see the descriptors that had a significant effect on the compound's activity, and the results are presented in Table 4. Based on Table 4, each descriptor model 6, model 7, model 9, and model 10 has a p-value descriptor < 0.05. Because model 9 and model 10 have a value of $R^2 \geq 0.6$, if the p-value requirements are combined with the R^2 value requirements, only model 6 and model 7 meet the R2 value and p-value criteria.

Models 6 and 7 of this study, compared with the previous model (Ketabforoosh et al., 2013), show that these two models have a better level of goodness of fit (Table 5). Models 6 and 7 have $R^2 \geq 0.6$, while the previous model has $R^2 \leq 0.6$. Model 6 uses MDEC22, MDEC23, JGI1, LogP, and BM descriptors. Model 7 uses MDEC22, MDEC23, JGI1, and BM descriptors, while the previous research model uses GATS1e and GATS3v. It indicates that the selection of the descriptor type can affect the quality of the obtained QSAR model. The goodness of fit level is very closely related to the significance of the descriptor effect as the independent variable and activity as the dependent variable. The higher fit in models 6 and 7 compared to the previous model indicates that the descriptor used in models 6 and 7 has a more significant effect than the descriptor in the previous model.

Table 4. Regression coefficient and p-value data from ten QSAR equation models

Model	1		2		3		4		5	
	Coefficient	**p-value**	**Coefficient**	**p-value**	**Coefficient**	**p-value**	**Coefficient**	**p-value**	**Coefficient**	**p-value**
Intercept	-9.940	0.211	-9.275	0.164	-10.984	0.005	-8.952	0.002	-8.441	0.003
MDEC22	0.525	0.024	0.501	0.005	0,.523	0.001	0.452	0.000	0.433	0.000
MDEC23	-0.789	0.039	-0,.759	0.018	-0.816	0.001	-0.669	0.000	-0.633	0.000
SlogP	-0.063	0.842	-	-	-	-	-	-	-	-
JGI1	83.418	0.065	78.601	0.024	86.361	0.000	83.469	0.000	80.362	0.000
JGI8	262.317	0.250	260.266	0.221	229.392	0.194	78.026	0.123	64.409	0.217
JGI10	207.046	0.395	204.134	0.368	167.397	0.360	-	-	-	
Hydrating Energy	0.058	0.750	0.054	0.750	-	-	-	-	-	-
LogP	-0.575	0.211	-0.532	0.155	-0.442	0.046	-0.376	0.061	-0.417	0.051
BM	0.009	0.138	0.008	0.051	0.008	0.032	0.006	0.025	0.007	0.023
Dipole Moment	0.022	0.546	0.025	0.377	0.026	0.328	0.038	0.126	-	-

Model	6		7		8		9		10	
	Coefficient	***p-value***	**Coefficient**	***p-value***	**Coefficient**	***p-value***	**Coefficient**	***p-value***	**Coefficient**	***p-value***
Intercept	-9.639	0.001	-6.548	0.005	-4.982	0.054	4.289	6.27E-09	4.530	4.6E-10
MDEC22	0.478	0.000	0.352	0.000	0.319	0.001	0.053	1.60E-01	-	-
MDEC23	-0.691	0.000	-0.603	0.000	-0.419	0.001	-0.054	5.21E-02	-0.025	1.6E-01
SlogP	-	-	-	-	-	-	-	-	-	-
JGI1	89.760	0.000	66.870	0.000	59.376	0.001	-	-	-	-
JGI8	-	-	-	-	-	-	-	-	-	-
JGI10	-	-	-	-	-	-	-	-	-	-
Hydrating Energy	-	-	-	-	-	-	-	-	-	-
LogP	-0.463	0.033	-	-	-	-	-	-	-	-
BM	0.008	0.006	0.008	0.011	-	-	-	-	-	-
Dipole Moment	-	-	-	-	-	-	-	-	-	-

Table 5. Results of statistical analysis of model 6, model 7, and previous research

Statistical Parameters	Model 6	Model 7	Previous Model*	Criteria
F_{rasio}	4,499	3,682	1,447	>1
R^2	0,853	0,783	0,415	≥ 0,6
R^2_{adj}	0,792	0,716	0,337	-
(R^2 - R^2_{adj})	0,061	0,067	0,078	< 0,3

Note: *Model according to Ketabforoosh *et al.* (2013)

Based on Table 5 and Table 4, two models of QSAR equations that meet these criteria can be drawn up: Equation (2) and Equation (3).

$$\boldsymbol{pIC_{50}} = -9{,}639 + 0{,}478\boldsymbol{MDEC22} - 0{,}691\boldsymbol{MDEC23} + 89{,}760\boldsymbol{JGI1} - 0{,}463\boldsymbol{logP} - 0{,}008\boldsymbol{BM} \quad (2)$$

$$\boldsymbol{pIC_{50}} = -6{,}548 + 0{,}352\boldsymbol{MDEC22} - 0{,}603\boldsymbol{MDEC23} + 66{,}870\boldsymbol{JGI1} - 0{,}008\boldsymbol{BM} \quad (3)$$

The QSAR model in Equation 2 contains a logP descriptor, while the QSAR model in Equation 3 does not contain a logP descriptor. The logP coefficient in Equation 2 is negative. If the logP is positive, the greater the logP value will result in a lower pIC_{50} activity value. On the other hand, if the logP is negative, the larger the logP value, the higher the pIC_{50} activity value. A positive logP value indicates the compound tends to be in a non-polar phase (hydrophobic). Conversely, a negative logP value indicates that the compound tends to be more soluble a in polar phase (hydrophilic). Thus, for non-polar compounds, is there a tendency that increasing the logP value will decrease the activity (pIC_{50}) of CAPE derivatives. On the other hand, for polar compounds, there is a tendency that increasing the logP value (which is negative) will increase the activity (pIC50) of CAPE derivatives. Thus, this logP parameter becomes particularly important in the design or development of CAPE derivative compounds, considering that CAPE compounds can be developed into polar or non-polar compounds (Hashimoto et al., 2021).

The QSAR model of equation (2) and equation (3) show that the JGI1 descriptor is the descriptor that has the most positive influence on the pIC_{50} value than the other descriptors. It indicates that the 1-Ordered Mean Topological Charge index is also important to consider in the design of CAPE-derived compounds with high potential as colorectal anticancer HT-29 cells.

3.3. Model Validation

The estimation of the two QSAR models' predictive power (equation (2) and equation (3)) was carried out using the LOO cross-validation technique test. The validity criterion used is that a model is said to be valid if the value of Q^2(LOO) > 0.5 (Veerasamy et al., 2011). The validation test results on Model 6 and Model 7 show that Model 6 has a Q^2(LOO) value of 0.702 while Model 7 has a Q^2(LOO) value of 0.569. Thus, these two models can be declared valid based on the Q^2(LOO) criteria.

In addition to estimating how robust the model predictions are for new compounds that are not in the data, the Q^2 value can also be used as a reference to assess the possibility of overfitting. This value can also be an indication of overfitting in the model, which is characterized by the difference between R^2 and Q^2 > 0.3 (Veerasamy et al., 2011). Based on Q^2 and R^2 values, it can be seen that model 6 has a Q^2 and R^2 difference of 0.151, while model 7 has a Q^2 and R^2 difference of 0.214. Therefore, it can be declared that there is no overfitting in model 6 and model 7.

Based on the Q^2(LOO) internal cross-validation test, it appears that model 6 and model 7 meet the criteria as valid models. However, if viewed from the value of the F_{ratio} and R^2, it appears that model 6 is better than model 7. In addition, model 6 has a PRESS value of 0.516 while model 7 was 0.745. It indicates that the addition of the hydrophobicity descriptor (logP) can improve the quality of the CAPE compound QSAR model as an anticancer HT-29. The comparison of the quality of model 6 (Equation (2)) and model 7 (Equation (3)) can be seen in the scatter diagram of the predicted activity value versus the

experimental activity value in Fig. 2. Fig. 2 shows that the goodness of fit level of model 6 is better than model 7.

Fig. 3 shows a comparison diagram of the predicted activity values of model 6 and model 7, which are very close to the experimental values. Fig. 3 also shows that model 6 has a predictive activity value closer to the experimental activity value than model 7. Overall, it can be stated that model 6 and model 7 are models that meet the Q^2(LOO) validity criteria, but model 6 has highest goodness of fit level than model 7. Based on Table 3, model 6 has a correlation coefficient value (r) of 0.924 while model 7 has a correlation coefficient value of 0.885. Thus, Equation (2) (derived from model 6) tends to have better predictive ability than Equation (3) (from model 7).

Based on Equation (2), to obtain CAPE-derived compounds with higher colorectal anticancer activity in HT-29 cells, new compounds can be developed by: increasing the value of the MDEC22 descriptor and increasing the value of JGI1 or decreasing the value of the MDEC23 descriptor. It should be noted that the derivatization in the production of new compound will generally result in a larger molecular weight even though the effect is relatively small, so the addition of a new group or side chain should not be too large. The design of new CAPE-derived compounds must also pay attention to molecular polarity. For non-polar compounds, a decrease in the logP value will tend to increase activity. On the other hand, for polar compounds, an increase in the logP value will increase the activity (pIC_{50}) of CAPE derivatives.

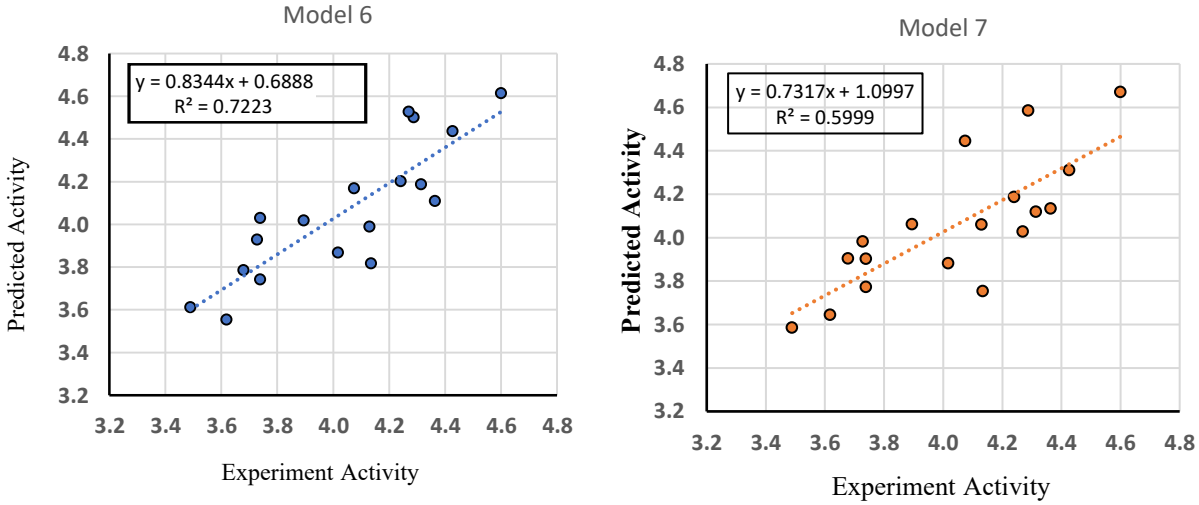

Figure 2. Scatter diagram of the relationship between the value of experimental activity vs. the predicted activity from the QSAR model Equation (2) and Equation (3).

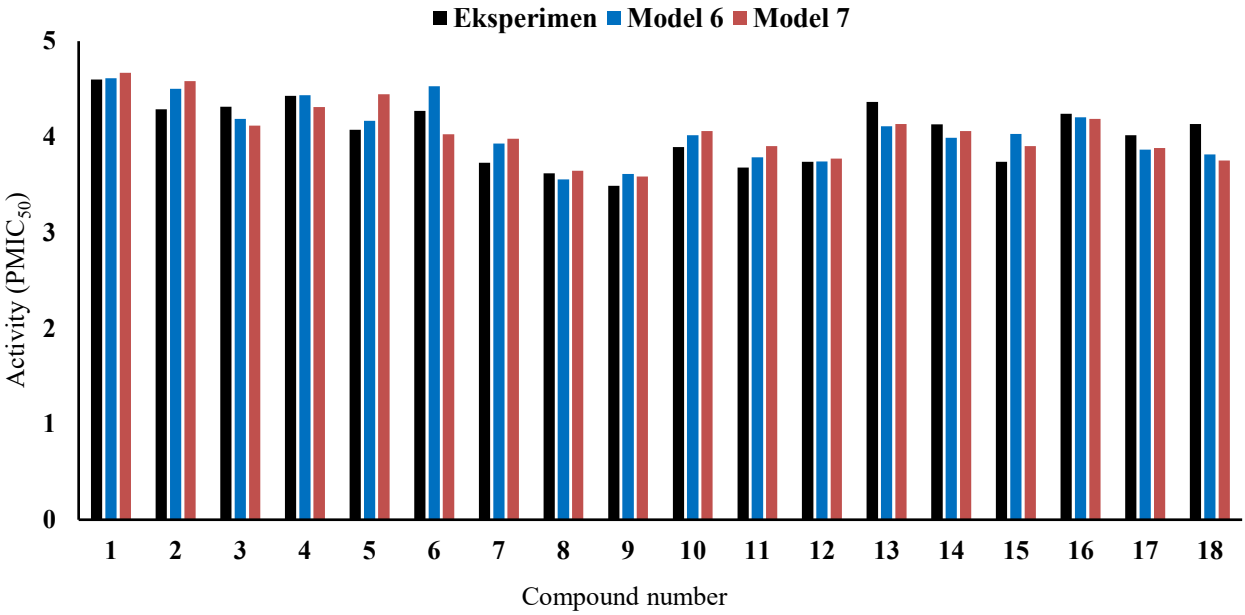

Figure 3. The predictive activity value of the QSAR model Equation 2 and the QSAR model Equation 3 are compared with the experimental activity values.

4. CONCLUSIONS

Based on the data from the research and discussion described, it can be concluded that by using four descriptors, namely MDEC22, MDEC23, JGI1, and BM, the QSAR model meets the validity criteria of Q^2(LOO). The addition of the LogP hydrophobic factor descriptor also resulted in an QSAR model that met the Q^2(LOO) validity criteria. The development of the QSAR model by adding the LogP descriptor resulted in the 5 descriptor QSAR model with higher goodness of fit level than the QSAR model without the LogP descriptor. Based on the goodness of fit and the validity of Q^2(LOO), these two QSAR models have the potential to be used as predictors or aids in the development of a new class of CAPE compounds as anticancer against HT-29 cells with higher activity.

LIST OF REFERENCES

American Cancer Society. (2020). *General Counsel American Cancer Society. Inc*. Atlanta, Georgia.

Galves, J., R. Garcia, M. T. Salabert, R. Soler. (1994). Charge Indexes New Topological Descriptors. *Journal of Chemical Information and Modeling*, *34*(3): 520-525.

Golbraikh A., Shen M., Xiao Z., Xiao Y.D., Lee K.H. & Tropsham A. (2003). Rational selection of training and test sets for the development of validated QSAR models. *Journal of Computer-Aided Molecular Design, 17*, 241–253. *https://doi.org/10.1023/:1025386326946*

Hashimoto R, Lai H, Fujita R, Hanaya K, Higashibayashi S, Inoue H, & Sugai T. (2021). *Global Cancer Observatory: Cancer Today*. Chemoenzymatic semisynthesis of caffeic acid β-phenethyl ester, an antioxidative component in propolis, from raw coffee bean extract. Bioscience, Biotechnology, and Biochemistry, 85 (3),476-480. *https://doi.org/10.1093/bbb/zbaa077*

Kabała-Dzik, A., Rzepecka-Stojko, A., Kubina, R, Jastrzebska-Stojko Z., Stojko, R., Wojtyczka, R.D., and Stojko, J. (2017). Comparison of Two Components of Propolis: Caffeic Acid (CA) and Caffeic Acid Phenethyl Ester (CAPE) Induce Apoptosis and Cell Cycle Arrest of Breast Cancer

Cells MDA-MB-231. *Molecules*, *22*(1554), 1-15.

Katzung, B. G., S. B. Masters & A. J. Trevor. (2013). Farmakologi Dasar & Klinik. EGC, Jakarta.

Ketabforoosh S.H.E., Amini M, Vosooghi M, Shafiee A, Azizi E. & Kobarfard F. (2013). Synthesis, evaluation of anticancer activity and QSAR study of heterocyclic esters of caffeic acid. *Iranian Journal of Pharmaceutical Research*, *12*(4), 705–719.

OECD. (2007). *Guidance Document On the Validation of (Quantitative) Structure-Activity Relationships [(Q)SAR] Models*. Organisation de Coopération et de Développement Economiques, France.

Roy, K., S. Kar & R. N. Das. (2015). *A Primer on QSAR/QSPR Modeling Fundamental Concepts*. Springer, New York.

Rocha, G. B., R. O. Freire, A. M. Simas & J. J. P. Stewart. (2006). RM1: A Reparameterization of AM1 for H, C, N, O, P, S, F, Cl, Br and I. *Wiley InterScience, 27*(10),1101-1111.

Siswandono. (2016). *Kimia Medisinal Jilid 1*. Airlangga Universitas Press, Jakarta.

Todeschini, R. & V. Consonni. (2000). *Handbook of Molecular Descriptor*. Wiley-VCH, Germany.

Veerasamy, R., H. Rajak, A. Jain, S. Sivadasan, C. P. Varghesel & R. K. Agrawal. (2011). Validation of QSAR Models Strategies and Importance. *International Journal of Drug Desain and Discovery, 2*, 511-519.

Wadhwa, R., Nigam, N., Bhargava, P, Dhanjal, J.K., Goyal, S, Grover, A., Sundar, D., Ishida, Y., Terao, K., Kau, S. (2016). Molecular characterization and enhancement of anticancer activity of caffeic acid phenethyl ester by γ cyclodextrin. *Journal of Cancer*, *7*(13), 1755–1771. *https://doi. org/10.7150/jca.15170*

Wildman, S. A. & G. M. Crippen. (1999). Prediction of Physicochemical Parameters by Atomic Contributions. *J.Chem.Inf.Comput.Sci, 39*(5), 868-873. *https://doi.org/10.1021/ci990307l*

JURNAL ILMIAH BERKALA SAINS DAN TERAPAN KIMIA

Jurnal Ilmiah Berkala: Sains dan Terapan Kimia
Vol. 16 No. 2, July 2022

Study of Microstructure and Optical Properties of Fe_2O_3/TiO_2 Composites as Functional Materials

Studi Mikrostruktur dan Sifat Optik Komposit Fe_2O_3/TiO_2 sebagai Material Fungsional

Rendy Muhamad Iqbal[1,2)], Erwin Prasetya Toepak[1)], Dyah Ayu Pramoda Wardani[1)], Elda Alyatikah[1)], Stevin Carolius Angga[1)], Luqman Hakim[3)]

[1)]Department of Chemistry, Faculty of Mathematic and Natural Science, Universitas Palangka Raya, Kampus UPR Tunjung Nyaho, Palangka Raya, 73111, Indonesia
[2)]Division of Natural and Applied Science, Center for Science, Technology and Peat Innovation, Universitas Palangka Raya, Palangka Raya, 73111, Indonesia
[3)]Department of Physic, Faculty of Mathematic and Natural Science, Universitas Palangka Raya, Kampus UPR Tunjung Nyaho, Palangka Raya, 73111, Indonesia

Email: iqbal.rm@mipa.upr.ac.id

ABSTRACT

Semiconductors have conductivity levels between insulators and conductors which can be applied in various fields such as photocatalytic, adsorption, and Dye Sensitizer Solar Cell (DSSC). However, some semiconductors are only active under ultraviolet light, therefore to improve their utilization, modifications are made by producing a hybrid combination of two or more materials or dopping materials. This study aims to obtain a semiconductor material with a low band gap energy from the Fe_2O_3/TiO_2 composite material. Fe_2O_3/TiO_2 composites were synthesized by the solid-state method and characterized by XRD, SEM-EDX, and UV-Vis. The characterization using XRD showed the peak intensity of TiO_2 and Fe_2O_3. The morphology of the material obtained using SEM-EDX showed an even distribution of particle size, as well as the distribution of Ti, Fe, and O elements. The optical properties of the composite showed strong absorbance in the UV region for higher TiO_2 compositions. On the other hand, composite materials with a higher Fe_2O_3 composition showed stronger absorbance in the visible light region.

Keywords: Fe_2O_3, microstructure, optic, TiO_2.

ABSTRAK

Semikonduktor adalah material dengan tingkat konduktivitas di antara material isolator dan konduktor yang dapat diaplikasikan dalam berbagai bidang seperti fotokatalitik, adsorpsi, Dye Sensitizer Solar Cell (DSSC) dan masih banyak lagi. Namun, beberapa semikonduktor hanya aktif dibawah sinar ultraviolet, sehingga untuk meningkatkan kinerja material semikonduktor dalam pemanfaatannya, umumnya dilakukan modifikasi berupa pembuatan komposit yakni kombinasi dua atau lebih material maupun material dopping. Penelitian ini bertujuan untuk membuat material komposit Fe_2O_3/TiO_2 untuk mendapatkan material semikonduktor dengan energi celah pita yang rendah. Material komposit Fe_2O_3/TiO_2 disintesis dengan metode solid state yang kemudian dikarakterisasi dengan XRD, SEM-EDX dan UV-Vis. Hasil karakterisasi menggunakan XRD menunjukkan adanya intensitas puncak dari TiO_2 dan Fe_2O_3. Morfologi material yang diperoleh menggunakan SEM-EDX menunjukkan distribusi ukuran partikel yang merata, serta sebaran unsur Ti, Fe dan O. Sifat optik dari komposit menunjukkan absorbansi yang kuat di daerah sinar UV untuk komposisi TiO_2 yang lebih tinggi. Sebaliknya, material komposit dengan komposisi Fe_2O_3 yang lebih tinggi menunjukkan absorbansi yang lebih kuat di daerah sinar tampak.

Keywords: Fe_2O_3, mikrostruktur, optik, TiO_2.

Received: December 9, 2021; **Accepted**: July 9, 2022: **Available online**: July 31, 2022

1. INTRODUCTION

Based on its ability to conduct electric current, a material can be divided into three types: conductors, insulators, and semiconductors. The structure of their band gap energies reveals the difference between the three materials. Semiconductors are substances with electrical conductivity between insulators and conductors and an energy gap between 0 and 4 eV. (Aminullah et al. 2019). Some semiconductor materials are metal oxides such as TiO_2, SnO_2, CuO, CaO, Fe_2O_3, and Fe_3O_4.

TiO_2 and Fe_2O_3 are semiconductor materials that are commonly found and used in various fields. TiO_2 (titanium dioxide) is a semiconductor material that is widely studied because of its good optical and electronic properties. In addition, this material has long-term stability, strong oxidation strength, low cost, and non-toxicity. Structurally, TiO_2 has three crystalline phases: anatase, rutile, and brochite. Anatase and rutile have a tetragonal crystal structure, while brookite has an orthorhombic crystal structure. The anatase and brookite phases are metastable phases that easily change to the rutile phase when heated. The band gap energy value of TiO_2 in the anatase phase is 3.2 eV, while in the rutile phase, it is 3.0 eV (Listanti et al. 2018). Some applications of TiO_2 include sensors, solar cells, photocatalysts, and health products.

Fe_2O_3 is known as hematite with a rhombohedral crystal structure. Fe_2O_3 is resistant to chemical reactions and temperature, environmentally friendly, widely used in semiconductor applications, and can absorb light (Nurrahmawati 2019). Fe_2O_3 can be used as a catalyst, gas sensor, solar cell, pigment, and lithium-ion battery.

The application of semiconductor materials such as photocatalytic generally requires specific criteria to achieve the optimal activity, both from the band gap energy factor or others. Researchers often combine two or more materials by dopping, composite manufacturing, and carriers to achieve this goal. Composite manufacturing is easier to conduct because it does not damage the basic structure of the material and is produced through physical reactions (Iqbal et al. 2020). The synthesized Fe_2O_3/TiO_2 composite was carried out to obtain optimal band gap energy to achieve the good photocatalytic activity, including degrading indigo carmine dye waste (Lubis et al. 2019) and methyl orange (Koohestani 2019).

In addition to optical properties, microstructural characteristics are important indicators of the material's identification. Microstructural characteristics can be in the form of diffraction patterns, elemental mapping, morphology, and topography. These aspects determine the physical characteristics of the material (Hasa 2007). Therefore, in this study, an assessment of the microstructure and optical properties of Fe_2O_3/TiO_2 composites was carried out.

2. MATERIALS AND METHODS

2.1. Materials

The materials used were TiO_2 (Merck, 99%), Fe_2O_3 (Merck, 99%), and methanol (Aldrich, 99%). The tools used were glassware, magnetic stirrer, oven, furnace, Panalytical XRD, SEM-EDX, and UV-Vis Diffuse Reflectance spectrophotometer Shimadzu-2450.

2.2. Methods

Fe_2O_3 and TiO_2 were mixed in a beaker with a ratio of 1, 2, 3, and 4. About 50 mL of methanol was added and stirred for 2-3 hours until homogeneous. The homogeneous mixture was allowed to stand at room temperature to obtain a Fe_2O_3/TiO_2 composite precipitate. The precipitate was separated, then dried in an oven at 90°C for 1 hour to evaporate the remaining methanol. Then it was calcined at 500°C for 1 hour. The obtained solids were characterized by XRD, SEM-EDX, and UV-Vis.

3. RESULTS AND DISCUSSION

The microstructure study of the Fe_2O_3/TiO_2 composite with mass ratios of 1, 2, 3, and 4 (Fig. 1) shows the diffraction pattern of the material according to JCPDS No. 21-1272 for TiO_2 and JCPDS No. 39-1346 for Fe_2O_3. The diffractogram identified peaks appearing at 25°, 32°, 47°, 53°, and 63° as TiO_2 peaks, and Fe_2O_3 peaks at 33°, 35°, 40°, 49°, and 62°. The combination of peaks that appear in one diffraction pattern indicates that the material

synthesis was successful. The mass ratio also affects the peak intensity. As shown in Fig. 1, the peak intensity of TiO_2 decreases as the amount of Fe_2O_3 increases.

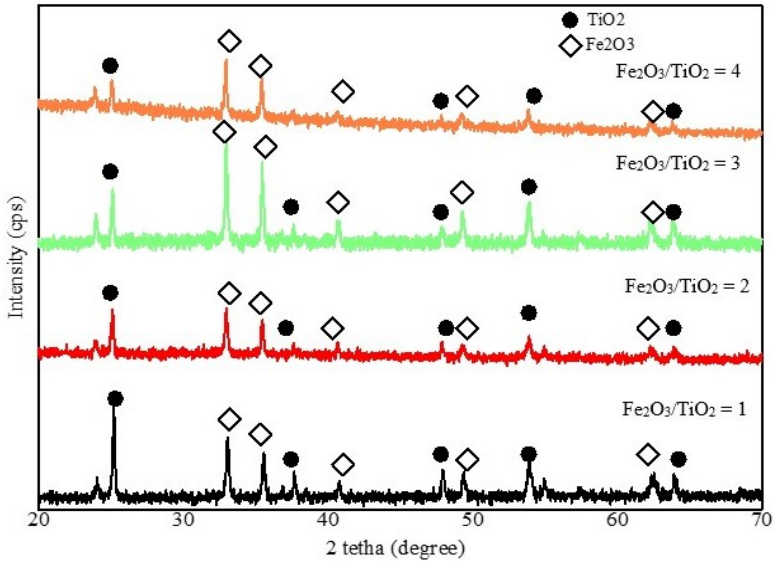

Figure 1. Diffraction pattern of Fe_2O_3/TiO_2 composite

The microstructural characteristics of the material are also supported by SEM-EDX data which shows the morphology and distribution of Fe_2O_3/TiO_2 composite elements (Fig. 2 and Fig. 3). Fig. 2(a) shows the composite morphology of Fe_2O_3/TiO_2 with a ratio of 1, and Fig. 2(b) with a ratio of 3. Both samples showed a uniform morphology. It indicates that the material synthesis was proceeding smoothly. Fig. 3 shows the distribution of Ti, Fe, and O elements of the Fe_2O_3/TiO_2 composite. Element O is indicated by the intensity of the bright blue color, which is relatively evenly distributed, but there are dark areas that are poor in oxygen. Fe elements are identified by red color and Ti by green color. It indicates a good distribution of the two elements.

The Fe_2O_3/TiO_2 composite's optical characteristics were identified by a UV-Vis instrument. Fig. 4 shows the difference in absorbance of Fe_2O_3/TiO_2 composite materials to light wavelengths at different ratios. Fe_2O_3/TiO_2 composites with a ratio of 1 had absorbance at a wavelength of around 300-600 nm. The Fe_2O_3/TiO_2 composite with a ratio of 4 experienced a shift in absorbance to around 350-650 nm. It can occur because Fe_2O_3 has a band gap energy of 2.2 eV, which is active under visible light, so the combination of Fe_2O_3 and TiO_2 materials can reduce the bandgap energy of TiO_2 (Iqbal et al. 2020).

The increasing amount of Fe_2O_3 in the Fe_2O_3/TiO_2 composite shifts the material's absorbance toward the visible light wavelength region. The absorbance at a given wavelength is inversely proportional to the band gap energy. Visible light has a longer wavelength than UV light, so materials with high absorbance in the visible light wavelength area have a smaller band gap energy value. Therefore, the Fe_2O_3/TiO_2 composite with a ratio of 4 has a smaller band gap energy value than the Fe_2O_3/TiO_2 composite with a ratio of 1 (Iqbal et al. 2020). It is supported by the reflectance data shown in Fig. 5.

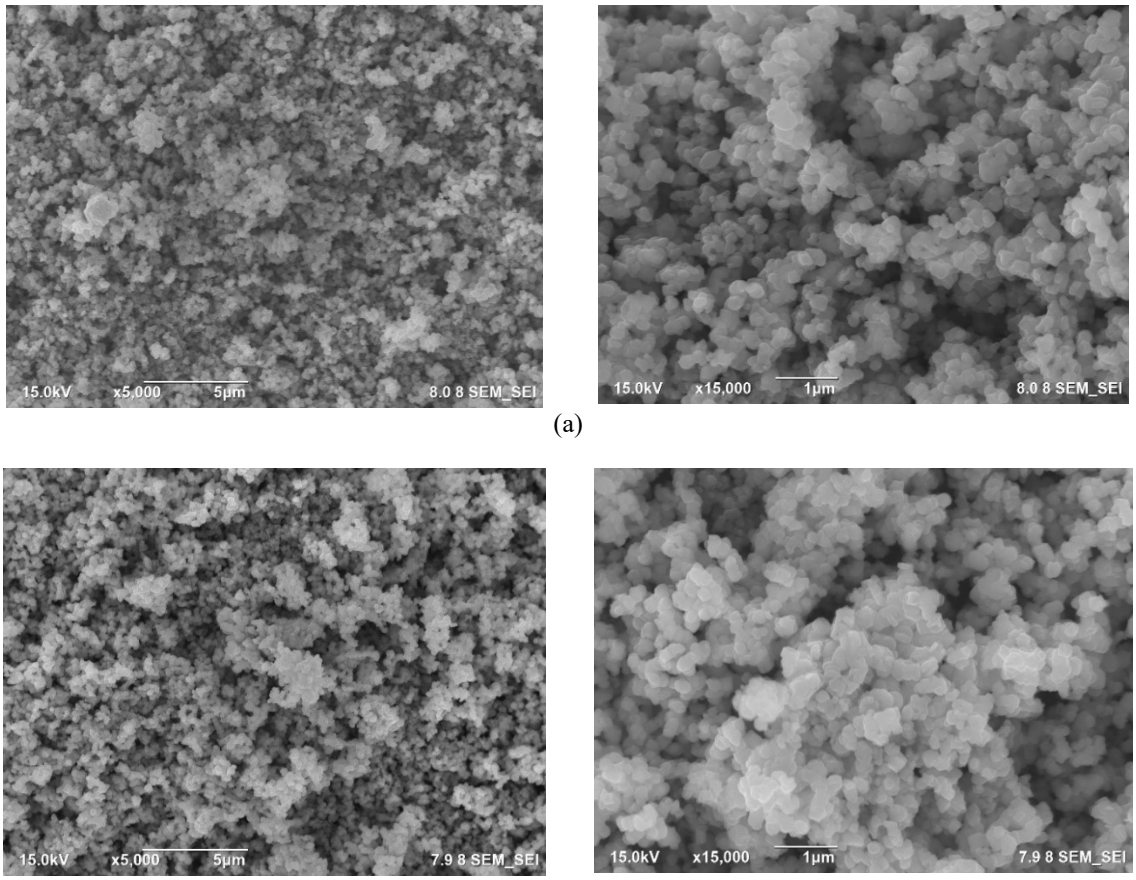

Figure 2. Characterization of Fe_2O_3/TiO_2 composites using SEM with mass ratios (a) 1 and (b) 3

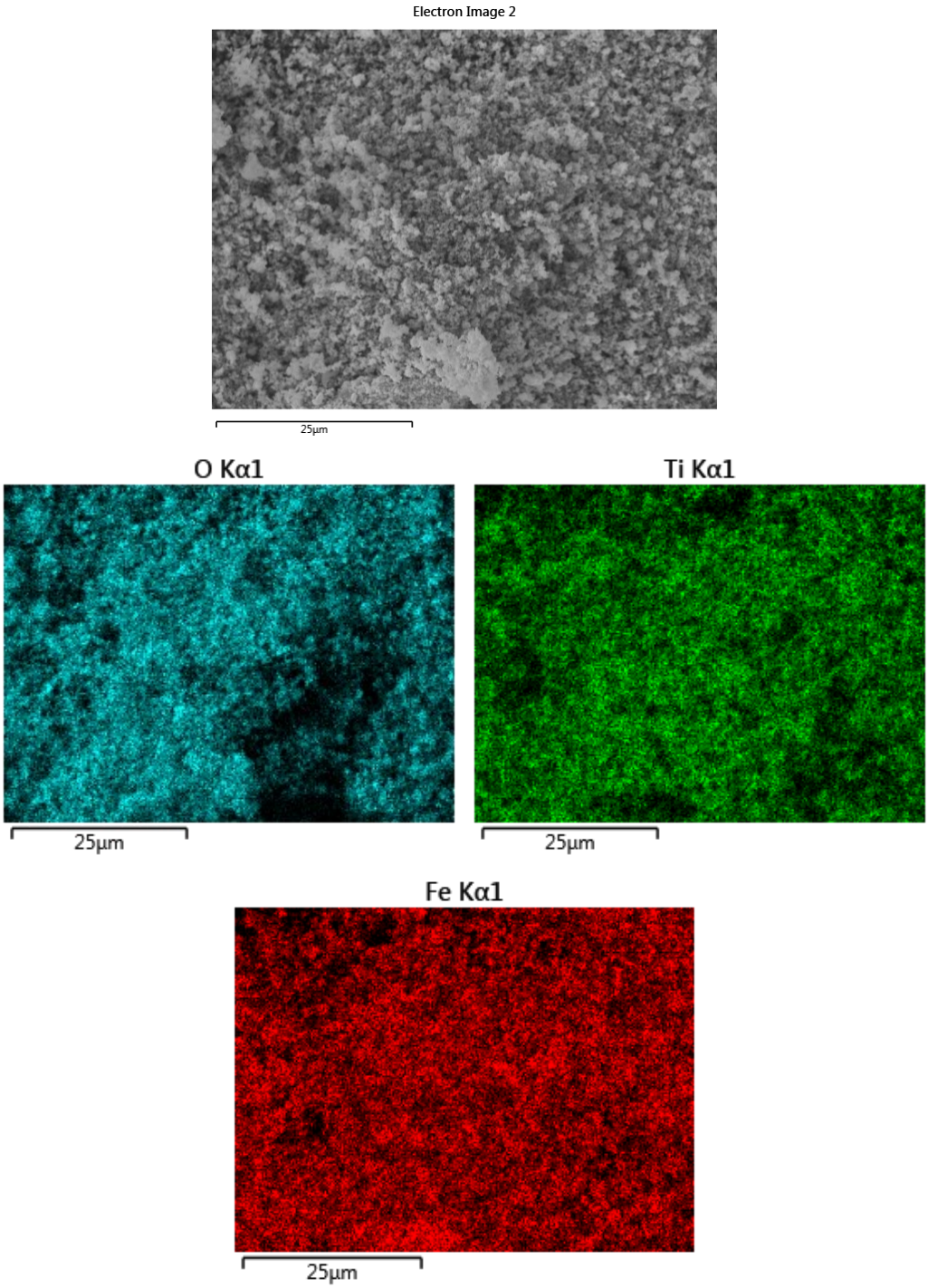

Figure 3. Distribution of Ti, Fe, and O elements in Fe_2O_3/TiO_2 composites

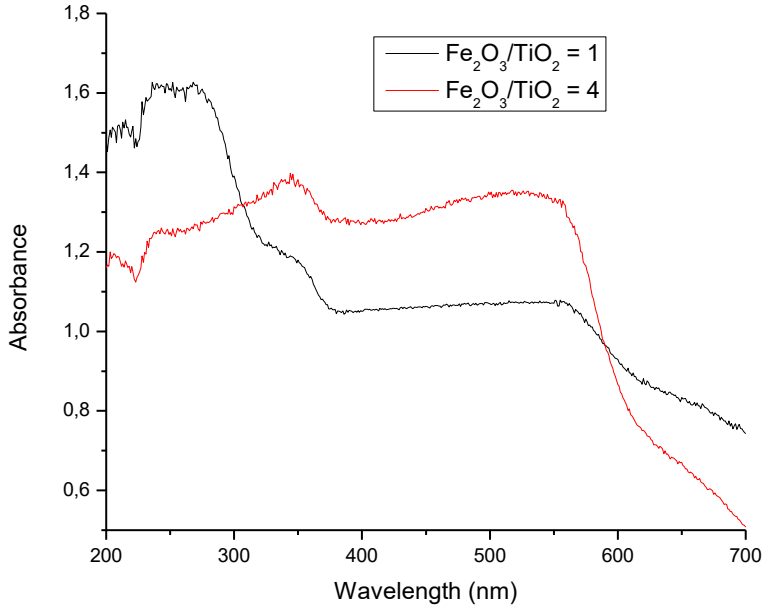

Figure 4. Absorbance spectra to the wavelength of Fe_2O_3/TiO_2 composites

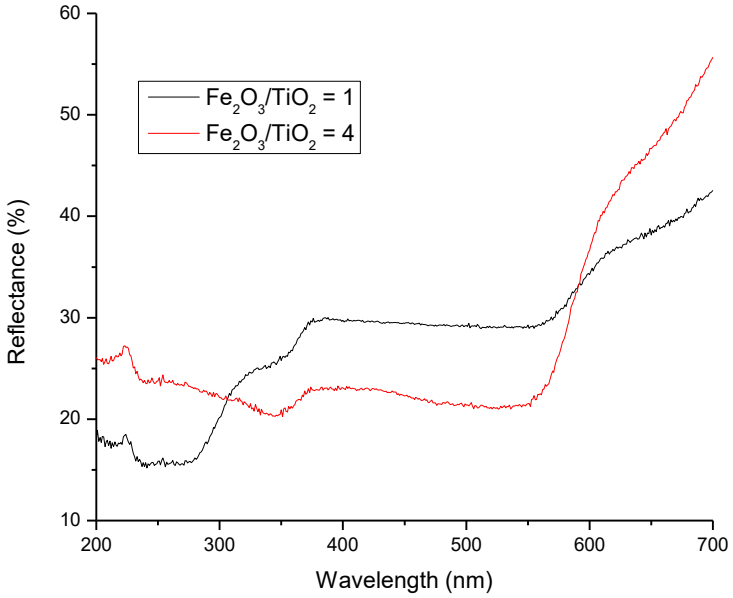

Figure 5. Reflectance spectra to the wavelength of Fe_2O_3/TiO_2 composites

4. CONCLUSIONS

The Fe_2O_3/TiO_2 composite had good microstructural characteristics based on the diffraction pattern, which showed conformity with JCPDS No. 21-1272 for TiO_2 and JCPDS No. 39-1346 for Fe_2O_3. Characterization using SEM-EDX showed good particle uniformity and elemental distribution. In addition, the optical characteristics of Fe_2O_3/TiO_2 composites indicate the absorbance of the material visible light wavelengths as the amount of Fe_2O_3 increases.

ACKNOWLEDGMENT

The authors acknowledge the LPPM Palangka Raya University for financial assistance "Basic Research Innovative Fiscal Year 2021" with contract number 307/UN24.13/PL/2021.

LIST OF REFERENCES

Aminullah, M. W., Setiawan, H., Huda, A., Samaulah, H., Haryati, S., & Bustan, M. D. (2019). Pengaruh Komposisi Material Semikonduktor Dalam Menurunkan Energi Band Gap Terhadap Konversi Gelombang Mikro. *Jurnal EECCIS*, *13*(2), 65-70.

Al Hasa, M. H. (2013). Karakterisasi Sifat Mekanik dan Mikrostruktur Paduan Intermetalik AlFeNi sebagai Bahan Kelongsong Bahan Bakar. *Jurnal Teknologi Bahan Nuklir*, *3*(2), 86–96.

Iqbal, R. M., Wardani, D. A. P., Hakim, L., Damsyik, A., Safitri, R., & Fansuri, H. (2020). The Structural and Optical Band Gap Energy Evaluation of TiO_2-Fe_2O_3 Composite. In *IOP Conference Series: Materials Science and Engineering*. *833*(1). https://doi:10.1088/1757-899X/833/1/012072

Koohestani, H. (2019). Synthesis and characterisation of TiO_2 Nanoparticles/Fe_2O_3 Waste Chips Composite. *Micro & Nano Letters*, *14*(6), 678-682. https://doi.org/10.1049/mnl.2018.5583

Listanti, A., Taufiq, A., Hidayat, A., & Sunaryono, S. (2018). Investigasi Struktur dan Energi Band Gap Partikel Nano TiO_2 Hasil Sintesis Menggunakan Metode Sol-Gel. *JPSE (Journal of Physical Science and Engineering)*, *3*(1), 8-15. http://dx.doi.org/10.17977/um024v3i12018p008

Lubis, S., Lelifajri, Sheilatina, & Ihsan, K. (2019). High Photocatalytic Activity of TiO_2/Fe_2O_3 Nanocomposite Prepared by Impregnation Method For Degradation of Indigo Carmine. *IOP Conference Series: Earth and Environmental Science*, *364*(1), 1–7. https://doi:10.1088/1755-1315/364/1/012014

Nurrahmawati, P. (2019). *Pengaruh Penambahan Al_2O_3 dan Fe_2O_3 pada SiO_2 Ekstraksi Lumpur Sidoarjo sebagai Dielektrik dan Penghambur Cahaya pada Dye Sensitized Solar Cells (DSSC)*. Doctoral dissertation, Institut Teknologi Sepuluh Nopember.

JURNAL ILMIAH BERKALA SAINS DAN TERAPAN KIMIA

Jurnal Ilmiah Berkala: Sains dan Terapan Kimia
Vol. 16 No. 2, July 2022

Adsorption of Organic Compounds in Leachate using Precipitated Calcium Carbonate (PCC) from Ale-Ale Shells

Adsorpsi Senyawa Organik Pada Lindi Menggunakan *Precipitated Calcium Carbonate* (PCC) dari Cangkang Kerang Ale-Ale

Yulistya Vidyaning Maulidya[1], Rudiyansyah[1], and Nelly Wahyuni[1]

[1]Program Studi Kimia, Universitas Tanjungpura Pontianak, 78124, Indonesia

Email: nellywahyuni@chemistry.untan.ac.id

ABSTRACT

Leachate waste from piles of garbage in the TPA has a high concentration of chemical oxygen demand (COD). High COD concentrations can cause a decrease in dissolved oxygen concentrations in the waters. Simple leachate treatment is carried out using the adsorption method with adsorbents derived from waste. This research used Precipitated Calcium Carbonate (PCC) adsorbent from Ale-ale shells. This study aims to evaluate the effect of particle size and calcination temperature variations on PCC yield and analyze the adsorption ability of PCC adsorbents in reducing COD concentrations. In addition, PCC was also characterized using an infrared spectrophotometer (FTIR) and an X-ray diffractometer (XRD). Determination of COD concentration was carried out by permanganometric titration. The optimum PCC yield of 57.75% was obtained from Ale-ale shells with a particle size of 40 mesh with a calcination temperature of 800oC. The functional groups in PCC are C-O at wave numbers 713 cm-1, 873 cm-1, and 1403 cm-1. XRD characterization showed the presence of a calcite phase with a high peak intensity at 2θ = 29.38o. The adsorption of organic matter on leachate by PCC (4.5 g/50 mL) with a stirring speed of 200 rpm for 240 minutes reduced the COD concentration of leachate from 1131.28 mg/L to 459.94 mg/L with an adsorption efficiency of 59.61%.

Keywords: adsorption, ale-ale shells, COD, leachate, PCC.

ABSTRAK

Limbah air lindi dari tumpukan sampah yang terdapat di TPA memiliki konsentrasi chemical oxygen demand (COD) yang tinggi. Dampak yang ditimbulkan dari tinggi nya konsentrasi COD tersebut adalah terjadi penurunan konsentrasi oksigen terlarut dalam perairan. Pengolahan lindi secara sederhana dilakukan menggunakan metode adsorpsi dengan adsorben yang berasal dari limbah. Pada penelitian ini digunakan adsorben Precipitated Calcium Carbonate (PCC) dari cangkang kerang ale-ale. Tujuan penelitian ini untuk mengetahui pengaruh variasi ukuran partikel dan suhu kalsinasi dalam pembuatan PCC terhadap rendemen yang dihasilkan serta mengetahui kemampuan adsorpsi adsorben PCC dalam menurunkan konsentrasi COD. Selain rendemen hasil, PCC yang dihasilkan juga dikarakterisasi menggunakan spekrofotometer infra merah (FTIR) dan difraktometer sinar-X (XRD). Penentuan konsentrasi COD dilakukan secara titrasi permanganometri. Rendemen optimum PCC sebesar 57,75% diperoleh dari cangkang kerang ale-ale ukuran partikel 40 mesh dengan suhu kalsinasi 800^{o}C. Gugus fungsi yang terdapat pada PCC dikarakterisasi menggunakan FTIR yang menunjukkan adanya gugus C-O pada bilangan gelombang 713 cm^{-1}, 873 cm^{-1}, dan 1403 cm^{-1}. Karakterisasi XRD menunjukan adanya fasa kalsit dengan intensitas puncak yang tinggi pada 2θ = 29,38^{o}. Adsorpsi bahan organik pada lindi oleh PCC (4,5 g/50 mL) dengan kecepatan pengadukan 200 rpm selama 240 menit mampu menurunkan konsentrasi COD lindi dari 1131,28 mg/L menjadi 459,94 mg/L dengan efisiensi adsorpsi 59,61%.

Kata Kunci: adsorpsi, cangkang ale-ale, COD, lindi, PCC.

Received: December 21, 2021; **Accepted**: June 26, 2022: **Available online**: July 31, 2022

1. INTRODUCTION

The leachate from TPA Batu Layang, Pontianak, West Kalimantan has a high concentration of COD. It indicates that many organic compounds decompose chemically in water using dissolved oxygen. The more organic compounds that decompose chemically, the lower the dissolved oxygen concentration, which can impact the water quality (Sumantri and Cordova 2011). Leachate is wastewater resulting from the dissolution of dissolved matter caused by the introduction of external water into the waste pile (Peraturan Menteri Pekerjaan Umum RI 2013). Therefore, leachate must be treated to reduce its COD concentration.

The leachate treatment system that has been carried out is to accommodate the leachate temporarily. It is feared that if the garbage pile rots, it will become a breeding ground for bacteria and disease (Sarwono et al.., 2017). In addition, there is a biological leachate treatment using aerobic and anaerobic bacteria to carry out the decomposition process of the leachate. However, this biological leachate treatment produces methane gas and residual sludge that requires further treatment (Said and Hartaja, 2015). Another alternative for leachate treatment is physicochemical treatment employing the adsorption method (Indrayani and Rahmah, 2018).

Adsorption is the removal of dissolved components in a fluid that occurs on the surface of the adsorbent (Setianingsih 2018). The adsorption process is simple and does not generate new pollutants. The adsorbent used in this study was Precipitated Calcium Carbonate (PCC) from Ale-ale shells (*Meretrix meretrix*) from Suka Bangun Village, Ketapang Regency, West Kalimantan. PCC results from a chemical reaction involving $CaCO_3$-containing materials (Jamarun et al., 2007). PCC has a greater degree of purity than other $CaCO_3$-containing materials because it is produced through chemical reaction stages (Erdogan and Eken, 2017). PCC is produced through calcination, hydration, and carbonation. It is believed that PCC adsorbent from Ale-ale shells reduces the COD concentration of leachate. Research conducted by Elystia et al. (2016) using PCC from blood clam shells showed that the adsorbent reduced the concentration of organic compounds in peat water with an adsorption efficiency of 99.86% at a composition of 5 g with a stirring speed of 150 rpm for 30 minutes.

This research used PCC adsorbent from Ale-ale shells. PCC adsorbents were prepared with variations in particle size and calcination temperature. The adsorption process was carried out in batches on an adsorbent mass of 4.5 g/50 mL with a stirring speed of 200 rpm for 240 minutes. This study aims to determine the variation of particle size and optimum calcination temperature on PCC yield in the adsorption of organic compounds in leachate from TPA Batu Layang.

2. MATERIALS AND METHODS

2.1. Materials

The materials used were nitric acid (Merck), oxalic acid (Merck), sulfuric acid (Merck), potassium permanganate (Merck), sodium carbonate (Smart-Lab), and Ale-ale shell waste from Suka Bangun Village, Ketapang Regency, West Kalimantan.

The tools used were various types of beakers, 40, 60, 80, and 100 mesh sieves, hotplate, hammer mill, magnetic stirrer, analytical balance, oven, Fourier Transform Infra-Red (FTIR) spectrophotometer Frontier Perkin Elmer FT-IR, UV-Vis spectrophotometer (UV-2600 Shimadzu), thermometer up to 110°C, and X-Ray Diffraction (XRD) XPERT PRO PANalytical PW30/40.

2.2. Synthesis of Precipitated Calcium Carbonate (PCC) (Azkiya dkk., 2016)

Ale-ale shells were washed, dried with various particle sizes of 40 mesh, 60 mesh, and 80 mesh, and calcined at a temperature of 800°C for 4 hours. A total of 5.6 g of each calcined product was added to a 20 mL beaker glass and added with 6 M HNO_3 and distilled water until the volume reached 200 mL, then stirred using a magnetic stirrer at 700 rpm 65°C for 30 minutes. After that, it was filtered to separate the filtrate and added with 159 mL of 1.5 M Na_2CO_3 solution slowly at a flow rate of 2.5 mL/minute for 60 minutes. The precipitate formed was filtered and washed with distilled water to pH seven and then dried in an oven at 105°C for three hours. The same steps were carried out for variations in calcination temperature of 900°C and

1000°C. The yield of $CaCO_3$ obtained was then calculated using the following equation:

$$\%\ yield = \frac{mass\ of\ product\ obtained}{theory\ mass} x\ 100\% \quad (1)$$

2.3. Adsorbent Characterization

The adsorbent was characterized using XRD instruments to determine the crystalline phase and FTIR to determine the functional groups in the adsorbent.

2.4. Leachate Characterization

The COD concentration of leachate before and after adsorption was analyzed based on SNI 06-6989.22-2004.

2.5. Organic Compound Adsorption in Leachate Using PCC Adsorbent

Adsorption was carried out on 50 mL leachate using 4.5 g of PCC adsorbent. The adsorption process was carried out in batches at 200 rpm for 240 minutes. The resulting filtrate was measured for its COD concentration to determine the efficiency of removing organic compounds from leachate based on equation (2).

$$\%R = \frac{C_{in} - C_{out}}{C_{in}} x100\% \quad (2)$$

3. RESULTS AND DISCUSSION

The preparation of PCC begins with a calcination process that aims to release CO_2 gas and decompose organic components contained in Ale-ale shells to initiate the decomposition of $CaCO_3$ into CaO (Cahyaningrum et al., 2017). The mass of calcined Ale-ale shells decreased from their original state due to releasing CO_2 gas after the calcination process (Amin dan Kurniasih, 2016). CaO obtained from the calcination is hygroscopic, which can absorb moisture from the air after being removed from the furnace (Khaira, 2011). The mass loss after the calcination is presented in Table 1. The reactions that occur in the calcination process follow Equation 1.

$$CaCO_{3(s)} \leftrightarrow CaO_{(s)} + CO_{2(g)} \quad (1)$$

Based on Table 1, the percentage reduction in the mass of Ale-ale shells produced was not significantly different because the time required for the calcination process for four hours was sufficient to decompose $CaCO_3$. It is evidenced in Fig. 1b. The XRD diffractogram produces peaks of CaO and $Ca(OH)_2$ according to ICDD 98-002-6959 for CaO and ICDD 98-020-2228 for $Ca(OH)_2$. The presence of $Ca(OH)_2$ occurs because the hygroscopic CaO has absorbed water vapor from the air. Based on the XRD characterization, the calcination process at 800°C has completely decomposed $CaCO_3$ into CaO, which is indicated by the absence of $CaCO_3$ minerals.

The utilization of HNO_3 as a solvent in the preparation of PCC is a modification of the PCC preparation using the caustic soda method by Azkiya et al. (2016). Modification with acidic solvents could increase the solubility of CaO compared to hydration with H_2O alone. Research by Zikri et al. (2015) in the PCC preparation using HNO_3 as a solvent found that the PCC yield was higher than that of other acid solvents such as HCl and CH_3COOH. Arief dan Jamarun (2009) tested various types of acids (HCl, HNO_3, and $HClO_4$) and found that the highest PCC yield was obtained from using HNO_3. The dissolution of CaO with HNO_3 will produce $Ca(NO_3)_2$ salt, which has a high solubility level to increase the yield of PCC produced (Meilianti 2017). The reaction that occurs follows Equation 2.

$$CaO_{(s)} + 2HNO_{3(aq)} \leftrightarrow Ca(NO_3)_{2(aq)} + H_2O_{(l)} \quad (2)$$

When Na_2CO_3 solution is added to the $Ca(NO_3)_2$ filtrate, the solution gradually becomes cloudy, and the turbidity increases as more Na_2CO_3 solution is added. It indicates the process of crystallization of $CaCO_3$ in a supersaturated solution condition. The reactions that occur are:

$$Ca(NO_3)_{2(aq)} + Na_2CO_{3(aq)} \rightarrow CaCO_3\downarrow_{(s)} + NaNO_{3(aq)} \quad (3)$$

Based on Reaction (3), the $CaCO_3$ product resulting from the precipitation process was the PCC. This study produced PCC with a pH of 12, so it must be washed with distilled water to achieve a neutral pH. $CaCO_3$ was washed with distilled water because the solubility of $CaCO_3$ in water is very small (Perry, 1984). After the pH of $CaCO_3$ was neutral, it was filtered using filter paper whose mass was known to separate the $CaCO_3$. The yield of $CaCO_3$ obtained as PCC is presented in Table 2.

Table 1. Percentage of mass loss

Particle size	Calcination temperature		
	800°C	900°C	1000°C
40 mesh	43.93%	44.36%	44.54%
60 mesh	43.91%	44.30%	44.48%
80 mesh	43.84%	44.16%	44.24%

Table 2. Yield of PCC

Particle size	Calcination temperature		
	800°C	900°C	1000°C
40 mesh	57.75%	57.51%	57.87%
60 mesh	58.20%	57.04%	56.98%
80 mesh	57.70%	58.12%	56.87%

Based on Table 2, the yield of PCC produced is not significantly different from the influence of particle size and calcination temperature. Therefore, the characterization and adsorbents production was carried out on PCC produced from 40 mesh Ale-ale shells with a calcination temperature of 800°C. Based on the diffractogram in Fig. 1c, PCC has a peak of $CaCO_3$ (calcite). It is in accordance with research by Malia (2018) that the crystal phase formed in PCC is calcite. Typical characteristics of calcite based on ICDD 01-076-2712 have a high peak intensity ranging from $2\theta = 29.39°$.

The resulting PCC has a C-O functional group with wave numbers of 1403 cm^{-1}, 873 cm^{-1}, and 713 cm^{-1}, which is in accordance with the interpretation of the functional group in Table 4. C-O at wave numbers 1420 cm^{-1}, 872 cm^{-1}, and 710 cm^{-1}. Based on Fig. 2b, the resulting PCC has a higher degree of purity than the Ale-ale shells, indicated by a sharper peak. PCC in this study functions as an adsorbent due to the attractive force generated by the C-O group. It occurs because of the difference in electronegativity between C and O atoms. Atom O has a greater electronegativity (Atkins et al., 2010). Due to the polarity of the C-O group on PCC, the polar adsorbate will be strongly bound (Hasyim 2015).

The initial COD concentration of the Batu Layang TPA leachate was 1131.28 mg/L. The decrease in COD concentration using PCC adsorbent resulted in an adsorption efficiency of 59.61% with a COD concentration of 456.936 mg/L, followed by an insignificant decrease in color intensity, as shown in Figure 3. The change in color intensity was based on the physicochemical activation process on the PCC adsorbent. According to Rahimawati et al. (2019), there was a decrease in the color intensity of drilled well water using physicochemical activated blood clam shell adsorbents because it can remove impurities that cover the pores of the adsorbent.

Changes in color intensity after adsorption using PCC adsorbent were measured at the maximum wavelength using a UV-Vis spectrophotometer. The maximum wavelength of leachate before adsorption was 254.6 nm, and after adsorption was 241.8 nm (Fig. 4). Based on this, there is a hypochromic shift with a smaller maximum wavelength because there is no auxochrome bound to the chromophore to form hydrogen bonds (Suhartati 2013).

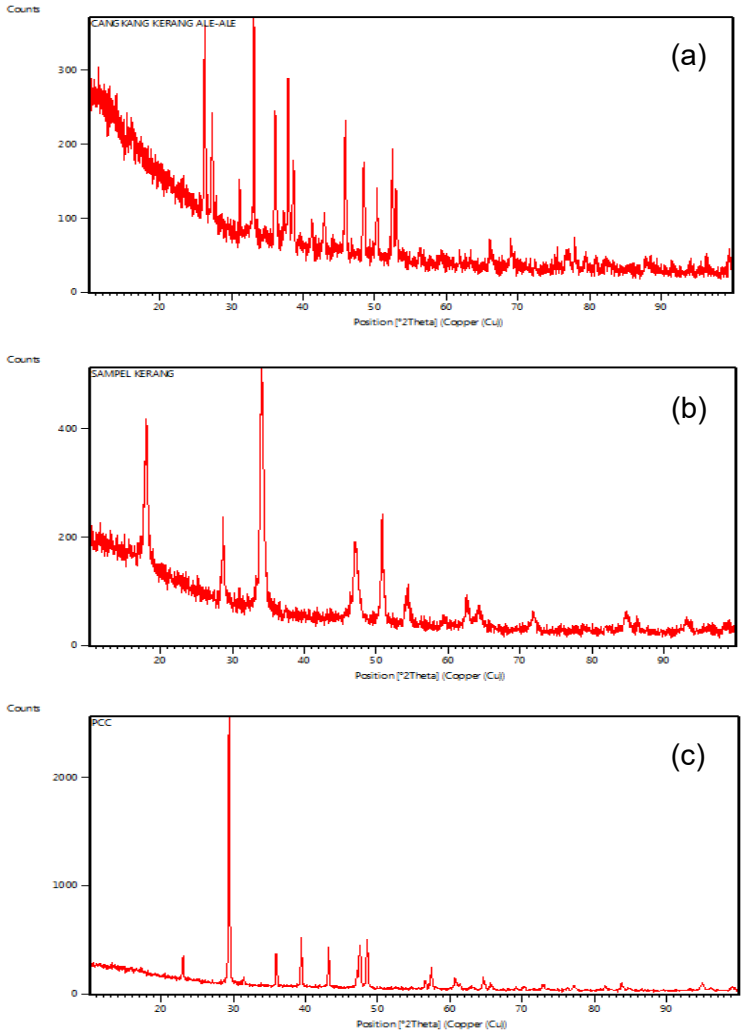

Figure 1. XRD diffractogram (a) Ale-ale shells, (b) 40 mesh Ale-ale shells after calcination at 800°C, and (c) PCC from 40 mesh Ale-ale shells and 800°C calcination temperature

Table 3. Crystal phase interpretation

Sample	Crystal phase	2 θ
Shells of Ale-ale	Aragonit ($CaCO_3$)	26.18°, 27.22°, 33.12°, 36.10°, 45.87°, 48.41°, and 52.42°
Shell of Ale-ale after calcining	Portlandite ($Ca(OH)_2$)	17.97°; 28.66°, 34.06°, 47.08°, 50.77°, 59.37°, 62.44°, 71.90°, and 84.60°
	Lime (CaO)	54.38° and 64.18°
PCC	Calcite ($CaCO_3$)	22.99°, 29.38°, 35.95°, 39.39°, 43.14°, 47.52°, 48.50°, 57.39°, and 64.65°

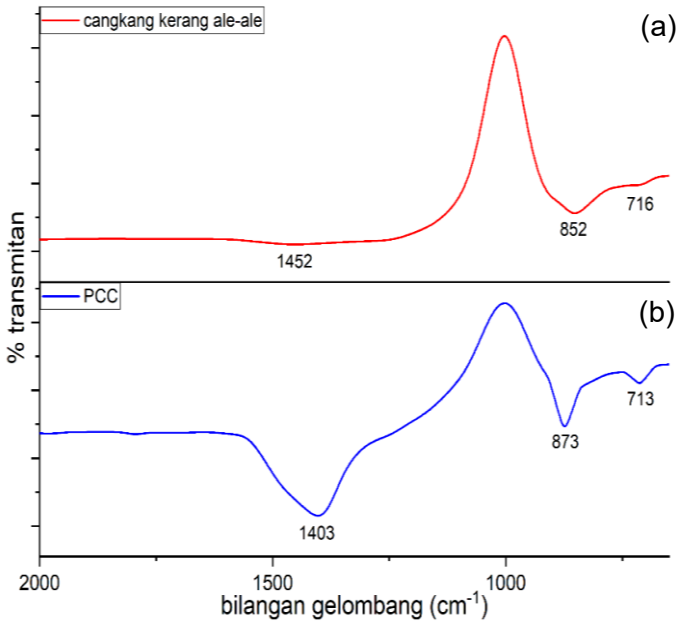

Figure 2. FTIR spectra of (a) Ale-ale shells and (b) PCC

Table 4. Functional group interpretation

Sample	Wave number (cm^{-1})	Functional group	Reference
Ale-ale shells	1452	C-O	Kamba, et al., 2013 Ramasary, et al., 2017
	852	C-O	
	716	C-O	
PCC	1403	C-O	Barhoum, et al., 2014 Munawaroh, et al., 2019
	873	C-O	
	713	C-O	

(a) (b)

Figure 3. Leachate (a) before adsorption and (b) after adsorption using PCC

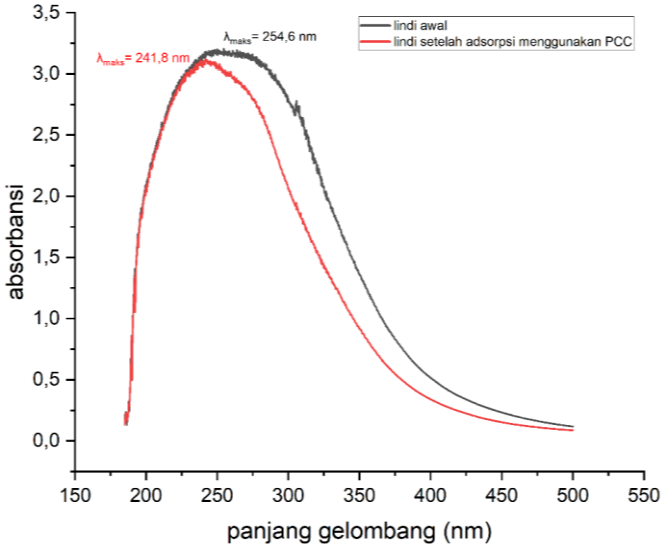

Figure 4. UV-Vis spectra of leachate before and after adsorption

4. CONCLUSIONS

PCC yields resulting from each variation in particle size and calcination temperature were not significantly different. The optimal yield at a particle size of 40 mesh with a calcination temperature of 800°C was 57.75%. The resulting PCC had a C-O functional group and a calcite crystal phase based on the characterization results. PCC adsorbent with a mass of 4.5 g with a stirring speed of 200 rpm for 240 minutes was able to reduce the COD concentration of 50 mL leachate to 456.94 mg/L with an adsorption efficiency of 59.61%. The COD concentration decreased due to the polar adsorbate binding by the polar C-O group on the PCC adsorbent.

LIST OF REFERENCES

Amin, M. & A. Kurniasih. (2016). Pengaruh Ukuran dan Waktu Kalsinasi Batu Kapur Terhadap Tingkat Perolehan Kadar CaO. *Prosiding Seminar Nasional Sains Matematika Informatika dan Aplikasinya IV*. Lampung.

Arief, S. & N. Jamarun. (2009). *Studi Pembentukan Precipitated Calcium Carbonate (PCC) dari Batu Kapur Alam Sumatera Barat.* Penelitian Hibah Strategis Nasional Jurusan Kimia Fakultas MIPA Universitas Andalas.

Atkins, P., T. Overton, J. Rourke, M. Weller, F. Armstrong, & M. Hagerman. (2010). *Shriver and Atkins Inorganic Chemistry Fifth Edition*. Oxford University Press. Great Britain.

Azkiya, N. I., F. Prasetia, E. D. Putri, A. Rosiana, & S. Wardhani. (2016). Sintesis *Precipitated Calcium Carbonate* (PCC) dari Batuan Kapur Alam dengan Metode Kaustik Soda (Kajian Konsentrasi HNO_3). *Jurnal Ilmu Dasar*, *17*(1), 31-34.

Barhoum, A., S. M. El-Sheikh, F. Morsy, S. El-Sherbiny, F. Reniers, T. Dufour, M. P. Delplancke, G. Van Assche, & H. Rahier. (2014). Preparation and Characterization of Ultra-Hydrophobic Calcium Carbonate Nanoparticles. *IOP Conf. Series: Materials Science and Engineering*, *64*, 1-5.

Cahyaningrum, S. E., N. Herdyastuty, D. Supangat, & B. Devina. (2017). Sintesis Hidroksiapatit dari Cangkang Telur Menggunakan Metode Pengendapan Basah. *Prosiding Seminar Nasional Kimia UNY*, Yogyakarta.

Elystia, S., Y. Azis, M. Reza, & D. S. Ermal. (2016). Penyisihan Zat Organik dari Air Gambut Menggunakan *Precipitated Calcium Carbonate* (PCC) dari Limbah Cangkang Kerang Darah (*Anadara granosa*). *Seminar Nasional Sains dan Teknologi Lingkungan II*. Padang.

Erdogan, N., & H. A. Eken. (2017). Precipitated Calcium Carbonate Production, Synthesis and Properties. *Physicochemical Problems of Mineral Processin, 53*(1), 57-68. https://doi.org/10.5277/ppmp170105

Hasyim, U. H. (2015). Modifikasi Permukaan *Precipitated Calcium Carbonate* (PCC) dengan *Coating Agents* Asam Stearat dan Gama Mercaptosilane sebagai *Reinforcing Filler* pada Pembuatan Kompon Karet. *Seminar Nasional Sains dan Teknologi*. Jakarta.

Indrayani, L., & N. Rahmah. (2018). Nilai Parameter Kadar Pencemar sebagai Penentu Tingkat Efektivitas Tahapan Pengolahan Limbah Cair Industri Batik. *Jurnal Rekayasa Proses*, *12*(1),41-50. https://doi.org/10.22146/jrekpros.35754

Jamarun, N., Yulfitrin, & S. Arief. (2007). Pembuatan *Precipitated Calcium Carbonate* (PCC) dari Batu Kapur dengan Metoda Kaustik Soda. *J. Ris. Kim*, *1*(1), 20-24.

Khaira, K. (2011). Pengaruh Temperatur dan Waktu Kalsinasi Batu Kapur Terhadap Karakteristik *Precipitated Calcium Carbonate* (PCC). *Jurnal Saintek*, *3*(1),33-43. http://dx.doi.org/10.31958/js.v3i1.39

Malia, E. N. (2018). *Skripsi: Aplikasi Precipitated Calcium Carbonate dari Batu Kapur sebagai Campuran Bahan Baku dalam Pembuatan Kertas*. Institut Pertanian Bogor.

Meilianti. (2017). Isolasi Kalsium Oksida (CaO) pada Cangkang Sotong (*Cuttlefish*) dengan Proses Kalsinasi Menggunakan Asam Nitrat dalam Pembuatan *Precipitated Calsium Carbonat* (PCC). *Distilasi*, *2*(1), 1-8. https://doi.org/10.32502/jd.v2i1.1131

Peraturan Menteri Pekerjaan Umum Republik Indonesia Nomor 03/PRT/M/2013. (2013). *Tentang Penyelenggaraan Prasarana dan Sarana Persampahan dalam Penanganan Sampah Rumah Tangga dan Sampah Sejenis Sampah Rumah Tangga.*

Perry, K. H. (1984). *Chemical Engineers Handbook 6th Edition*. Mc Graw Hill Book Company, New York.

Rahimawati, R., Nurhasanah, & M. Nurhanisa. (2019). Pengaruh Penambahan Massa Cangkang Kerang Darah (*Anadara granosa*) Teraktivasi pada Peningkatan Kualitas Air Sumur Bor. *Prima Fisika*, *7*(3), 312-318. http://dx.doi.org/10.26418/pf.v7i3.38764

Said, N. I., & D. R. K. Hartaja. (2015). Pengolahan Air Lindi dengan Proses Biofilter Anaerob-Aerob dan Denitrifikasi. *JAI*, *8*(1), 1-20. https://doi.org/10.29122/jai.v8i1.2380

Sarwono, E., W. A. Azis, & B. N. Widiarti. (2017). Pengaruh Variasi Waktu Tinggal Terhadap Kadar BOD, COD, dan TSS pada Pengolahan Lindi TPA Bukit Pinang Samarinda Menggunakan Sistem Aerasi Bertingkat dan Sedimentasi. *Jurnal Teknologi Lingkungan*, *1*(2), 20-26.

Setianingsih, T. (2018). *Karakterisasi Pori dan Luas Muka Padatan*. UB Press, Malang.

Suhartati, T. (2013). *Dasar-Dasar Spektrofotometri UV-Vis dan Spektrometri Massa untuk Penentuan Struktur Senyawa Organik*. CV Anugrah Utama Raharja, Bandar Lampung.

Sumantri, A., & M. R. Cordova. (2011). Dampak Limbah Domestik Perumahan Skala Kecil Terhadap Kualitas Air Ekosistem Perairan dan Dampaknya Terhadap Kesehatan Masyarakat. *JPSL, 2*(1), 127-134. https://doi.org//10.19081/jpsl.2011.1.2.127

Zikri, A., A. Amri, Zultiniar, & Yelmida. (2015). Sintesa *Precipitated Calcium Carbonate* (PCC) dari Cangkang Kerang Darah (*Anadara granosa*) dengan Variasi Jenis Asam dan Waktu Karbonasi. *JOM FTEKNIK*, *2*(2), 1-6.

JURNAL ILMIAH BERKALA SAINS DAN TERAPAN KIMIA

Jurnal Ilmiah Berkala: Sains dan Terapan Kimia
Vol. 16 No. 2, July 2022

Adsorption of Organic Compounds in Leachate using Precipitated Calcium Carbonate (PCC) from Ale-Ale Shells

Adsorpsi Senyawa Organik Pada Lindi Menggunakan *Precipitated Calcium Carbonate* (PCC) dari Cangkang Kerang Ale-Ale

Yulistya Vidyaning Maulidya[1], Rudiyansyah[1], and Nelly Wahyuni[1]

[1]Chemistry Study Program, Tanjungpura University Pontianak, 78124, Indonesia

Email: nellywahyuni@chemistry.untan.ac.id

ABSTRACT

Leachate waste from piles of garbage in the landfill (TPA) has a high concentration of Chemical Oxygen Demand (COD). High COD concentrations can cause a decrease in dissolved oxygen concentrations in the waters. Simple leachate treatment is carried out using the adsorption method with adsorbents derived from food waste. This research used Precipitated Calcium Carbonate (PCC) adsorbent from ale-ale shells. This study aims to evaluate the effect of particle size and calcination temperature variations on PCC yield and analyze the adsorption ability of PCC adsorbents in reducing COD concentrations. In addition, PCC was characterized using an infrared spectrophotometer (FTIR) and an X-ray diffractometer (XRD). Determination of COD concentration was carried out by permanganometric titration. The optimum PCC yield of 57.75% was obtained from Ale-ale shells with a particle size of 40 mesh with a calcination temperature of 800°C. The functional groups in PCC are C-O at wave numbers 1403 cm^{-1}, 873 cm^{-1}, and 713 cm^{-1}. XRD characterization showed the presence of a calcite phase with a high peak intensity at 2θ = 29.38°. The adsorption of organic matter on leachate by PCC (4.5 g/50 mL) with a stirring speed of 200 rpm for 240 minutes reduced the COD concentration of leachate from 1131.28 mg/L to 456.94 mg/L with an adsorption efficiency of 59.61%.

Keywords: adsorption, ale-ale shells, COD, leachate, PCC.

ABSTRAK

Limbah air lindi dari tumpukan sampah yang terdapat di Tempat Pembuangan Akhir (TPA) memiliki konsentrasi Chemical Oxygen Demand (COD) yang tinggi. Dampak yang ditimbulkan dari tinggi nya konsentrasi COD tersebut adalah terjadi penurunan konsentrasi oksigen terlarut dalam perairan. Pengolahan lindi secara sederhana dilakukan menggunakan metode adsorpsi dengan adsorben yang berasal dari limbah makanan. Pada penelitian ini digunakan adsorben Precipitated Calcium Carbonate (PCC) dari cangkang kerang ale-ale. Tujuan penelitian ini untuk mengetahui pengaruh variasi ukuran partikel dan suhu kalsinasi dalam pembuatan PCC terhadap rendemen yang dihasilkan serta mengetahui kemampuan adsorpsi adsorben PCC dalam menurunkan konsentrasi COD. PCC yang dihasilkan dikarakterisasi menggunakan spekrofotometer infra merah (FTIR) dan difraktometer sinar-X (XRD). Penentuan konsentrasi COD dilakukan secara titrasi permanganometri. Rendemen optimum PCC sebesar 57,75% diperoleh dari cangkang kerang ale-ale ukuran partikel 40 mesh dengan suhu kalsinasi 800°C. PCC memiliki gugus fungsi C-O yang terdapat pada bilangan gelombang 1403 cm^{-1}, 873 cm^{-1}, dan 713 cm^{-1}. Karakterisasi XRD menunjukan adanya fasa kalsit dengan intensitas puncak yang tinggi pada 2θ = 29,38°. Adsorpsi bahan organik pada lindi oleh PCC (4,5 g/50 mL) dengan kecepatan pengadukan 200 rpm selama 240 menit mampu menurunkan konsentrasi COD lindi dari 1131,28 mg/L menjadi 456,94 mg/L dengan efisiensi adsorpsi 59,61%.

Kata Kunci: adsorpsi, cangkang kerang ale-ale, COD, lindi, PCC.

Received: December 21, 2021; **Accepted**: June 26, 2022: **Available online**: July 31, 2022

1. INTRODUCTION

The leachate from TPA Batu Layang, Pontianak, West Kalimantan has a high concentration of COD. It indicates that many organic compounds decomposed chemically in water using dissolved oxygen. The more organic compounds that decomposed chemically, the lower the dissolved oxygen concentration, which can impact the water quality (Sumantri and Cordova, 2011). Leachate is wastewater resulting from the dissolution of dissolved matter caused by external water entry into the waste pile (Peraturan Menteri Pekerjaan Umum RI, 2013). Therefore, leachate must be treated to reduce its COD concentration.

The leachate treatment system that has been carried out is to accommodate the leachate temporarily. It is feared that if the garbage pile rosts, it will become a breeding ground for bacteria and disease (Sarwono et al., 2017). In addition, there is a biological leachate treatment using aerobic and anaerobic bacteria to carry out the decomposition process of the leachate. However, this biological leachate treatment produces methane gas and residual sludge that requires further treatment (Said and Hartaja, 2015). Another alternative for leachate treatment is physicochemical treatment employing the adsorption method (Indrayani and Rahmah, 2018).

Adsorption is the removal of dissolved components in a fluid that occurs on the surface of the adsorbent (Setianingsih, 2018). The adsorption process is simple and does not generate new pollutants. The adsorbent used in this study was Precipitated Calcium Carbonate (PCC) from ale-ale shells (*Meretrix meretrix*) from Suka Bangun Village, Ketapang Regency, West Kalimantan. PCC results from a chemical reaction involving $CaCO_3$-containing materials (Jamarun et al., 2007). PCC has a greater degree of purity than other $CaCO_3$-containing materials because it is produced through chemical reaction stages (Erdogan and Eken, 2017). PCC is produced through calcination, hydration, and carbonation. It is believed that PCC adsorbent from ale-ale shells reduces the COD concentration of leachate. Research conducted by Elystia et al. (2016) using PCC from blood clam shells showed that the adsorbent reduced the concentration of organic compounds in peat water with an adsorption efficiency of 99.86% at a composition of 5 g with a stirring speed of 150 rpm for 30 minutes.

This research used PCC adsorbent from ale-ale shells. PCC adsorbents were prepared with variations in particle size and calcination temperature. The adsorption process was carried out in batches on an adsorbent mass of 4.5 g/50 mL with a stirring speed of 200 rpm for 240 minutes. This study aims to determine the variation of particle size and optimum calcination temperature on PCC yield in the adsorption of organic compounds in leachate from TPA Batu Layang.

2. MATERIALS AND METHODS

2.1. Materials

The materials used were nitric acid (Merck), oxalic acid (Merck), sulfuric acid (Merck), potassium permanganate (Merck), sodium carbonate (Smart-Lab), and ale-ale shells waste from Suka Bangun Village, Ketapang Regency, West Kalimantan.

The tools used were various types of beakers, 40, 60, 80, and 100 mesh sieves, hotplate, hammer mill, magnetic stirrer, analytical balance, oven, Fourier Transform Infra-Red spectrophotometer (FTIR) (Frontier Perkin Elmer FT-IR), UV-Vis spectrophotometer (UV-2600 Shimadzu), thermometer up to 110°C, and X-Ray Diffraction (XRD) (XPERT PRO PANalytical PW30/40).

2.2. Synthesis of Precipitated Calcium Carbonate (PCC) (Azkiya et al., 2016)

Ale-ale shells were washed, dried with various particle sizes of 40 mesh, 60 mesh, and 80 mesh, and calcined at a temperature of 800°C for 4 hours. A total of 5.6 g of each calcined product was added to a beaker glass and added with 20 mL of 6 M HNO_3 and distilled water until the volume reached 200 mL, then stirred using a magnetic stirrer at 700 rpm 65°C for 30 minutes. After that, it was filtered to separate the filtrate and added with 150 mL of 1.5 M Na_2CO_3 solution slowly at a flow rate of 2.5 mL/minute for 60 minutes. The precipitate formed was filtered and washed with distilled water to pH 7 and then dried in an oven at 105°C for 3 hours. The same steps were carried out for variations in calcination temperature of 900°C and 1000°C. The yield of $CaCO_3$

obtained was then calculated using the following equation:

$$\%\ yield = \frac{mass\ of\ product\ obtained}{theory\ mass}\ x\ 100\% \quad (1)$$

2.3. Adsorbent Characterization

The adsorbent was characterized using XRD instruments to determine the crystalline phase and FTIR to determine the functional groups in the adsorbent.

2.4. Leachate Characterization

The COD concentration of leachate before and after adsorption was analyzed based on SNI 06-6989.22-2004.

2.5. Organic Compound Adsorption in Leachate Using PCC Adsorbent

Adsorption was carried out on 50 mL leachate using 4.5 g of PCC adsorbent. The adsorption process was carried out in batches at 200 rpm for 240 minutes. The resulting filtrate was measured for its COD concentration to determine the efficiency of removing organic compounds from leachate based on Equation (2).

$$\%R = \frac{C_{in} - C_{out}}{C_{in}} x100\% \quad (2)$$

3. RESULTS AND DISCUSSION

The preparation of PCC begins with a calcination process that aims to release CO_2 gas and decompose organic components contained in ale-ale shells to initiate the decomposition of $CaCO_3$ into CaO (Cahyaningrum et al., 2017). The mass of calcined ale-ale shells decreased from their original state due to releasing CO_2 gas after the calcination process (Amin and Kurniasih, 2016). CaO obtained from the calcination is hygroscopic, which can absorb moisture from the air after being removed from the furnace (Khaira, 2011). The mass loss after the calcination is presented in Table 1. The reactions that occur in the calcination process follow Equation 3.

$$CaCO_{3(s)} \leftrightarrow CaO_{(s)} + CO_{2(g)} \quad (3)$$

Based on Table 1, the percentage reduction in the mass of ale-ale shells produced was not significantly different because the time required for the calcination process for 4 hours was sufficient to decompose $CaCO_3$. It is evidenced in Fig. 1b. The XRD diffractogram produces peaks of CaO and $Ca(OH)_2$ according to ICDD 98-002-6959 for CaO and ICDD 98-020-2228 for $Ca(OH)_2$. The presence of $Ca(OH)_2$ occurs because the hygroscopic CaO has absorbed water vapor from the air. Based on the XRD characterization, the calcination process at 800°C has completely decomposed $CaCO_3$ into CaO, which is indicated by the absence of $CaCO_3$ minerals.

The utilization of HNO_3 as a solvent in the preparation of PCC is a modification of the PCC preparation using the caustic soda method by Azkiya et al. (2016). Modification with acidic solvents could increase the solubility of CaO compared to hydration with H_2O alone. Research by Zikri et al. (2015) in the PCC preparation using HNO_3 as a solvent found that the PCC yield was higher than that of other acid solvents such as HCl and CH_3COOH. Arief dan Jamarun (2009) tested various types of acids (HCl, HNO_3, and $HClO_4$) and found that the highest PCC yield was obtained from using HNO_3. The dissolution of CaO with HNO_3 will produce $Ca(NO_3)_2$ salt, which has a high solubility level to increase the yield of PCC produced (Meilianti, 2017). The reaction that occurs follows Equation 4.

$$CaO_{(s)} + 2HNO_{3(aq)} \leftrightarrow Ca(NO_3)_{2(aq)} + H_2O_{(l)} \quad (4)$$

When Na_2CO_3 solution is added to the $Ca(NO_3)_2$ filtrate, the solution gradually becomes cloudy, and the turbidity increases as more Na_2CO_3 solution is added. It indicates the process of crystallization of $CaCO_3$ in a supersaturated solution condition. The reactions that occur are:

$$Ca(NO_3)_{2(aq)} + Na_2CO_{3(aq)} \rightarrow CaCO_3\downarrow_{(s)} + NaNO_{3(aq)} \quad (5)$$

Based on Reaction (5), the $CaCO_3$ product resulting from the precipitation process was the PCC. This study produced PCC with a pH of 12, so it must be washed with distilled water to achieve a neutral pH. $CaCO_3$ was washed with distilled water because the solubility of $CaCO_3$ in water is very small (Perry, 1984). After the pH of $CaCO_3$ was neutral, it was filtered using filter paper whose mass was known to separate the $CaCO_3$. The yield of $CaCO_3$ obtained as PCC is presented in Table 2.

Table 1. Percentage of mass loss

Particle size	Calcination temperature		
	800°C	900°C	1000°C
40 mesh	43.93%	44.36%	44.54%
60 mesh	43.91%	44.30%	44.48%
80 mesh	43.84%	44.16%	44.24%

Table 2. Yield of PCC

Particle size	Calcination temperature		
	800°C	900°C	1000°C
40 mesh	57.75%	57.51%	57.87%
60 mesh	58.20%	57.04%	56.98%
80 mesh	57.70%	58.12%	56.87%

Based on Table 2, the yield of PCC produced is not significantly different from the influence of particle size and calcination temperature. Therefore, the characterization and adsorbents production was carried out on PCC produced from 40 mesh ale-ale shells with a calcination temperature of 800°C. Based on the diffractogram in Fig. 1c, PCC has a peak of $CaCO_3$ (calcite). It is in accordance with research by Malia (2018) that the crystal phase formed in PCC is calcite. Typical characteristics of calcite based on ICDD 01-076-2712 have a high peak intensity ranging from $2\theta = 29.39°$.

The resulting PCC has a C-O functional group with wave numbers of 1403 cm^{-1}, 873 cm^{-1}, and 713 cm^{-1}, which is in accordance with the interpretation of the functional group in Table 4. C-O at wave numbers 1420 cm^{-1}, 872 cm^{-1}, and 710 cm^{-1}. Based on Fig. 2b, the resulting PCC has a higher degree of purity than the ale-ale shells, indicated by a sharper peak. PCC in this study functions as an adsorbent due to the attractive force generated by the C-O group. It occurs because of the difference in electronegativity between C and O atoms. Atom O has a greater electronegativity (Atkins et al., 2010). Due to the polarity of the C-O group on PCC, the polar adsorbate will be strongly bound (Hasyim, 2015).

The initial COD concentration of the Batu Layang TPA leachate was 1131.28 mg/L. The decrease in COD concentration using PCC adsorbent resulted in an adsorption efficiency of 59.61% with a COD concentration of 456.94 mg/L, followed by an insignificant decrease in color intensity, as shown in Figure 3. The change in color intensity was based on the physicochemical activation process on the PCC adsorbent. According to Rahimawati et al. (2019), there was a decrease in the color intensity of drilled well water using physicochemical activated blood clam shell adsorbents because it can remove impurities that cover the pores of the adsorbent.

Changes in color intensity after adsorption using PCC adsorbent were measured at the maximum wavelength using a UV-Vis spectrophotometer. The maximum wavelength of leachate before adsorption was 254.6 nm, and after adsorption was 241.8 nm (Fig. 4). Based on this, there is a hypochromic shift with a smaller maximum wavelength because there is no auxochrome bound to the chromophore to form hydrogen bonds (Suhartati, 2013).

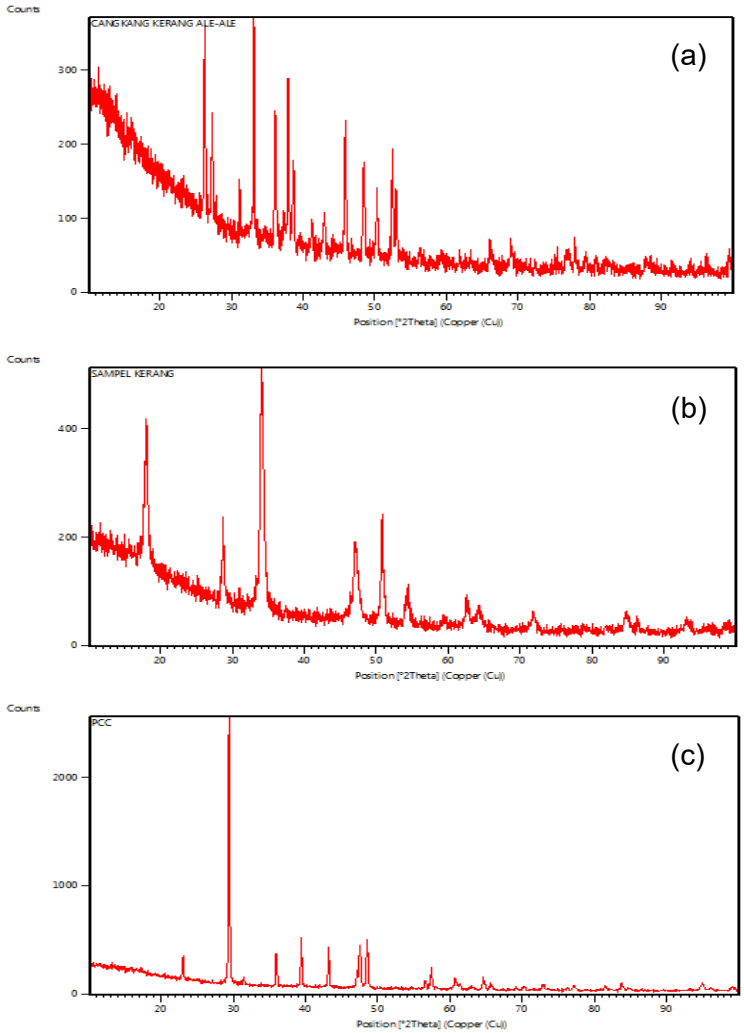

Figure 1. XRD diffractogram (a) ale-ale shells, (b) 40 mesh ale-ale shells after calcination at 800°C, and (c) PCC from 40 mesh ale-ale shells and 800°C calcination temperature

Table 3. Crystal phase interpretation

Sample	Crystal phase	2θ
Shells of ale-ale	Aragonit ($CaCO_3$)	26.18°, 27.22°, 33.12°, 36.10°, 45.87°, 48.41°, and 52.42°
Shell of ale-ale after calcining	Portlandite ($Ca(OH)_2$)	17.97°; 28.66°, 34.06°, 47.08°, 50.77°, 59.37°, 62.44°, 71.90°, and 84.60°
	Lime (CaO)	54.38° and 64.18°
PCC	Calcite ($CaCO_3$)	22.99°, 29.38°, 35.95°, 39.39°, 43.14°, 47.52°, 48.50°, 57.39°, and 64.65°

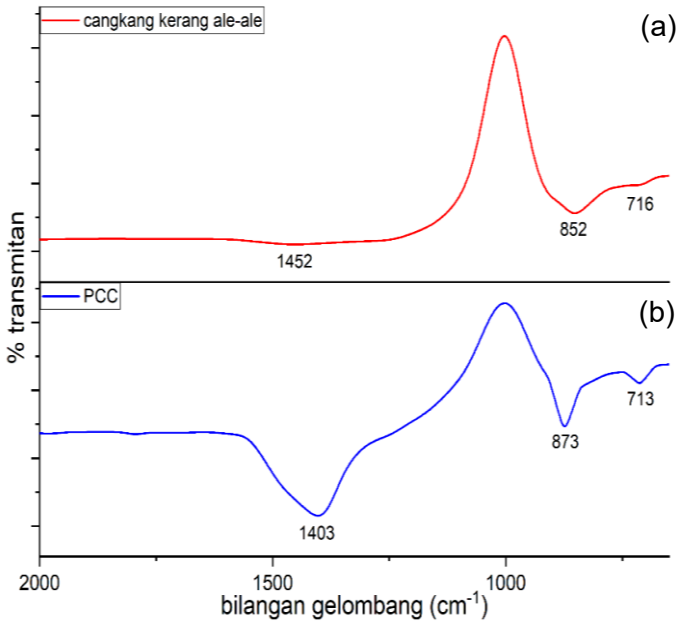

Figure 2. FTIR spectra of (a) ale-ale shells and (b) PCC

Table 4. Functional group interpretation

Sample	Wave number (cm^{-1})	Functional group	Reference
Ale-ale shells	1452	C-O	Kamba, et al., 2013 Ramasary, et al., 2017
	852	C-O	
	716	C-O	
PCC	1403	C-O	Barhoum, et al., 2014 Munawaroh, et al., 2019
	873	C-O	
	713	C-O	

(a) (b)

Figure 3. Leachate (a) before adsorption and (b) after adsorption using PCC

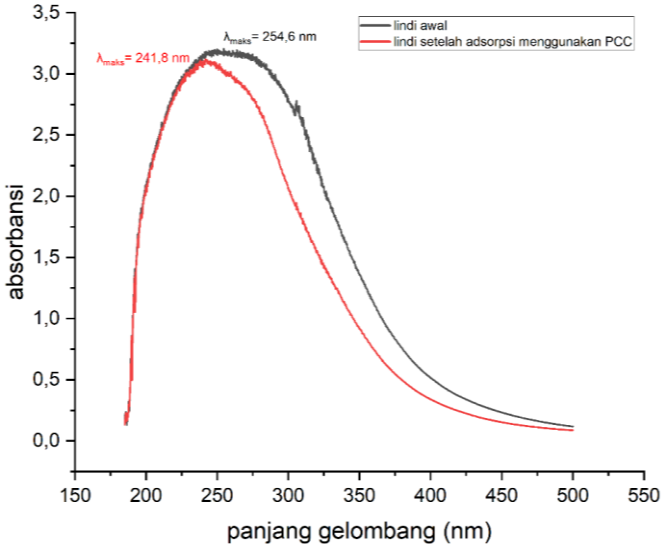

Figure 4. UV-Vis spectra of leachate before and after adsorption

4. CONCLUSIONS

PCC yields resulting from each variation in particle size and calcination temperature were not significantly different. The optimal yield at a particle size of 40 mesh with a calcination temperature of 800°C was 57.75%. The resulting PCC had a C-O functional group and a calcite crystal phase based on the characterization results. PCC adsorbent with a mass of 4.5 g with a stirring speed of 200 rpm for 240 minutes was able to reduce the COD concentration of 50 mL leachate to 456.94 mg/L with an adsorption efficiency of 59.61%. The COD concentration decreased due to the polar adsorbate binding by the polar C-O group on the PCC adsorbent.

LIST OF REFERENCES

Amin, M. & A. Kurniasih. (2016). Pengaruh Ukuran dan Waktu Kalsinasi Batu Kapur Terhadap Tingkat Perolehan Kadar CaO. *Prosiding Seminar Nasional Sains Matematika Informatika dan Aplikasinya IV*. Lampung.

Arief, S. & N. Jamarun. (2009). *Studi Pembentukan Precipitated Calcium Carbonate (PCC) dari Batu Kapur Alam Sumatera Barat.* Penelitian Hibah Strategis Nasional Jurusan Kimia Fakultas MIPA Universitas Andalas.

Atkins, P., T. Overton, J. Rourke, M. Weller, F. Armstrong, & M. Hagerman. (2010). *Shriver and Atkins Inorganic Chemistry Fifth Edition*. Oxford University Press. Great Britain.

Azkiya, N. I., F. Prasetia, E. D. Putri, A. Rosiana, & S. Wardhani. (2016). Sintesis *Precipitated Calcium Carbonate* (PCC) dari Batuan Kapur Alam dengan Metode Kaustik Soda (Kajian Konsentrasi HNO_3). *Jurnal Ilmu Dasar*, *17*(1), 31-34.

Barhoum, A., S. M. El-Sheikh, F. Morsy, S. El-Sherbiny, F. Reniers, T. Dufour, M. P. Delplancke, G. Van Assche, & H. Rahier. (2014). Preparation and Characterization of Ultra-Hydrophobic Calcium Carbonate Nanoparticles. *IOP Conf. Series: Materials Science and Engineering*, *64*, 1-5.

Cahyaningrum, S. E., N. Herdyastuty, D. Supangat, & B. Devina. (2017). Sintesis Hidroksiapatit dari Cangkang Telur Menggunakan Metode Pengendapan Basah. *Prosiding Seminar Nasional Kimia UNY*, Yogyakarta.

Elystia, S., Y. Azis, M. Reza, & D. S. Ermal. (2016). Penyisihan Zat Organik dari Air Gambut Menggunakan *Precipitated Calcium Carbonate* (PCC) dari Limbah Cangkang Kerang Darah (*Anadara granosa*). *Seminar Nasional Sains dan Teknologi Lingkungan II*. Padang.

Erdogan, N., & H. A. Eken. (2017). Precipitated Calcium Carbonate Production, Synthesis and Properties. *Physicochemical Problems of Mineral Processin, 53*(1), 57-68. https://doi.org/10.5277/ppmp170105

Hasyim, U. H. (2015). Modifikasi Permukaan *Precipitated Calcium Carbonate* (PCC) dengan *Coating Agents* Asam Stearat dan Gama Mercaptosilane sebagai *Reinforcing Filler* pada Pembuatan Kompon Karet. *Seminar Nasional Sains dan Teknologi*. Jakarta.

Indrayani, L., & N. Rahmah. (2018). Nilai Parameter Kadar Pencemar sebagai Penentu Tingkat Efektivitas Tahapan Pengolahan Limbah Cair Industri Batik. *Jurnal Rekayasa Proses*, *12*(1),41-50. https://doi.org/10.22146/jrekpros.35754

Jamarun, N., Yulfitrin, & S. Arief. (2007). Pembuatan *Precipitated Calcium Carbonate* (PCC) dari Batu Kapur dengan Metoda Kaustik Soda. *J. Ris. Kim*, *1*(1), 20-24.

Khaira, K. (2011). Pengaruh Temperatur dan Waktu Kalsinasi Batu Kapur Terhadap Karakteristik *Precipitated Calcium Carbonate* (PCC). *Jurnal Saintek*, *3*(1),33-43. http://dx.doi.org/10.31958/js.v3i1.39

Malia, E. N. (2018). *Skripsi: Aplikasi Precipitated Calcium Carbonate dari Batu Kapur sebagai Campuran Bahan Baku dalam Pembuatan Kertas*. Institut Pertanian Bogor.

Meilianti. (2017). Isolasi Kalsium Oksida (CaO) pada Cangkang Sotong (*Cuttlefish*) dengan Proses Kalsinasi Menggunakan Asam Nitrat dalam Pembuatan *Precipitated Calsium Carbonat* (PCC). *Distilasi*, *2*(1), 1-8. https://doi.org/10.32502/jd.v2i1.1131

Peraturan Menteri Pekerjaan Umum Republik Indonesia Nomor 03/PRT/M/2013. (2013). *Tentang Penyelenggaraan Prasarana dan Sarana Persampahan dalam Penanganan Sampah Rumah Tangga dan Sampah Sejenis Sampah Rumah Tangga.*

Perry, K. H. (1984). *Chemical Engineers Handbook 6th Edition*. Mc Graw Hill Book Company, New York.

Rahimawati, R., Nurhasanah, & M. Nurhanisa. (2019). Pengaruh Penambahan Massa Cangkang Kerang Darah (*Anadara granosa*) Teraktivasi pada Peningkatan Kualitas Air Sumur Bor. *Prima Fisika*, *7*(3), 312-318. http://dx.doi.org/10.26418/pf.v7i3.38764

Said, N. I., & D. R. K. Hartaja. (2015). Pengolahan Air Lindi dengan Proses Biofilter Anaerob-Aerob dan Denitrifikasi. *JAI*, *8*(1), 1-20. https://doi.org/10.29122/jai.v8i1.2380

Sarwono, E., W. A. Azis, & B. N. Widiarti. (2017). Pengaruh Variasi Waktu Tinggal Terhadap Kadar BOD, COD, dan TSS pada Pengolahan Lindi TPA Bukit Pinang Samarinda Menggunakan Sistem Aerasi Bertingkat dan Sedimentasi. *Jurnal Teknologi Lingkungan*, *1*(2), 20-26.

Setianingsih, T. (2018). *Karakterisasi Pori dan Luas Muka Padatan*. UB Press, Malang.

Suhartati, T. (2013). *Dasar-Dasar Spektrofotometri UV-Vis dan Spektrometri Massa untuk Penentuan Struktur Senyawa Organik*. CV Anugrah Utama Raharja, Bandar Lampung.

Sumantri, A., & M. R. Cordova. (2011). Dampak Limbah Domestik Perumahan Skala Kecil Terhadap Kualitas Air Ekosistem Perairan dan Dampaknya Terhadap Kesehatan Masyarakat. *JPSL, 2*(1), 127-134. https://doi.org//10.19081/jpsl.2011.1.2.127

Zikri, A., A. Amri, Zultiniar, & Yelmida. (2015). Sintesa *Precipitated Calcium Carbonate* (PCC) dari Cangkang Kerang Darah (*Anadara granosa*) dengan Variasi Jenis Asam dan Waktu Karbonasi. *JOM FTEKNIK*, *2*(2), 1-6.

JURNAL ILMIAH BERKALA SAINS DAN TERAPAN KIMIA

Jurnal Ilmiah Berkala: Sains dan Terapan Kimia
Vol. 16 No. 2, July 2022

Antioxidant and Antibacterial Activity of The Stem Bark Extract of *Sterculia Foetida* L.

Aktivitas Antioksidan dan Antibakteri Ekstrak Kulit Batang Tumbuhan *Sterculia Foetida* L.

Theodore Y. K. Lulan[*)], Febri O. Nitbani, Reinner I. Lerrick

Chemistry Department, Faculty of Science and Engineering, Nusa Cendana University
[2]Institute Research, Institution, Address, City, Zip Code, Country

Email: theodore_lulan@staf.undana.ac.id

ABSTRACT

Free radicals are compounds that contain one or more unpaired electrons which are very reactive, causing damage to cells or tissues and implication in the emergence of various degenerative diseases. Several methods of exploring medicinal plants have been carried out to find new sources of natural antioxidants and antibacterials that can reduce the use of synthetic drugs. This study aimed to examine the antioxidant and antibacterial activity of the stem bark extract of the plant Sterculia foetida L. The antioxidant activity of S. foetida was tested using the ABTS radical method (2,2-Azinobis 3-ethyl benzothiazoline 6-sulfonic acid). The principle of this method is that the color intensity or absorbance of the ABTS solution is inversely proportional to the concentration of antioxidant compounds. ABTS absorbance measurements were carried out at a wavelength of 734 nm. The results showed that the bark extract of the plant S. foetida could inhibit ABTS radicals with an IC50 value of 5.54 g/mL. The antibacterial activity of S. foetida was tested by measuring the optical density (OD) at a wavelength of 630 nm and expressed by the Inhibition Concentration 50 (IC50) value of 10442.29 g/mL.

Keywords: *Sterculia foetida L.* plant, antioxidant, antibacterial, ABTS, phytochemical

ABSTRAK

Radikal bebas merupakan suatu senyawa yang mengandung satu atau lebih elektron yang tidak berpasangan yang sangat reaktif sehingga menyebabkan kerusakan sel atau jaringan, dan berimplikasi pada timbulnya berbagai penyakit degeneratif. Beberapa metode eksplorasi tumbuhan obat dilakukan untuk menemukan sumber baru antioksidan dan antibakteri alami yang mampu mengurangi penggunaan obat sintetik. Penelitian ini bertujuan untuk menguji aktivitas antioksidan dan antibakteri dari ekstrak kulit batang tumbuhan Sterculia foetida L. Pengujian aktivitas antioksidan S. foetida dilakukan menggunakan metoda radikal ABTS (2,2-Azinobis 3-ethyl benzothiazoline 6-sulfonic acid). Prinsip dari metode ini adalahintensitas warna atau absorbansi larutan ABTS berbanding terbalik dengan konsentrasi senyawa antioksidan. Pengukuran absorbansi ABTS dilakukan pada panjang gelombang 734 nm. Hasil penelitian menunjukkan bahwa ekstrak kulit batang tumbuhan S. foetida memiliki kemampuan menghambat radikal ABTS dengan nilai IC_{50} sebesar 5,54 µg/mL. Pengujian aktivitas antibakteri S. foetida dilakukan dengan mengukur densitas optik (OD) pada panjang gelombang 630 nm dan dinyatakan dengan nilai Inhibition Concentration 50 (IC_{50}) sebesar 10442,29 µg/mL.

Kata Kunci: Tumbuhan *Sterculia foetida L.*, antioksidan, antibakteri, ABTS, fitokimia

Received: November 21, 2021; **Accepted**: March 9, 2022: **Available online**: July 31, 2022

1. INTRODUCTION

In recent years, the use of natural ingredients as traditional medicine in Indonesia has increased, and some natural ingredients have even been mass-produced. Traditional medicine is believed to have fewer side effects compared to chemically-derived drugs. Additionally, raw materials for traditional medicine are readily available and relatively inexpensive (Alam et al., 2012; Muchtadi et al., 2013).

Many studies have been conducted to test the active ingredients found in plants or natural ingredients. Purgiyanti (2019) tested the antioxidant mechanism of the active ingredients of *Centella asiatica* extract against free radicals. Torokano et al. (2018) tested the inhibitory capacity of red jatropha leaf extract to inhibit the growth of *Staphylococcus aureus*, *Salmonella typhi*, and *Escherichia coli* bacteria, while Monalisa et al. (2011) tested *Elephantopus scaber* leaves to inhibit *Staphylococcus aureus* and *Salmonella typhi* bacteria.

Antioxidants stabilize free radicals by interrupting chain reactions so that free radical reactions can be halted (Winarsi, 2007; Babalola, 2012; El-sherei et al., 2016). Free radical chain reactions due to unpaired electrons cause free radicals to become highly reactive compounds against body cells, causing various chronic, degenerative diseases to cell or tissue damage (Bosenberg & Zyl, 2008; Tuba & Gülçin, 2008). Antibacterial is a substance that kills or suppresses bacteria's growth and reproduction (Vital et al., 2010; Hebbar et al., 2014). Based on their activity, antibacterial substances can be bactericidal (kill bacteria), bacteriostatic (inhibit bacterial growth) or inhibit the germination of bacterial spores (Murray et al., 2003). Some bacteria, such as *Escherichia coli*, *Staphylococcus aureus*, *Salmonella typhosa*, and *Vibrio cholera*, can cause various diseases for living things (Griffin, 1981; Silalahi, 2006).

Medicinal plants have the potential to contain secondary metabolites such as alkaloids, flavonoids, terpenoids, and steroids that can act as antioxidants, antibacterial, antifungal, and antidiabetic compounds (Gressler et al., 2008; Li et al., 2009; Lin et al., 2010; Widodo & Rahayu, 2010; Tarak et al., 2011; Wibowo et al., 2014; Hairani et al., 2016;). One of the medicinal plants that have the potential as natural antioxidants and antibacterial agents is *Sterculia foetida* L. (Heyne et al., 1987; Forest Watch Indonesia, 2001; Ministry of Forestry, 2002). This plant is intriguing to examine because it is proven to be efficacious in overcoming various health problems based on the empirical experience of the local NTT community. *S. foetida* is known by the people of NTT as the Nitas tree (Hall for the Establishment of Forest Areas Region XIV, 2008). The leaves, bark, and roots of *S. foetida* are used to treat wounds in livestock. People also take advantage of the ripe fruit skin of *S. foetida* to treat stomach and kidney diseases (Njurumana, 2011; Siswadi et al., 2013).

Other studies have shown that *S. foetida* has antibacterial and antioxidant activity. An antioxidant test by Gunawan and Karda (2015) proved that the bark essential oil from the stem of *S. foetida* has the potential as an antioxidant compound. The antifeedant activity test by Rani and Rajaskharreddy (2009) proved that the leaves of *S. foetida* contain triterpene and alkaloid compounds that have potential as antifeedant compounds. An anti-inflammatory test by Naik et al. (2003) proved that *S. foetida* contains the taraxer-14-en-3β-ol, which has the potential to be an anti-inflammatory compound. Based on these studies, it is known that the *S. foetida* plant contains phenolic compounds that have the potential as antioxidant agents (Asih et al., 2010). It is known that plants with a high concentration of phenolic compounds possess antioxidant properties (Mujumdar et al., 2011; Huang et al., 2013; Cahyani et al., 2019). Based on the data from the literature study that has been carried out, this research will determine the antioxidant and antibacterial activity test of the stem bark extract of the plant *Sterculia foetida* L. originating from East Nusa Tenggara.

2. MATERIALS AND METHODS

2.1. Materials

The materials used were stem bark samples of *S. foetida*, ABTS and quercetin (Sigma-Aldrich), $K_2S_2O_8$, sodium chloride, potassium chloride, sodium hydrogen phosphate, potassium dihydrogen phosphate, $AlCl_3$, Mayer's reagent, Wagner's reagent, Dragendorff's reagent, magnesium, chloroform, DMSO, anhydrous acetic acid, $HgCl_2$, KI, and Iodine from Merck (Darmstadt, Germany). In addition, 10% $FeCl_3$, 25% NH_3, methanol, ethanol, 2M HCl, concentrated sulfuric acid, distilled water, and Whatman filter paper were also used on an analytical scale.

The tools used were knife, oven, blender, sieve, analytical balance, extraction equipment, test tube, test tube rack, dropper, beaker, measuring cup, rotary evaporator, incubator, and UV-Vis Thermo Genesys 10S spectrophotometer.

2.2. Extraction

A total of 600 grams of *S. foetida* bark powder was extracted by maceration using 1.5 liters of methanol for 3 x 24 hours. The results of the macerate were filtered with filter paper to obtain the filtrate. The filtrate was then evaporated using a rotary evaporator at a temperature of 60°C.

2.3. Phytochemical Test

A. Alkaloids

A total of 500 mg of extract was dissolved with methanol in a test tube, and then 3 - 5 drops of Wagner reagent were added. The sample was then observed until it was cloudy or a precipitate was formed. Positive alkaloids are characterized by brown deposits (Tiwari et al., 2011; Atun, 2014).

B. Flavonoids

A total of 500 mg of extract was dissolved with methanol in a test tube, then two drops of concentrated HCl and Mg metal were added and shaken vigorously. Positive flavonoids are indicated by the presence of foam and a red/yellow/orange color solution (Atun, 2014).

C. Saponins

A total of 500 mg of extract was dissolved with methanol in a test tube, then two drops of 1 M HCl were added and shaken. Positive saponins are indicated by the presence of foam with much intensity and are consistent for 10 minutes (Atun, 2014).

D. Tannins

A total of 500 mg of extract was dissolved in methanol in a test tube, then ten drops of 10% $FeCl_3$ were added. Positive tannins are indicated by a dark blue and blue-black/greenish-black color solution (Atun, 2014).

E. Triterpenoids/steroids

A total of 500 mg of extract was dissolved in methanol in a test tube. Ten drops of glacial acetic acid and two drops of concentrated H_2SO_4 were added, then shaken slowly. Positive triterpenoids are indicated by a red/brown color solution, while steroid positives are indicated by a blue, purple/green color solution (Atun, 2014).

2.4. Determining Antioxidant Activity Preparation of Quercetin Stock Solution

A stock solution of 1000 g/mL quercetin was prepared by dissolving 10 mg of quercetin with ethanol p.a in a 10 mL volumetric flask.

2.5. Preparation of ABTS Solution and Reagents

a. ABTS solution: 18 mg ABTS (7 mM) was dissolved with distilled water in a 5 mL volumetric flask.
b. $K_2S_2O_8$ solution: 14 mg potassium persulfate (2.45 mM) was dissolved with distilled water in a bottle to 20 mL.
c. ABTS stock solution: 5 mL of ABTS solution was added with 5 mL of potassium persulfate solution and incubated in a dark room at 22-24°C for 12-16 hours before use to produce ABTS with a dark blue color.
d. Phosphate Buffer Saline (PBS) solution pH 7.4: 8 g sodium chloride, 0.2 g potassium chloride, 1.42 g sodium hydrogen phosphate, 0.24 potassium dihydrogen phosphate were dissolved in distilled water to 1 L.

2.6. ABTS Maximum Absorption

Wavelength Measurement

A total of 0.1 mL of PBS solution pH 7.4 was mixed with 2 mL of ABTS stock solution and incubated for six minutes. Then the absorbance of the solution was measured by UV-Vis spectrophotometry at the maximum wavelength.

2.7. ABTS Test with Quercetin (Comparison)

Quercetin stock solution 100 g/mL was pipetted into a 5 mL volumetric flask as much as 3.09 g/mL, 6.19 g/mL, 12.38 g/mL, 24.75 g/mL, and 49.5µg/mL, or pipette 0.15 mL, 0.31 mL, 0.62 mL, 1.24 mL, and 2,475 mL, respectively. Then the volume was added up to the mark with ethanol p.a. From each concentration, 0.1 mL of solution was taken and added with 2 mL of ABTS stock solution. The solution was incubated for six minutes, and the absorbance was measured using UV-Vis spectrophotometry at the maximum wavelength.

2.8. Measurement of Antioxidant Activity

The stock solution of 1000 g/mL methanol extract sample was pipetted into a 5 mL volumetric flask as much as 25 g/mL, 50 g/mL, 100 g/mL, 200 g/mL, and 400 g/mL or as much as 0.125 mL, 0.25 mL, 0.5 mL, 1 mL and 2 mL. Then the volume was added up to the limit with ethanol p.a. From each concentration, 0.1 mL of the extract solution was added with 2 mL of ABTS stock solution, incubated for six minutes, and the absorbance was measured using UV-Vis spectrophotometry at the maximum wavelength. Sample concentration and percent inhibition were plotted on the x and y axes of the linear regression equation (Y = ax + b, respectively). This equation is used to determine the IC_{50} value. The amount of antioxidant activity was calculated by the formula:

$$Percent\ Inhibition\ (\%) = \left(\frac{control\ absorbance\ \ sample\ absorbance}{control\ absrbance}\right) \times 100\%$$

2.9. Evaluating Antibacterial Activity

A. Media

In the antibacterial bioactivity test, tools and media were sterilized using an autoclave for 15 minutes at 120°C and 1 atm. Solid media was prepared by inserting 20 g of Mueller Hinton Agar into 500 mL of distilled water, then put into an Erlenmeyer, covered with cotton, and heated until it boiled and thickened. The agar medium was then sterilized using an autoclave at 105°C for 15 minutes.

Liquid media (Nutrient Agar) was prepared by dissolving 20 g of Nutrient Agar (NA) in 250 mL of distilled water, then put into an Erlenmeyer and covered with cotton. The suspension was then heated to boiling while stirring and cooled to room temperature. The media was sterilized in an autoclave at 105°C for 15 minutes.

2.10. Preparation of Isolated Bacterial Colony

The tube containing the bacteria was removed from the –80°C freezer and thawed. A total of 5 mL of Nutrient Broth (NB) was poured into a sterile test tube and added with 50 µl of bacteria. The test tubes were then covered with parafilm and incubated at 37°C for 18 hours. A vortex was used to even out the bacterial suspension. A total of 200 µl of bacterial suspension was spread evenly on the NA plate in a machine, covered with parafilm, and incubated at 37°C for 18 hours to obtain isolated colonies.

2.11. Preparation of Bacterial Suspension For Antibacterial Evaluation

A total of 5 mL of NB was poured into a sterile test tube. One colony of bacteria with a sterile yellow tip was taken and put into a 5 mL NB tube. The bottom of the test tube was pressed to dissolve the bacteria in the NB. The tube was then covered with parafilm and incubated on a shaker at 37°C for 18 hours.

2.12. Sample Preparation

The extract was dissolved in a solvent (e.g., 1 mL) to the highest concentration (record the amount of extract to reach the maximum concentration). Dissolve the ethanol extract in DMSO (e.g., 1 mL) to the highest concentration (record the amount of extract to reach the maximum concentration). Sonification was carried out so that all extracts were wholly dissolved.

2.13. Measurement of Optical Density (OD) of Cell Suspensions

A total of 500 µL of bacterial suspension

was mixed with 500 µL of NB, and the OD630 was measured at 630 nm. The bacterial suspension was then prepared at OD630 = 0.4. Then the calculations were carried out.

2.14. Colony Inspection

Serial dilutions of the bacterial suspension were carried out: 10^9, 10^8 10^7 10^6 10^5 10^4 10^3 for each bacteria used. A total of 100 µL of 10^3 bacteria were spread on NA, covered with parafilm, and incubated at 37°C for 18 hours. After that, the colonies of each bacterium were counted.

2.15. Experiment

A 500 L mixture was made from 445 µL NB + 50 µL bacterial suspension (using 104 cells and the remaining 105 cells) + 5 µL samples, then repeated for the rest of the samples. Vortex was used for leveling. A premix of 150 µL was used for each sample, three replication for each sample, and twice for the blank. It was then tightly closed with sealing paper and fitted with a well cover. It was incubated at 37°C for 18 hours, and the cell density was measured at OD630.

3. RESULTS AND DISCUSSION

Based on Table 1, phytochemical tests on the methanol extract of Nitas stem bark showed the presence of secondary metabolites, namely flavonoids and tannins. The results of the antioxidant activity test of the methanol extract of the Nitas stem bark against ABTS are presented in Table 2, with a percent radical inhibition of 88.3%.

From Table 2 and Fig. 1, it can be explained that the greater the sample concentration, the greater the inhibition of the sample against free radicals. Fig. 1 shows the logarithmic regression equation that can be used to calculate the IC_{50} value (5.54 g/mL). These results indicate that the methanol extract of the stem bark of *S. foetida* has a powerful antioxidant activity. Antibacterial activity of methanol extract of Nitas bark against *Staphylococcus aureus* bacteria is presented in Fig. 2.

The results of the measurement of bacterial growth inhibition are presented in Fig. 2. From Fig. 2, it can be seen that the effectiveness of the methanol extract of Nitas stem bark as an antibacterial against *S. aureus* bacteria was 47.11%, indicated by an IC_{50} value of 10442.29 g/mL.

Based on the research that has been done, the methanol extract of the bark of Nitas can inhibit the growth of *S. aureus* bacteria. It is supported by the presence of tannins and flavonoids in the extract. As an antibacterial, flavonoids work by inhibiting the synthesis of nucleic acids located in ring B, which plays a vital role in the intercalation process or hydrogen bonding by accumulating nucleic acid bases, which can inhibit the formation of DNA and RNA (Cushnie et al., 2005). As an antibacterial, tannins work by inhibiting the reverse transcriptase and DNA topoisomerase enzymes, causing bacterial cells to fail to form (Nuria et al., 2009). In *S. aureus* bacteria, administration of antibacterial compounds from the methanol extract of Nitas stem bark can inhibit the assembly of the cell wall and fail to join the glycan chain with the peptidoglycan of the cell wall causing bacterial death. Without a cell wall, bacteria will not be able to survive outside influences, so bacteria tend to die shortly.

Table 1. Phytochemical test results of methanol extract of Nitas bark

Identification	Result	Description

Alkaloids	Reagen wagner: brick-red	-
Flavonoids	Orange color solution	+
Saponins	Golden-brown	-
Tannins	Greenish black	+
Triterpenoids/Steroids	Turbid yellow	-

*Note: (+) = positive contains compounds
(-) = negative contains compounds

Table 2. Data on the percentage of inhibition of samples from various concentrations

Sample concentration (µg/mL)	(%) inhibition
3.09	33.88
6.19	51.28
12.38	73.91
24.75	85.73
49.5	88.3

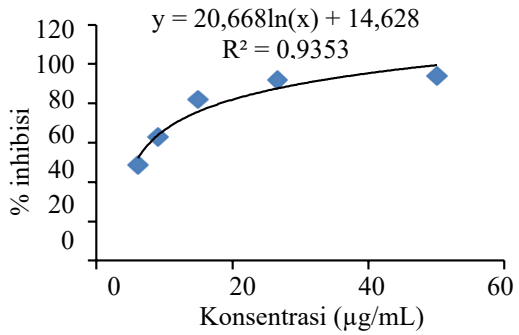

Figure 1. Antioxidant activity of plant extract of *S. Foetida*

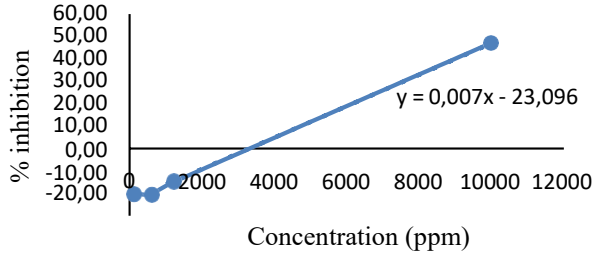

Figure 2. Antibacterial activity of the plant extract of *S. foetida*

4. CONCLUSIONS

Based on the results of the research conducted, it can be concluded that:

1. The methanolic extract of the bark of Nitas (*Sterculia foetida* L.) contains secondary metabolites in the form of flavonoids and tannins that have the potential as antioxidants and

antibacterials.

2. Antioxidant and antibacterial activity of the methanolic extract of the bark of Nitas (*Sterculia foetida* L.) with inhibition of 88.3% and 47.11%, respectively, with IC50 values of 5.54 g/mL and 10.442.29 g/mL.

LIST OF REFERENCES

Alam, Md. R., Raton, Md., Hassan, Md. M., Kadir, M. F., Islam, S. M. A., Haque, Md. A. (2012). Anthelmintic and diuretic activity of bark extracts of *Sterculia villosa*. *J. Appl. Pharm. Sci.*, *2*(10), 86-89. https://doi.org/10.7324/JAPS.2012.21017

Asih, I. A. R. A., Gunawan, I. W. G. & Ariani N. M. D. (2010). Isolasi dan Identifikasi Senyawa Golongan Triterpenoid Dari Ekstrak n-Heksana Daun Kepuh (*Sterculia foetida* L.) Serta Uji Aktivitas Antiradikal Bebas. *Jurnal Kimia*, *4*(2), 135-140.

Atun, Sri. (2014). Metode Isolasi dan Identifikasi Struktural Senyawa Organik Bahan Alam. *Jurnal Konservasi Cagar Budaya*. https://doi.org/10.33374/jurnalkonservasicagarbudaya.v8i2.132

Bani A.P., & Tiara M.N. (Ed.). (2003), *Biokimia Harper*. Jakarta, Penerbit Buku Kedokteran EGC.

Babalola, I. T., Adelakun, E. A., Wang, Y., Shode, F. O. (2012). Anti-TB Activity of *Sterculia setigera.* Del., Leaves (*Sterculiaceae*), *J. Pharmacogn. Phytochem, 1*(3), 17-23.

Balai Pemantapan Kawasan Hutan Wilayah XIV. (2008). *Laporan Statistik Kehutanan wilayah XIV Kupang tahun 2008,* Kupang.

Bosenberg, L. H. dan Zyl, D. G. V. (2008). The mechanism of action of oral antidiabetic drugs : A review of recent literature. *J. Endocrinol. Metab. Diabetes South Africa*, *13*(3).

Cahyani, N. P. S. E., Susiarni, J., Dewi, K. C. S., Melyandari, N. L. P., Putra, K. W. A. & Swastini, D. A. (2019). Karakteristik Dan Skrining Fitokimia Ekstrak Etanol 70% Batang Kepuh (*Sterculia foetida* L.). *Jurnal Kimia*, *13*(1): 22-28.

Cushnie TP, Tim L, Andrew J. (2005). Antimicrobial activity of flavonoids. *International Journal of Antimicrobial Agents*, *26*(3), 343-356. https://doi.org/10.1016/j.ijantimicag.2005.09.002

Departemen Kehutanan. (2002). *Informasi Umum Kehutanan*, Departemen Kehutanan, Jakarta.

El-sherei, M. M., Ragheb, A. Y., Kassem, M. E. S., Marzouk, M. M., Mosharrafa, S. A., Saleh, N. A. M. (2016). Phytochemistry, biological activities and economical uses of the genus *Sterculia* and the related genera: A review. *Asian Pacific J. Trop. Dis., 6*(6), 492-501. https://doi.org/10.1016/S2222-1808(16)61075-7

Forest Watch Indonesia/Global Forest Watch, (2001), Keadaan Hutan Indonesia, Bogor, Indonesia.

Gressler, V., Stuker, C. Z., Dias, G. O. C, Dalcol, I. I., Burrow, R. A., Schmidt, J., Wessjohann, L., Morel, A. F. (2008), Quinolone alkaloids from *Waltheria douradinha, Phytochemistry, 69*, 994-999.

Griffin, H. D. (1981). *Fungal Physiology.* John Wiley and Sons. New York.

Gunawan & Karda (2015). Identifikasi senyawa minyak atsiri dan uji aktivitas antioksidan ekstrak etanol kulit batang Kepuh (*Sterculia foetida* L.). *Jurusan Kimia FMIPA Universitas Udayana*. *8*(1).

Hairani, R., Mongkol, R., Chavasiri, W. (2016), Allyl and Prenyl Ethers of Mansonone G, New Potential Semisynthetic Antibacterial Agents. *Bioorganic Med. Chem. Lett., 26*, 5300-5303. https://doi.org/10.1016/j.bmcl.2016.09.044

Hebbar, Deepa R.dan , Nalini, M .S. (2014). Phytochemical Screening, Total

Phonolic Content and In vitro Antioxidant Studies of Leaf, Bark and Flower Extracts of Schefflera Spp. (Araliaceae). *Journal of Applied Pharmacognosy And Phytochemistry*, *2*(5),10-14. https://doi.org://10.7324/JAPS.2013.31117.

Heyne, K. (1987), *Tumbuhan Berguna Indonesia*, Jilid II, Yayasan Sarana Wana Jaya, Jakarta.

Huang, Q., Huang, R., Wei, L., Yongxing, C., Lv, S., Liang, C., Zhang, X., Yin, F., Li, H., Zhuo, L., Lin, X. (2013). Antiviral activity of methyl helictere isolated from *Helicteres angustifolia* (Sterculiaceae) against hepatitis B virus. *Antiviral Res*., *100*, 373-381.

Li, S., Shia, Y., Shang, X. Y., Cui, B. S., Yuana, Y., Chena, X. G. (2009), Triterpenoids from the roots of *Pterospermum heterophyllum* Hance, *J.Asian Nat. Prod. Res., 11*(7), 652–657.

Lin, L., Song, Z., Xu, H., (2010), A new phenylpropanoid galactoside and other constituents from *Pterygota alata* (Roxb.) R. Brown, *Biochem. Syst. Ecol.*, *38*, 1238–1241.

Maryanti, A. & Hendrati, R. L. (2014), Budidaya Kepuh (Sterculia foetida L.) untuk Antisipasi Kondisi Kering. Bogor: IPP Press.

Monalisa, D., Handayani, T., dan Sukmawati., D. (2011). Uji Daya Anti Bakteri Ekstrak Daun Tapak Liman (*Elephantopus Scaber* .L) Terhadap *Staphylococcus Aureus* dan *Salmonella Typhi*. *Jurnal BIOMA*, *9*(2), 13-20.

Muchtadi, D. (2013). *Antioksidan dan Kiat Sehat di Usia Produktif.* Bandung: Alfabeta. 91-95.

Mujumdar, A. M., Naik, D. G., Waghole, R. J., Kulkarni, D. K. & Kumbhojkar, M. S. (2011). Pharmacological Studies On Sterculia foetida Leaves. *0209*.

Naik, D. G., Mujumdar, A. M., Waghole, R. J., Misar, A. V, Bligh, S. W. A., Bashall, A., & Crowder, J. (2003), *matory Compound from Sterculia*. *100*, 40–41.

Njurumana, G. N. (2011), Ekologi Dan Pemanfaatan Nitas (*Sterculia foetida* L.) di Kabupaten Timor Tengah Selatan, Nusa Tenggara Timur. *Jurnal Penelitian Hutan Dan Konservasi Alam*.

Nuria, Maulita C, Faizaitun, Arvin, Sumantri. (2009), Uji aktivitas antibakteri ekstrak etanol daun jarak pagar (*Jatropha Curcas* L.) terhadap bakteri *Staphylococcus aureus* Atcc 25923, *Escherichia coli* Atcc 25922, dan *Salmonella thypi* Atcc 14808. Mediagro, *5*(2), 26-77

Purgiyanti, Purba, V. A., Winarno, H., (2019). Penentuan Kadar Fenol Total Dan Uji Aktivitas Antioksidan Kombinasi Ekstrak Herba Pegagan (*Centella Asiatica* L. Urban), *Dan*,*8*(2), 40–45. http://dx.doi.org/10.30591/pjif.v8i2.1395

Rani, P. U., & Rajasekharreddy, P. (2009), Toxic and antifeedant activities of *Sterculia Foetida* L.*)* seed crude extract against *Spodoptera litura* F. and *Achaea Janata* L. *2*(2), 161–164.

Silalahi, J. (2006). *Makanan Fungsional*. Yogyakarta: Kanisius. (pp. 40-41, 52, 54).

Siswadi, Saragih, S. G., Rianawati, H. (2013). Potential Distributions and Utilization of Faloak (*Sterculia quadrifida* R. Br. 1844) on Timor Island, East Nusa Tenggara, In *Forest and Biodiversity*. Editor Langi, M., Tasirin, J., Walangitan, H., and Masson, G. Manado Forestry Research Institute, Manado, 165–172.

Tarak, D., Namsa, N. D., Tangjang, S., Arya, S. C., Rajbonshi, B. (2011). An inventory of the ethnobotanicals used as anti-diabetic by a rural community of Dhemaji district of Assam, Northeast India. *J. Ethnopharmacol, 138*, 345-350.

Tiwari, P., Kumar, B., Mandeep, K., Kaur, G., & Kaur, H. (2011). Phytochemical

screening and Extraction: A Review. *Internationale Pharmaceutica Sciencia*.

Torokano, S., Akhmad Khumaidi, dan Arsa Wahyu Nugrahani. (2018). Aktivitas Antibakteri Ekstrak Etanol Daun Jarak Merah (Jatropha gossypifolia) Terhadap Bakteri Escherichia coli dan Staphylococcus aureus. Natural Science: *Journal of Science and Technology*, *7*(1), 117–126.

Tuba, A. K., Gülçin, I. (2008), Antioxidants and radical scavenging properties of curcumin. *Chemico-Biological Interaction*, *174*, 27-37.

Vital, P. G., Velasco, R. N., Demigillo, J. M. & Rivera, W. L., (2010), Antimicrobial activity, cytotoxicity and phytochemical screening of Ficus septica Burm and Sterculia foetida L. leaf extracts. *4*(1),58-63.

Wibowo A., Ahmat N., Hamzah A. S., Latif F. A., Norrizah J. S. dan Khong H. Y. (2014), Identification and biological activity of secondary metabolites from *Dryobalanops beccarii*. *Phytochem. Lett. 9*, 117–122. https://doi.org/10.1016/j.phytol.2014.05.001

Widodo, G. P. dan Rahayu, M. P. (2010). Aktivitas Antimalaria Ekstrak Etil Asetat Kulit Batang Mundu *(Garcinia dulcis* Kurz*)*. *Majalah Farmasi Indonesia*. *21*(4), 238-242.

Winarsi, H. (2007). *Antioksidan Alami dan Radikal Bebas*. Yogyakarta: Kanisius. (pp. 87-93).

JURNAL ILMIAH BERKALA SAINS DAN TERAPAN KIMIA
Jurnal Ilmiah Berkala: Sains dan Terapan Kimia
Vol. 16 No. 2, July 2022

Characteristics and Chemical Composition of Fly Ash From Pulang Pisau's Power Plant as A Potential Material for Synthesis of Aluminosilicate Materials

Karakteristik dan Komposisi Kimia Abu Layang PLTU Pulang Pisau Sebagai Bahan Baku Potensial untuk Sintesis Material Aluminosilikat

Rendy Muhamad Iqbal[1,2], Akhmad Damsyik[1], Retno Agnestisia[1], Siswo[1], Ni Wayan Prema Mulya Sari[1], Fildzah 'Adany[3]

[1]Department of Chemistry, Faculty of Mathematic and Natural Science, Universitas Palangka Raya, Kampus UPR Tunjung Nyaho, 73111, Indonesia
[2]Divison of Natural and Applied Science Center for Development of Science, Technology and Peat Innovation, Universitas Palangka Raya, Kampus UPR Tunjung Nyaho, 73111, Indonesia
[3]Research Center for Chemistry, National Research and Innovation Agency, Kawasan Puspitek, 15314, Indonesia

Email: Iqbal.rm@mipa.upr.ac.id

ABSTRACT

The Steam-Electric Power Station (PLTU) is one of the initiatives to meet the nation's current electricity requirements. The use of fuel for steam power plant is still dominated by fossil fuels such as coal. Even though domestic energy needs are met, steam power plant turns out to be a contributor to gas emissions that cause global warming, as well as a by-product in the form of fly ash which can cause environmental and ecosystem problems. Fly ash contains silica oxide (SiO_2) and aluminum oxide (Al_2O_3) compounds which can be used as raw materials for synthesizing aluminosilicate-based materials such as geopolymers and zeolites. This study tested the characteristics and composition of chemical compounds in fly ash from Pulang Pisau's power plant, Central Kalimantan. Characterization using X-Ray Diffraction (XRD) showed that peaks of quartz material dominated fly ash from Pulang Pisau's power plant at 2θ=20.82°;26.61° and mullite minerals at 2θ= 31.2°;33.1°; 35.4°;39.2°;59.8°. The results of the chemical compound composition were tested using the ASTM-D3682-12 standard. Fly ash has a composition of 29.00% SiO_2, 9.98% Al_2O_3, 13.75% Fe_2O_3, and 28.37% CaO. Fly ash from Pulang Pisau's power plant is classified as type C fly ash, which can potentially be used as a source of aluminosilicate-based material synthesis.

Keywords: PLTU, fly ash, aluminosilicate.

ABSTRAK

Pembangkit Listrik Tenaga Uap (PLTU) merupakan salah satu upaya untuk memenuhi kebutuhan listrik dalam negeri saat ini. Pemakaian bahan bakar untuk PLTU masih didominasi oleh bahan bakar fosil seperti batu bara. Batu bara merupakan sumber energi yang menjadi bahan bakar utama untuk sumber listrik di Indonesia. Meskipun kebutuhan energi dalam negeri terpenuhi, ternyata Pembangkit Listrik Tenaga Uap (PLTU) merupakan salah satu tempat kontribusi penyumbang emisi gas yang menyebabkan pemanasan global, serta produk samping yakni abu layang (fly ash) yang menimbulkan permasalahan bagi lingkungan dan ekosistem. Abu layang mengandung senyawa silika oksida (SiO_2) dan aluminium oksida (Al_2O_3) yang dapat digunakan sebagai bahan baku sintesis material berbasis aluminosilikat seperti geopolimer, zeolit dan lain-lain. Pada penelitian ini, dilakukan pengujian karakteristik dan komposisi senyawa kimia pada abu layang PLTU Pulang Pisau Kalimantan Tengah. Berdasarkan karakterisasi menggunakan X-Ray Diffraction (XRD) menunjukkan bahwa abu layang PLTU Pulang Pisau didominasi oleh puncak material kuarsa pada 2θ=20,82°;26,61° dan mineral mullite pada 2θ= 31,2°;33,1°;35,4°;39,2°;59,8°. Hasil komposisi senyawa kimia di uji dengan menggunakan standar ASTM-D3682-12. Berdasarkan data yang diperoleh pengujian komposisi kimia abu layang memiliki

komposisi senyawa SiO_2; Al_2O_3; Fe_2O_3; CaO tertinggi dengan persentase masing-masing 29,00%;9,98%;13,75%; 28,37%. Berdasarkan komposisi senyawa kimia, abu layang PLTU Pulang Pisau diklasifikasikan sebagai abu layang tipe C. Dari data tersebut dapat disimpulkan bahwa, abu layang dari PLTU Pulang Pisau sangat berpotensi untuk digunakan sebagai sumber sintesis material berbasis aluminosilikat.

Kata Kunci: PLTU, abu layang, aluminosilikat.

Received: December 14, 2021; **Accepted**: June 29, 2022: **Available online**: July 31, 2022

1. INTRODUCTION

As the global population is expected to rise, so will the yearly energy demand. One of the most critical energy demands is the domestic supply of electrical energy. According to PLN's 2020 Statistical Data, PLN's total production is 274,852.18 GWh, an increase of 14.205 from the previous year (PLN Statistics, 2020). Numerous power plants are utilized to meet demands for electrical energy. Steam-Electric Power Station (PLTU) is one of them. There are 127 PLTU in Indonesia, which is expected to increase annually in parallel with population growth.

Steam power plant produces electricity using coal-based raw materials (Rasyid et al., 2017). Coal is a fossil fuel in the form of sedimentary rock with burning properties formed due to the deposition of organic matter, especially plants. Coal is composed of dominant chemical elements in the form of carbon (C), hydrogen (H) and oxygen (O) (Surahman et al., 2020). Steam power plant have an advantage over other power plants due to the relatively abundant availability of coal in Indonesia. In general, Indonesia's coal type has low calories, so it is less attractive to the export market. In addition to having a positive impact on fulfilling the domestic electricity supply, steam power plant has a negative impact in the form of dangerous fly ash.

Steam power plant contributes to emitting fly ash waste generated from the coal combustion process. Fly ash is a hazardous material that, when disposed into the environment, will cause serious environmental problems, especially in living ecosystems (Sutarno et al., 2019). Fly ash contains heavy metals which will negatively impact the environment, such as reducing soil fertility and polluting waters. In addition to impacting the environment, fly ash can disrupt the health system of living things that are exposed to irritation of the eyes, nose, throat, respiratory system disorders, and nervous disorders that can reduce the ability of the brain system (Sulistiyani, 2016).

Based on previous research, it was reported that fly ash contains oxide compounds such as silicon oxide (SiO_2), aluminium oxide (Al_2O_3), calcium oxide (CaO), and iron oxide (Fe_2O_3) (Abidin & Leksono, 2021). This high content of silicon oxide and aluminium oxide has the potential to be used as the raw material for the production of aluminosilicate-based materials such as geopolymers and zeolites.

Geopolymer is an inorganic polymer material that is synthesized geochemically. Geopolymer is formed due to the polymerization reaction between silica (Si) elements and Aluminum (Al). Geopolymers are getting higher attention because of their advantages such as hard material properties, weather resistance, good thermal stability, porosity, and good compressive strength (Oktaviastuti & Yurnalisdel, 2020). Zerfu et al. (2016) stated that the quality of geopolymer material depends on the type of fly ash and the coal combustion process. Quality geopolymers contain 70% (wt%) total silicon oxide, aluminium oxide, and iron oxide (Zerfu & Ekaputri, 2016).

Zeolite is an aluminosilicate-based material with a very regular structure, high porosity, and good thermal stability properties. Zeolites can be produced from natural materials such as clay, bagasse, kaolin, and lateritic soils (Sukmaladewi, 2017; Iqbal et al., 2018; Endang et al., 2019). In addition to natural zeolites, many synthetic zeolites have been developed, of which there are more than 215 frameworks. Synthetic zeolites that have been identified include the NaY zeolite (Rachman et al., 2018), Y zeolite (Rahayu et al., 2019), and

the ZSM-5 zeolite (Hartanto et al., 2018). Fly ash, which is rich in silica and alumina, has the potential to be used as a raw material in the production of zeolite. Therefore, in this study, the chemical characteristics of fly ash obtained from the steam power plant in Central Kalimantan will be studied to determine the chemical composition and characteristics of fly ash crystals as a raw material for synthesizing aluminosilicate materials.

2. MATERIALS AND METHODS

2.1. Materials

The material used was fly ash taken from the Pulang Pisau's power plant Central Kalimantan, which was analyzed using the ASTM-D3682-12 standard. The tool used was X-Ray Diffraction (XRD) (Rhigaku Miniflex600).

2.2. Methods

The fly ash studied was obtained from the Central Kalimantan steam power plant located in the Pulang Pisau Regency area. The fly ash was characterized using X-Ray Diffraction (XRD). Analysis of the fly ash's chemical composition using a method that met the standards according to ASTM-D3682-12.

3. RESULTS AND DISCUSSION

Fly ash was characterized using the X-ray diffraction method to determine the constituent material. The diffractogram in Fig. 1 gives the diffraction pattern at an angle of 2θ. Based on the characterization test using X-Ray Diffraction (XRD), the fly ash of the Pulang Pisau's power plant was dominated by peaks of quartz material at 2θ=20.82°;26.61 and mullite minerals at 2θ= 31.2°;33.1°;35,4°;39,2°;59,8°. Sunarti and Nazudin (2021) stated that the X-ray diffraction pattern of quartz and mullite materials in fly ash indicated the presence of Si and Al elements. The higher intensity of the quartz peaks, when compared to the mullite peaks' intensity, indicates that the silica content in fly ash is higher than that of alumina and other oxides. Based on this high silica and alumina composition, fly ash has the potential to be developed as a raw material for aluminosilicate-based materials such as geopolymers and zeolites.

The chemical composition of fly ash depends on the type of coal being burned. The chemical composition of fly ash from Pulang Pisau's power plant is presented in Table 1. The composition of chemical compounds was tested using the ASTM-D3682-12 standard. The chemical composition of fly ash was 29.00% SiO_2, 9.98% Al_2O_3, 13.75% Fe_2O_3, and 28.37% CaO. The high percentage of SiO_2, Al_2O_3, Fe_2O_3, and CaO will potentially be used as raw materials for the synthesis of aluminosilicate-based materials.

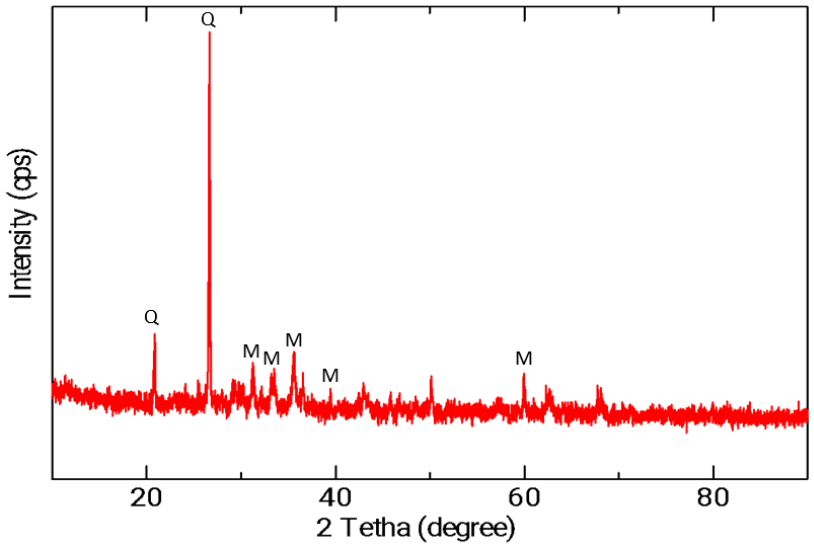

Figure 1. Fly Ash XRD Diffractogram Pattern from Pulang Pisau's Power Plant

Table 1. Chemical Compound Composition of Fly Ash from Pulang Pisau's Power Plant

Chemical Compound	Percentage
SiO_2	29.00
Al_2O_3	9.98
Fe_2O_3	13.75
CaO	28.37
MgO	9.03
SO_3	5.82
P_2O_5	0.32
Na_2O	0.67
K_2O	0.71
TiO_2	1.16
MnO_2	0.28

*Source: original processed data

The type of fly ash influences the quality of aluminosilicate-based materials. Fly ash is generally classified into two types based on its chemical composition (type C and F). Based on the American Society for Testing Material (ASTM) C618 standard, fly ash type F contains more than 70% (wt%) SiO_2, Al_2O_3, and Fe_2O_3 and less than 20% CaO. Type C fly ash contains less than 70% wt% SiO_2, Al_2O_3, and Fe_2O_3 and a CaO content of more than 10% (Hidayati et al., 2020). Based on the ASTM C618 standard, the fly ash from the Pulang Pisau's power plant can be categorized as type C. Table 2 illustrates the classification of fly ash classes from various steam power plants.

Previous research by Wattimena et al. (2017) reported that geopolymers synthesized with high calcium content would have high compressive characteristics. Over time, apart from the geopolymerization reaction, a hydration reaction will occur. Based on this fact, the fly ash of the Pulang Pisau's power plant, which is classified as type C with a very high CaO content, is suitable as a raw material for the synthesis of geopolymer materials. In contrast to zeolite materials, the calcium content in fly ash will affect the crystallinity of the zeolite during the synthesis process. Zeolite synthesized with type C fly ash will produce a residue characteristic of quartz, whereas when the zeolite is synthesized with type C fly ash, it will produce residues of quartz and mullite. Hence, the zeolite synthesized from type C fly ash will have a higher crystallinity than the zeolite synthesized from type F fly ash (Kunecki et al., 2020). Therefore, fly ash from Pulang Pisau's power plant with high CaO content is suitable as raw material for zeolite synthesis.

Table 2. Classification of Fly Ash Class from Various Steam Power Plant in Indonesia

Source of Fly Ash	Classification	Reference
Pacitan Power Plant	Type F	
Semen Gresik	Type C	
Petrokimia Gresik	Type F	Sari et al., 2018
Abu Layang PT. IPMOMI	Type F	
Pulang Pisau's Power Plant	Type C	Results of this study

4. CONCLUSIONS

The characteristics of fly ash will affect the quality of fly ash used as a raw material for synthesizing aluminosilicate materials. Peaks of quartz and mullite material dominate the characteristics of fly ash based on the XRD test. Based on the ASTM C618 standard, the fly ash of the Pulang Pisau's power plant is classified as type C, which is very suitable as a raw material for the synthesis of aluminosilicate materials such as geopolymers and zeolites.

ACKNOWLEDGMENT

The Research Team acknowledges the Faculty of Mathematics and Natural Sciences, University of Palangka Raya, for the research grant with contract number 422/UN24.10/KP/2021 and the Pulang Pisau PLTU for the fly ash samples.

LIST OF REFERENCES

Endang, P. S., Rahadian, A. R., Ulva, T. I. M., Alvin, R. W., Rendy, M. I., & Nurul, W. (2019). The MnO_2/Zeolite NaY Catalyzed Oxidation of CO Emission in Catalytic Converter System. *Materials Science Forum*, *964*, 199-208. https://doi.org/10.4028/www.scientific.net/MSF.964.199

Hartanto, D. et al. (2017). Effect of H2O/SiO2 Molar Ratio on Direct Synthesis of ZSM-5 from Bangka's Kaolin Without Pretreatment. *Malaysian Journal of Fundamental and Applied Sciences, 13*(4), 817–820.

Hidayati, R. E., Anindika, G. R., Faradila, F. S., Hidayati, I., Prasetyoko, D., & Fansuri, H. (2020). Geopolymerization of Fly Ashes From 6 Indonesian Power Plants Using A Standardized Recipes. In *IOP Conference Series: Materials Science and Engineering*. *864*(1). IOP Publishing. https:// doi:10.1088/1757-899X/864/1/012017

Iqbal, R. M., Wardhani, S., Darjito, D., & Karelius, K. (2018). Fabrication and Performance of Laterite East Kotawaringin-Zeolite/Chitosan Composite as Slow Release of Iron Fertilizer. *Molekul*, *13*(2), 148-154.

Jurnal, R. T. (2017). Studi Kelayakan Pembangunan Pembangkit Listrik Tenaga Uap 2x50 Mw dengan Menggunakan Boiler Circulating Fluidized Bed Combustion di Kendari, Sulselrabar. *Energi & Kelistrikan*, *9*(2), 147-156. https://doi.org/10.33322/energi.v9i2.46

Kunecki, P., Panek, R., Wdowin, M., Bień, T., & Franus, W. (2021). Influence of the fly ash fraction after grinding process on the hydrothermal synthesis efficiency of Na-A, Na-P1, Na-X and sodalite zeolite types. *International Journal of Coal Science & Technology*, *8*, 291-311. https://doi.org/10.1007/s40789-020-00332-1

Leksono, E. B., & Abidin, A. (2021). Pemanfaatan Limbah Fly Ash Batubara sebagai Koagulan dengan Konsep Reverse Logistics. *Jurnal INTECH Teknik Industri Universitas Serang Raya*, *7*(1), 39-44. https://doi.org/10.30656/intech.v7i1.2736

Oktaviastuti, B., & Yurnalisdel, Y. (2020). Studi Kuat Tekan Beton Geopolymer Dengan Fly Ash Sebagai Perkerasan Kaku Di Pesisir Pantai. *Fondasi: Jurnal Teknik Sipil*, *9*(2), 201-214. http://dx.doi.org/10.36055/jft.v9i2.8515

Rachman, R. A., Martia, U. T. I., Aulia, W., Iqbal, R. M., Widiastuti, N., & Kurniawan, F. (2018). Combination of microbial fuel cell and zeolite Na-Y adsorption for chromium removal. In *AIP Conference Proceedings*, *2049*(1). AIP Publishing LLC. https://doi.org/10.1063/1.5082478

Rahayu, E. S., Bentang, D., & Fauziyyah, G. (2020). Penggunaan Kembali Limbah Cair dari Sintesis Zeolit Y sebagai Sumber Silika untuk Sintesis Zeolit Y secara Hidrotermal. *Jurnal Teknik Kimia Indonesia*, *18*(2), 53-60. http://dx.doi.org/10.5614/jtki.2019.18.2.4

Sari, D. K., Setyaningsih, E. P., Fansuri, H., & Susanto, T. E. (2018). Kajian Karakteristik Kimia dan Fisika Abu Layang yang Menjadi Penentu Kekuatan Mekanik Perekat Geopolimer Berbahan Dasar Abu Layang. *Akta Kimia Indonesia*, *3*(2), 222-235.

Sugiyanto, C., & Kurniawati, E. (2021). Pengaruh Struktur Umur Penduduk terhadap Pertumbuhan Ekonomi di Indonesia. *Jurnal Ekonomi dan Pembangunan Indonesia*, *21*(1), 41-58. https://doi.org/10.21002/jepi.v21i1.1209

Sukmaniar, S., & Saputra, W. (2020). Transmigrasi Wilayah Perbatasan di Indonesia. *UNM Geographic Journal*, *3*(1), 41-50. https://doi.org/10.26858/ugj.v3i1.14599

Sukmaladewi. (2017). *Sintesis Zeolit dari Campurab Lempung dan Blotong*. Skripsi Program Sarjana, UIN ALAUDDIN, Makassar.

Sulistyani. (2016). Berbagai Potensi Abu Terbang (FLY ASH) Hasil Pembakaran Batu Bara Pada PLTU, *Prosiding Seminar Nasional Kimia.*

Surahman, S. (2020). Prosedur Penanganan Loading Batu Bara Pada Kapal Capesize Mv. Mineral Haiku Agar Mencapai Target Di Adang Bay Anchorage Pada Pt Bahtera Adhiguna (Cabang Tanah Grogot). *Jurnal Maritim*, *10*(1), 44-50. http://dx.doi.org/10.46964/jmarit.v10i1.582

Sutarno, S., Kusdiyono, K., Wahjoedi, W., & Mawardi, M. (2019). Kajian Pengaruh Kebakaran Terhadap Sifat Karakteristik Bata Beton Geopolimer dari Fly Ash Dan Bottom Ash Limbah PLTU Tanjung Jati. *Bangun Rekaprima: Majalah Ilmiah Pengembangan Rekayasa, Sosial dan Humaniora*, *5*(1), 21-28. http://dx.doi.org/10.32497/bangunrekaprima.v5i1.1406

Sunarti, S. (2021). Sintesis Zeolit A dari Abu Dasar Batubara (Coal Bottom Ash) dengan Metode Peleburan dan Hidrotermal. *Molluca Journal of Chemistry Education (MJoCE)*, *11*(1), 8-16. https://doi.org/10.30598/MJoCEvol11iss1pp8-16

Walker, R. J. (2016). Population growth and its implications for global security. *American Journal of Economics and Sociology*, *75*(4), 980-1004. https://doi.org/10.1111/ajes.12161

Wattimena, O. K., Antoni, & Hardjito, D. (2017). A review on the effect of fly ash characteristics and their variations on the synthesis of fly ash based geopolymer. *AIP Conference Proceedings*, *1887*(1).

Zerfu, K. E. F. I. Y. A. L. E. W., & Ekaputri, J. J. (2016). Review on alkali-activated fly ash based geopolymer concrete. *Materials Science Forum*, *841*, 162-169. https://doi.org/10.4028/www.scientific.net/MSF.841.162